TÉCNICO LISBOA

Detailed Modelling of Catalytic Partial Oxidation Processes

Ethylene Oxide Production

Maria Isabel Luiz Gomes Pereira Coutinho

Thesis to obtain the Master of Science Degree in

Chemical Engineering

Advisors:
Prof. Dr. Henrique Aníbal Santos de Matos
Dr. Štěpán Špatenka

Examination Committee

Chairperson: Prof. Dr. Francisco Manuel Da Silva Lemos
Advisor: Prof. Dr. Henrique Aníbal Santos de Matos
Member of the Committee: Dr. Ana Catarina Gouveia Braz

Instituto Superior Técnico - Universidade de Lisboa

October 2019

Declaração

Declaro que o presente documento é um trabalho original da minha autoria e que cumpre todos os requisitos do Código de Conduta e Boas Práticas da Universidade de Lisboa.

Declaration

I declare that this document is an original work of my own authorship and that it fulfills all the requirements of the Code of Conduct and Good Practices of the Universidade de Lisboa.

Acknowledgments

I would first like to thank my thesis advisors Prof. Dr. Henrique Matos and Dr. Štěpán Špatenka for their unsurpassed guidance and availability. Their knowledge and advice offered on a variety of subjects was crucial in this endeavor.

I would also like to express my gratitude to Vasco Manaças, whose input was imperative in the success of this work.

I am grateful for the enriching experience of writing my dissertation in Process Systems Enterprise Ltd, endorsed by my university. It was truly a wonderful opportunity, with an extremely welcoming and helpful environment.

I would like to express my special gratitude to Petkim Petrokimya Holding A.Ş. for providing the experimental data which was instrumental for the completion of this work's objectives.

Finally, I must profoundly thank my family and friends for their infallible support, without whom this accomplishment would be impossible.

Isabel Pereira Coutinho

Abstract

Reactor modelling has previously focused on fluid dynamics, using simplified kinetic rate expressions. Although this method has proven to be sufficient in the past, it has a limited range of applicability. This limitation hinders various ends for which reactor models are created: sizing, optimisation, control, etc.

This work aims to use detailed microkinetics of the intervening reactions in a catalytic partial oxidation process to generate a comprehensive reactor model.

The use of a detailed model for the reaction's kinetics additionally provides a better understanding of the reaction's mechanism and the impact of specific changes on the overall scheme.

A microkinetic model for ethylene epoxidation was selected from literature. The detailed kinetics were tested independently and within a gPROMS catalytic multitubular fixed bed reactor model.

Sensitivity analysis were carried out to evaluate the capability of the microkinetics in predicting plausible effects: selectivity and activity trends. This analysis was further successful in identifying the rate-determining reaction steps. These steps were then selected for parameter estimation.

A parameter estimation was performed using experimental data provided by Petkim Petrokimya Holding A.Ş.. An enhanced model adapted to industrial catalysts was parameterised accordingly.

The last stage focused on possible model extensions. The moderator effect and catalyst deactivation were studied due to their prevailing presence in an industrial setting.

A deactivation expression was developed for the current microkinetic model, as well as suggestions on incorporating the moderator.

Keywords: Ethylene oxide production, ethylene partial oxidation, ethylene epoxidation, microkinetics, modelling, gPROMS

Resumo

A dinâmica de fluidos tem sido o foco dos últimos desenvolvimentos na área da modelação de reatores. Pouca relevância tem sido atribuída à cinética das reações, que geralmente é simplificada.

Esta abordagem tem previamente gerado bons resultados, porém é limitada, visto que inibe o progresso de inúmeras aplicações, nomeadamente dimensionamento, otimização e controlo de reatores.

Esta dissertação utiliza a micro-cinética das reações intervenientes num processo catalítico de oxidação parcial para construir um modelo de reator universal. Ademais, uma melhor compreensão do mecanismo das reações, bem como o impacto de perturbações em certas variáveis, são especificados pela utilização de modelos de cinética detalhados.

Um mecanismo micro-cinético para a epoxidação do etileno foi selecionado da literatura. A cinética deste modelo foi testada independentemente e em conjunto com um modelo de um reator multitubular de leito fixo na plataforma gPROMS.

A capacidade preditiva do modelo foi aferida via análise de sensibilidade, com a seletividade e atividade do modelo como âmago da análise. Adicionalmente, os passos reacionais limitantes foram identificados, sendo posteriormente utilizados na etapa da estimativa de parâmetros.

Dados experimentais fornecidos pela Petkim Petrokimya Holding A.Ş. permitiram a estimativa de certos parâmetros cinéticos, de modo a adaptar o modelo à indústria.

A etapa final consistiu em averiguar possíveis extensões do modelo. Dois fenómenos predominantes na indústria de produção de oxido de etileno foram considerados: o efeito de modificadores e a desativação do catalisador.

Uma expressão para a desativação foi incorporada no modelo e sugestões para integrar o efeito do modificador foram discutidas.

Keywords: Produção de óxido de etlieno, oxidação parcial de etilieno, epoxidação de etileno, micro-cinética, modelação, gPROMS

Contents

List of Tables

List of Figures

Acronyms

1D	1-Dimensional. 16, 22, 33
AML:FBCR	Advanced Model Library for Fixed-Bed Catalytic Reactors. 15, 23
APE	Approach to Equilibrium. 33
DFT	Density Functional Theory. 6, 10, 11
EDC	Ethylene Dichloride. 12, 53
EO	Ethylene Oxide. xiii, 2, 11, 17, 21, 23, 24, 27–29, 31, 32, 34–37, 47–50, 53–57, 61–63, 75, 76
EOS	Equation of State. 16
GC	Gas Chromatography. 25
gPLE	general Power-Law Expression. 8, 9, 12, 57
gPROMS	general Process Modelling System. 15–17, 19–23, 27–29, 44, 54, 61
GSA	Global Systems Analysis. 15, 54, 55
HREELS	High-Resolution Electron Energy Loss Spectroscopy. 9, 10
IP	Initialisation Procedure. 20, 21
IR	Infrared. 9
KPI	Key Performance Indicator. 22–24, 34, 36–38, 44, 50, 58, 59, 63
LHHW	Langmuir-Hinshelwood-Hougen-Watson. 1, 9, 11, 13
MFC	Mass Flow Controllers. 25
PET	Polyethylene Terephthalate. 4

POX Partial Oxidation. 1, 3, 4, 9, 11

PSE Process Systems Enterprise. 15

QSSA Quasi-Steady-State Assumption. 19

RDS Rate-Determining Step. 32, 34, 49, 62

STEM Scanning Transmission Electron Microscope. 64

SVR Support Vector Regression. 13

SVS Saved Variable Set. 21

TOX Total Oxidation. 9, 11

TPD Temperature Programmed Desorption. 9

UHV Ultra-high Vacuum. 11

VCM Vinyl Chloride. 22, 25, 27–29, 47, 53–56, 63, 64

1. Motivation

Chemical production plants have long been a source of great profit. The search for the most lucrative plant design has progressively become more competitive. Methods for sizing and designing the various equipment, as well as the plant as a whole, have evolved to reach near optimal configurations.

Nonetheless, obtaining optimal configurations represents a higher challenge for a few sets of processes. This is the case of the processes that involve catalytic partial oxidation (POX) reactions.

Using conventional methods to design catalytic partial oxidation applications is arduous. It is necessary to test different variables under industrial conditions, and through a recursive method determine the intrinsic kinetics of the reaction and the best design for the reactor.

The demand for a detailed model of these POX reactions arises from the necessity of uncoupling these two steps. Simultaneously, it provides comprehensive and exact knowledge of the reactor, allowing to accurately predict the reactor's performance for a wide range of operating conditions, and enabling the optimisation of the reactor's design with scarcely any additional data.

1.1 Purpose

This dissertation aims to develop a general model that can accurately predict the inner workings of a POX catalytic reactor with high fidelity.

As an example of a partial oxidation reaction, ethylene epoxidation was chosen, due to ethylene oxide's prominent growing demand and to the reaction's complex kinetics. Moreover, the microkinetic approach has been successful for similar applications, namely the partial oxidation of methanol to formaldehyde [1].

Ethylene partial oxidation competes with other two reactions, ethylene and ethylene oxide total oxidation, as shown in Fig. 1.1.

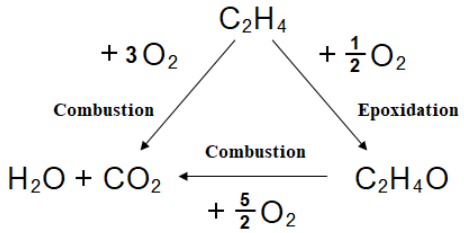

Figure 1.1: Simplified ethylene oxidation scheme

Previous modelling approaches focused on obtaining the extent of each one of these three reactions through rate expressions. The expressions could be power-laws or Langmuir-Hinshelwood-Hougen-Watson (LHHW) formulations, both with fitted parameters.

However, the proposed detailed modelling involves the intermediate steps for each reaction. The discrimination of the steps provides a deeper understanding of the reactions and their respective driving forces. Additionally, it establishes the nature of the relationships between the three main reactions.

This work attempts to develop an enhanced model, based on the detailed kinetics proposed by Stegelmann et al. [2]. The model would presumably be applicable in a wide range of industrial conditions when used within the fixed bed reactor model. It would additionally include phenomena not considered in the original model: deactivation and the moderator effect.

Incorporating these effects would be crucial for the applications outlined, since every plant experiences catalyst deactivation and adds moderators to improve the selectivity.

1.2 Outline

The first stage of this work was an extensive literature review on the industry's stance on the process. Different approaches for partial oxidation processes implementation, as well as a more refined review on ethylene selective oxidation, were explored. Common catalysts, promoters, moderators and reactors were identified. The various advantages and disadvantages were outlined.

Bearing the goal of this work in mind, the kinetics were characterised in higher extent. A timeline for the major advances in this field was established and different proposed mechanisms were discussed. Several techniques for modelling and optimisation were also studied and a multi-step reaction scheme was selected from literature.

The second stage consisted in the implementation of the model. The kinetics were modelled using white-box principles. The selected reaction scheme was implemented within a fixed bed reactor model to demonstrate its potential and limitations. Literature parameters were used as initial points to be examined afterwards, in light of the real data. An uncertainty analysis was carried out for key parameters. These parameters were then re-evaluated in the next step, when the model was consolidated.

Subsequently, a parameter estimation (third stage) was applied using experimental data. It focused on model parameters which had been identified as having a high degree of uncertainty in the previous stage.

The fourth stage, model validation, had the goal of assessing the applicability of the model. Using varying operating conditions, the performance of the model was compared to experimental results, and conclusions were drawn accordingly.

Finally, a sensitivity analysis was performed to identify if the model could include additional effects commonly observed in ethylene oxide (EO) plants. The chosen additions included catalyst deactivation and the effect of a moderator.

2. Literature Review

Detailed modelling of a catalytic partial oxidation process may focus on several topics. This initial review aspired to better understand partial oxidation reactions and their particularities. Furthermore, a focus on a specific case study, a POX reaction, ensured that significant information on mechanisms, promotion, catalysts, previous modelling, among others was obtained.

2.1 Partial Oxidation Processes

POX processes have been extensively reviewed throughout literature, however their rigorous characterisation still remains amiss to this day [3] which leads to most POX processes currently still operating far from optimal conditions, prompting oversized reactors, sub-optimal productivity, and profit loss.

The difficulty in the exact characterization of these processes stems from the fast nature of the POX reactions coupled with the fact that most have accentuated thermal effects. Since the majority of these reactions occur appreciably fast, they often become mass-transfer limited under industrial production conditions, accounting for the unknown kinetics for that range (e.g. CO oxidation) [3].

Most of these processes still use sub-optimal pellets, which cause serious diffusion limitations, since the surface area contacted by the fluid in mass-transfer limited process is much lower than the reaction-controlled processes [3].

The POX high exothermic attribute confers numerous complications, including possible safety concerns in respect to run-away reactions and/or regular operating conditions; the need for intensive heat transfer and thermal stability; and the formation of gradients within the catalyst, which may achieve steady-state multiplicity [3].

The usual scale-up procedure is hampered by the above mentioned effects, hence the need to use industrial conditions (pressure, temperature, feed, etc) and reactors to test kinetic parameters and catalysts with adequate accuracy. Moreover, solutions employed in other reaction, such as feed dilution, cause the experimentally-deduced kinetics to stray from the industrial kinetics [3].

There are multiple well-established POX processes. The following are noteworthy: catalytic oxidation of ammonia to NO, ammoxidation of methane to HCN, partial oxidation of methanol to formaldehyde, ammoxidation of propylene to acrylonitrile, oxidative coupling of methane to produce ethylene, partial oxidation of butane or maleic anhydride, partial oxidation of methane to synthesis gas and partial oxidation of ethylene to ethylene oxide [3, 4].

The use of tubular fixed bed reactors is the norm for partial oxidation process. The cooling is provided in a variety of forms, including using tubes (multitubular reactor), cold shots, arrangements of multistage adiabatic reactors with inter-stage cooling and more [3, 5].

However, the previously mentioned ammoxidation of propylene is an exception, since it uses a fluidized bed reactor. Likewise, the partial oxidation of butane began to employ a circulating fluidized bed in 1988 [3].

2.2 Ethylene Oxide Production

Ethylene oxide (oxirane in accordance to IUPAC nomenclature) is the simplest cyclic ether. It decomposes above 400 ℃, possibly in an explosive manner. One of its most hazardous properties, being a very reactive compound, is simultaneously the main reason for its popularity [6]. This aspect enables this chemical intermediate to be applied in a variety of chemical reactions, increasing its demand throughout the chemical industry.

Some of its primary uses include disinfectants, sterilizing agents and fumigants [6]. In respect to the derivative uses, the most significant industry is ethylene glycol production, which is used in applications such as antifreeze and manufacturing polyester fibers. Other derivatives include amines and polyethylene glycols, triethylene glycol, ethylene glycol ethers, ethanolamine and ethylene carbonate [6–8].

The typical specifications of ethylene oxide are presented below (Table 2.1).

Table 2.1: Typical specifications of ethylene oxide [6]

Boiling point @ 101.3 kPa (℃)	10.8
Water content (mg kg^{-1})	50
CO_2 content (mg kg^{-1})	10
Aldehyde content (mg kg^{-1})	50
Ethylene oxide purity, minimum (%)	99.5

In 2018, Northeast Asia, Middle East, and North America's combined ethylene oxide production accounted for 77% of the global value [9]. The growing demand in emerging countries such as Brazil, Russia, and India has been associated with the increasing consumption of Polyethylene Terephthalate (PET) packaging. Its properties, such as 100% recyclability, rigidity and transparency, have gained notoriety, namely amongst environmentally conscious consumers.

2.2.1 Process and technology

The partial oxidation of ethylene is the most broadly applied process for ethylene oxide manufacture [10]. Early production was performed via the Chlorohydrin process which had a moderately high (around 80% [2, 11]) selectivity. However, there was formation of dangerous byproducts (calcium chloride and other chlorine-containing compounds) which accounted for loss in efficiency and increase of pollution; which promoted the search for improved processes [6].

The field advanced towards direct oxidation. Both air and oxygen-based production are applied nowadays (Fig. 2.1), with a higher emphasis on the latter [8]. The oxygen-based process has gained popularity as the most economical choice [6].

As mentioned previously, the strong thermal effects of POX reactions must be adequately controlled to ensure no reaction runaway. For this purpose, a cooling media is used within the shell of the multitubular reactor. Since the heat generated varies with the aging of the catalyst (the combustion reaction is more exothermic), the cooling fluid must be able to change accordingly. Nonetheless, the temperature is dictated by the maximum allowed coolant pressure drop [6].

Water and high-boiling hydrocarbons (~190 ℃) are frequently used while extracting heat and may be achieved through pumping or evaporation of the coolant. When using evaporative cooling, the organic coolant is flammable at high temperatures and requires high-pressure water (steam generation) for regeneration. A control valve is also required to keep the cooling medium at boiling point. Nevertheless, using water entails higher costs due to the elevated pressures. This option is mostly used for smaller reactors which operate at

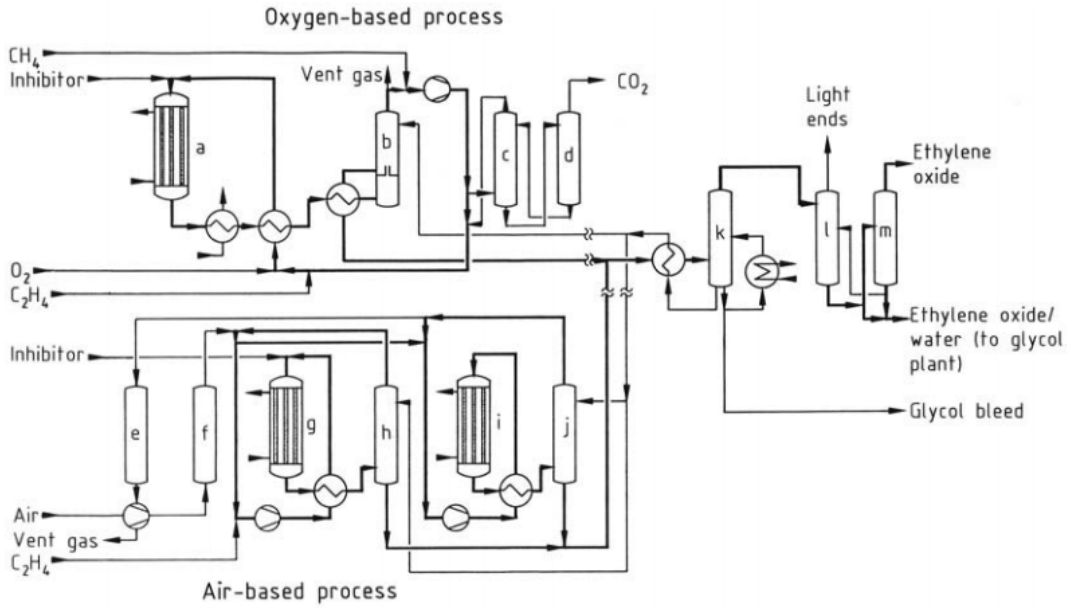

Figure 2.1: Ethylene oxide production scheme through the air-based and oxygen-based process [6]

low temperature with high-selectivity catalysts [6].

The main benefit of using evaportive cooling is the need for a small volume of the medium, since latent heat is being transferred. In contrast, the circulation cooling requires significant pumping power but allows for a defined temperature profile control in the gas flow direction [6].

As part of the efficient heat integration of the plant, the effluent is used to pre-heat the feed and/or generate steam. Furthermore, the hydrocarbons may be used to heat the recycle stream or for steam generation [6].

The feed to the reactors is closely watched: mixing devices are necessary to avoid reaching flammability limits locally. Ethylene feeds must be treated to remove sulfur and acetylene [6, 12]. The presence of the former in the reaction mixture can have serious repercussions (catalyst poisoning).

Several steps are taken for the recovery and purification of the product from the effluent. Firstly, ethylene and carbon dioxide scrubbers are used. These remove trace amount of carbon dioxide, nitrogen, methane, ethylene and others (e.g. argon, aldehydes). Secondly, a small purge (0.1-0.2% (v/v)) of the effluent is combusted to prevent inert accumulation [6].

The outlet follows into an ethylene oxide desorber where the product is retrieved on the top. A stripper removes low-boiling components with the posterior distillation column separating the product from water [6].

The recycle stream must be compressed, scrubbed with a hot aqueous potassium carbonate solution, and treated. This treatment is optional, based on the needs of the feed stream: adding diluent, ethylene, oxygen or modifiers, as required [6].

Air-based oxidation processes require bigger purges to ensure that the nitrogen that enters as air does not accumulate. Although this measure is undesirable, it does benefit from some positive aspects, namely it removes carbon dioxide to an extent where scrubbing is unnecessary. Overall, the weakest point of the air-based process is the higher conversions which conduce to lower selectivities [6]. A more extensive comparison of both production pathways is presented in Table 2.2.

Table 2.2: Ethylene oxide production through air-based and oxygen-based processes comparison [6]

	Air-based	Oxygen-based
C_2H_4 concentration (vol%)	2-10	15-40
O_2 concentration (vol%)	4-8	5-9
CO_2 concentration (vol%)	5-10	5-15
C_2H_4 concentration (vol%)	0-1	0-2
Ar concentration (vol%)		5-15
CH_4 concentration (vol%)		1-60
Temperature (℃)	220-275	220-275
Pressure (MPa)	1-3	1-2.2
GHSV (h^{-1})	2000-4500	2000-4000
Pressure drop (kPa)	40-200	
C_2H_4 conversion (%)	20-65	7-15
Selectivity (%)	80	80-90

Future developments contemplate alternative routes such as electrochemical oxidation, enzymatic oxidation and thallium catalysed oxidation, but these are far from being applied in the commercial context. There are also developments in producing ethylene glycol via alternative raw materials: carbon dioxide and formaldehyde [6].

2.2.2 Reactions

Three competing reactions (eq. 2.1-2.3 [13]) are predominant during the direct-oxidation processes: partial oxidation of ethylene (eq. 2.1), total oxidation (combustion) of ethylene (eq. 2.2) and decomposition of ethylene oxide (eq. 2.3) to the combustion products, carbon dioxide and water [6, 8, 10]. The latter may be considered negligible for low temperatures, [6] (which is not the case for industrial processes).

$$C_2H_4 + \frac{1}{2}O_2 \rightarrow C_2H_4O \qquad \Delta H^\circ = -105 \text{ kJ kmol}^{-1} \tag{2.1}$$

$$C_2H_4 + 3O_2 \rightarrow 2CO_2 + 2H_2O \qquad \Delta H^\circ = -1323 \text{ kJ kmol}^{-1} \tag{2.2}$$

$$C_2H_4O + \frac{5}{2}O_2 \rightarrow 2CO_2 + 2H_2O \qquad \Delta H^\circ = -1218 \text{ kJ kmol}^{-1} \tag{2.3}$$

Thermodynamically, total combustion is markedly more favourable; ethylene oxide is only the kinetic product [2].

Experimental data points to the ethylene oxide decomposition pathway only occurring in the absence of gaseous oxygen and at high temperature [14]. This is not a relevant condition for steady state kinetics but suggests that adsorbed oxygen promotes carbon dioxide formation [15]. Nonetheless, some authors [16] still state that ethylene combustion occurs preferentially via ethylene oxide and have supporting Density Functional Theory (DFT) calculations [17].

One unusual property displayed by this process is the reverse isotope effect, i.e. higher rates displayed for ethylene oxide formation using deuterated ethylene [2, 11, 18–20]. In contrast, the conventional isotope effect is shown by the the combustion reaction. Furthermore, geometric isomer studies have noted that there is a necessary rotation of the C-C bond for the selective reaction to occur [18].

Experimental studies [19, 21] have revealed that there is a change in the apparent order of the reactants at different partial pressures. For low ethylene partial pressure (at constant remaining conditions) the order reported is 1, while at high partial pressures it changes to a small positive number [2] (e.g. 0.71 [16, 18]). The same applies to oxygen [19, 21].

The presence of no negative apparent orders led authors [19, 21] to believe there was no competition between oxygen and ethylene. This was later discredited, since both species adsorb in the same active sites, (corroborated in Stegelmann et al's model [2]). Stegelmann et al.'s [2] model predicted the oxygen reaction order as 1.5 at low ethylene pressures decreasing to -0.5 at high pressures and the ethylene reaction order as 1 at low oxygen pressures decreasing to -2 at high pressures.

2.2.3 Reactor

High reaction heats account for the need for efficient means of heat transfer, at times considered the determining process in the reaction kinetics [2, 7]. Multitubular arrangements with coolant circulation through the shell-side are therefore employed for this purpose. The inlet is fed in gas-phase, with the alternative of air and oxygen-based processes [6, 8]. Residence time in the reactor usually is registered under the 1 second order of magnitude, with reaction temperatures and pressures in the range of 230-290 ℃ and 1-3 MPa, respectively [2, 6, 8].

The tube bundles consists of thousand of tubes which are 6-13 meters long and have 20-40 mm internal diameter (to ensure proper heat transfer). The catalyst is located inside the tubes [6].

Although ethylene oxide is not corrosive, mild steels (e.g. stainless steel) are used for the reactor, since the process may reach relatively high temperatures. Additionally, this prevents rust, which promotes isomerisation, polymer formation, and increases the viscosity [6, 16].

Early processes required 1 to 3 reactors, with very low conversions (around 40%) in the first reactor to confer acceptable selectivity [2, 8]. Modern designs use pure oxygen in a single-stage apparatus [8]. Recycling of recovered reactants is standard to ensure acceptable process yields and to increase profit. The reactors' feed has a high ethylene content (25-30%), and the oxygen content is subject to the reaction mixture remaining above the upper flammability limit [2, 8, 16], rendering the surface reaction step more relevant (low oxygen coverage promotes oxygen dissociation) [18]. This new configuration achieves overall higher yields in smaller equipment [8].

Unfortunately, attempts of using fluidized bed in a commercial setting have failed so far, due to sintering and strong abrasion, combined with low selectivity [6]. Considering the reactions have strong exothermic effects, this would be the preferable arrangement if it were possible.

2.2.4 Catalyst, promoters and modifiers

The catalyst usually elected by the industry is silver finely dispersed (7-20%) on a porous matrix (pore diameter within 0.5 to 50 µm) of α-alumina (higher than 99% purity) [2, 6, 16, 18]. It has low specific surface area (around 2 m^2 g^{-1}) [2, 6, 8] which confers less activity but higher selectivity, and slows down diffusion to inhibit further oxidation. Hydroxyl groups must be removed from the support through silane treatment to avoid promoting catalytic isomerisation to acetaldehyde.

The catalyst is used in the form of spheres or rings with diameters that range from 3 to 8 mm. The lower bound is fixed by pressure drop while the upper is stipulated by gas mixing. Low-selectivity catalysts usually operate at lower temperatures (200 ℃) since they are very active. High-selectivity catalysts operate around 240 ℃. Other supports such as γ-alumina, SiO_2, MgO, SiC, TiO_2, Y_2O_3, ZrO_2 have been tested [6].

The quantity of active sites (site density), their corresponding dispersion, and accessibility are parameters which determine the catalyst's activity. To produce higher activity catalysts the quality of the catalyst's preparation and activation must be monitored. The activity among batches may be similar, but is rarely identical.

Promoting the catalyst with alkali salts has become widespread [6, 8, 11], usually in the range of 100-500 mg kg^{-1}. It is noteworthy that residual acidity in the support is highly unfavourable for the process selectivity, since it promotes the combustion reaction [8]; hence the need for the previously mentioned alkali salts, (which reduce density of acid sites). These also enhance oxygen dissociation [8].

Cesium or a combination of rhenium, sulfur, tungsten and molybdenum can significantly affect selectivity, which may thus reach the 80% threshold. Cesium is said to create a silver film that decreases the support's importance [22–24], and increases the selectivity. Nevertheless, their use has been reported to decrease catalyst life [6, 16].

The use of chlorine-based modifiers [6, 8, 10, 11, 14–16, 25] is also of the utmost importance. These compounds (e.g. 1,2-dichloroethane, vinyl chloride, and ethyl chloride) are added to the reactor's feed to provide a higher selectivity for the epoxidation reaction, while simultaneously decreasing the rate of both epoxidation and combustion reactions [8, 10, 16].

The method of how these moderators work is still uncertain, although their positive effects are clear throughout literature [10]. There are two major (non-exclusive) theories of how these modifiers promote the selectivity. The first consists of enhancing the electrophilic effect of silver [8, 15, 18]. The electrophilic effect can be considered as the modifier, acting as a surrogate for subsurface oxygen, since chlorine atoms draw electron density from the metal surface, or as the rehybridization of valence band orbitals [15]. This is supported by the increase in apparent heat of adsorption reported by ethylene at higher modifier concentrations [16].

The second theory considers that chlorine acts as a suppressor [8, 15], occupying vacant sites that neighbor the intermediates and preventing total oxidation to occur. The latter site-blocking theory is corroborated by the fact that at high concentrations chlorine becomes an inhibitor, poisoning the catalyst and preventing oxygen chemisorption [15, 26].

Other authors [6] state the modifiers ensure an even coverage.

2.2.5 Deactivation

Various processes may lead to the deactivation of the Ag-based catalysts, the most significant being sintering, poisoning (e.g. sulfur from ethylene) and wearing [25, 27]. Processes such as abrasion and dust formation are adverse for the stability of the catalyst [6].

The commonly employed solution to counter-effect the loss of activity due to sintering is to increase the reaction temperature [10, 27]. In practice, plants gradually increase feed or coolant temperature to compensate for this aging effect of the catalyst, since the silver surface decreases to 50% its initial value in two years [6]. However, there is an upper limit for the feed temperature (flammability limits): when this condition is reached, the catalyst must be replaced. The frequency of catalyst replacement is dependent on the type of catalyst, the rate at which the process is run, and the purity of the feed. In general, highly selective catalysts require to be traded every 2 years, while lower selectivity catalysts last for 5 years [6].

Regeneration of the catalyst has been explored with no success, using a methanolic solution of cesium salts being the most promising lead. Recovery of silver, at high purity, from used catalysts is achievable and industrially applied. The same cannot be stated for the support [6].

It is relevant that the increase of reaction temperature also has an adverse effect on the catalyst, since it promotes sintering[1] [10, 27]. A process which is equally relevant is coking (specific type of poisoning) which occurs on the catalyst surface. For oxygen rich feeds, this deactivation process is not an issue since the catalyst displays a "self-cleaning" behaviour by reducing the deposited coke to CO_2 [27].

Boskovic et al. [27] has recently parameterised a general power-law expression (gPLE) that translates

[1] Sintering is the process at which heated dispersed metal particles are conduced to migrate into a cluster in order to minimize their surface energy.

the loss of activity with time. This equation assumes that the deactivation never drops to 0, but has a constant lower bound, which is consistent with industry. The determined equation was in good agreement with experimental data.

2.2.6 Mechanism

Although thoroughly investigated, the scientific community has not reached a consensus for the mechanism that entails ethylene partial oxidation [2, 12, 28]. Much of the uncertainty related to the intricacies of this process originates from the difficulty in tracking the intermediates. Since this reaction is very rapid, the intermediates are short-lived. The predominant methods used are TPD[2], HREELS[3] and manipulation of adsorbates, at low temperature, using voltage pulses [18].

Early mechanisms established molecular oxygen as the only active oxygen species [6, 29]. This implied that there was a 6/7 upper bound for the epoxidation selectivity. It was stipulated that combustion displayed an ensemble effect, which dictated that this reaction required a larger amount of sites to occur [16]. At the time, all experimental data corroborated this mechanism. More recently, promoted catalysts have reached selectivies as high as 90%, disproving this theory [6, 16].

Experiments with the decomposition of N_2O show that it can partially oxidize ethylene (with very low selectivity), proving that the active species is in fact atomic oxygen. Additional investigation with norbene and styrene have supported atomic oxygen as the active species [6, 18].

Kung [11] proposed a mechanism in 1992, which combined adsorbed ethylene and oxygen as active species. The surface reaction occurred after the migration of the adsorbed oxygen. It further propagated by migration of other oxygen atoms to react with the adsorbed species. The premise was that for epoxidation this step occurred only once, while the remaining unselective products required subsequently oxidation.

Schouten, Borman and Westerterp [12, 30, 31] collected data from experiments in an internal recycle reactor to determine rates for the intervening reactions. Temperature and concentrations gradients were therefore avoided, ensuring the absence of temperature and mass transfer limitations. Inhibiting effects of the product (ethylene oxide) and nitrogen were studied, and the carbon dioxide concentration was monitored at the outlet, using IR. The experiment yielded batches of catalyst with varying activity, owed to sintering, poisoning and changes in oxidation state. The authors assure this would not change the determined kinetics parameters, only the deactivation.

Three rate expression (LHHW) were tested (parameters estimated), each considering a different mechanism. The oxygen active species varied between mechanisms: gaseous, molecularly adsorbed, and dissociatively adsorbed oxygen. The third was found to model the results most precisely. This third mechanism produced distinct rates for TOX and POX, by assuming these occur on different active sites. It also enabled to establish the deactivation of each reaction independently, although they were found to be nearly identical. However, this model's applicability was limited to an operating range, since it reported different adsorption constants for the same species in distinct reaction rates. Furthermore, the expression used for the ethylene oxide combustion was simply a gPLE deduced from experiments in the absence of ethylene (its extent negligible in the operating conditions).

Authors Grant and Lambert [32] originally proposed the presence of two types of adsorbed oxygen: a low-valence charge "selective" oxygen and a high-valence charge oxygen (which took part in hydrogen abstraction) [33].

Reports of the existence of three types of oxygen [2, 8, 16, 32, 34–36]: adsorbed atomic oxygen, subsurface atomic oxygen and molecular oxygen, are fairly universal. The subsurface oxygen is usually described as adsorbed oxygen that has migrated into lattice positions. The same phenomenon is reported for other

[2] Temperature Programmed Desorption
[3] High-Resolution Electron Energy Loss Spectroscopy

transition metals such as rhodium and palladium [8].

Recent developments in this field has evolved to believe that the subsurface oxygen is an active species in the process [6, 8, 32]. The electronic effect is considered to be its contribution. By removing electron density from the silver particles which are bonded to the atomic oxygen, it provides an electrophilic character to the metal-adsorbate compound. This promotes the interaction of the adsorbed oxygen with the ethylene C-C bond by drawing electron density to the catalyst's surface [6, 8, 37, 38].

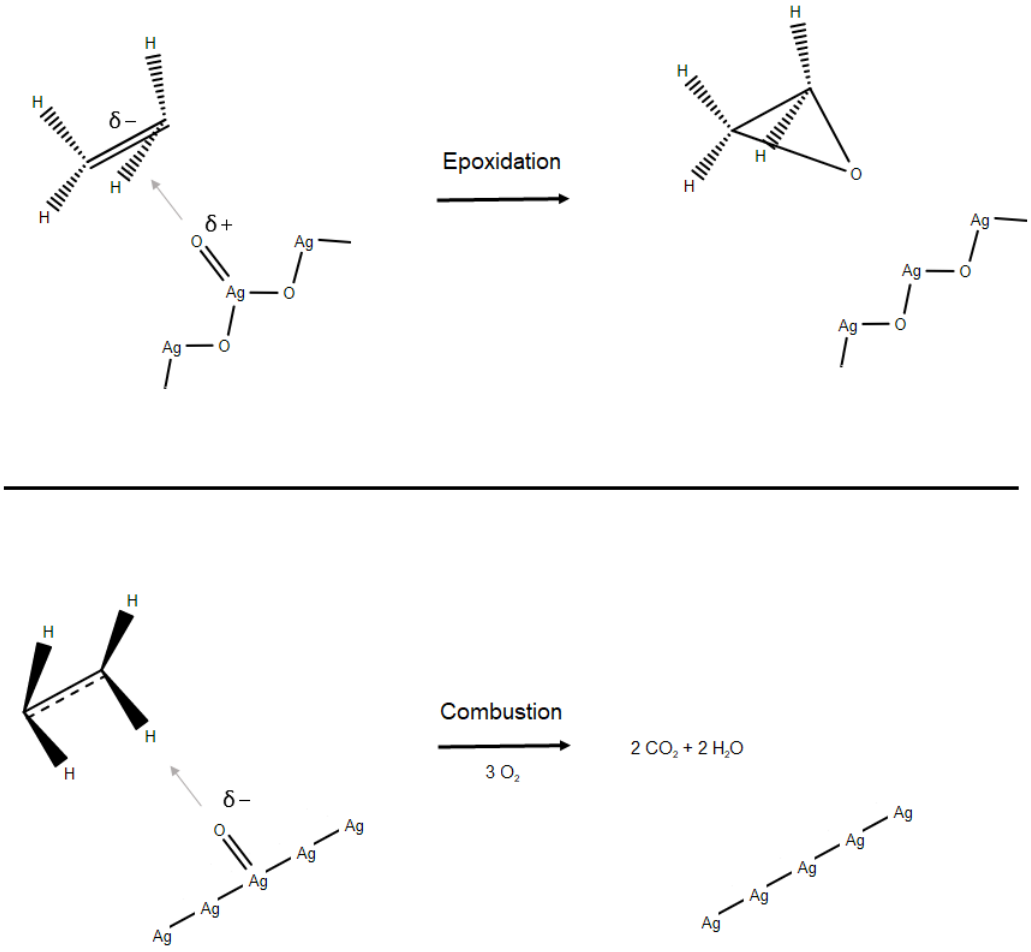

Figure 2.2: Subsurface oxygen promotion of epoxidation scheme[4]

Some authors [2, 15, 39] defend that the subsurface oxygen uptake is too slow to be relevant for steady-state kinetics. The diffusion is only fast for oxidized surfaces. Rocha et al. [2, 15, 39] additionally conclude that the subsurface oxygen must then only act as and oxygen reservoir, providing it with a crucial role in transient kinetics.

Waugh an Hague's [40] investigation on kinetic parameters provided additional insight on the mechanism. By observing that both epoxidation and combustion have similar activation energies, it is considered that a possible common intermediate to both reactions may be present in one of the rate-determining steps [2, 16, 24, 26, 40]. They also enlighten on the role of the cesium promoter, which inhibits the formation of the unselective silver-oxygen bonds.

Linic and Barteau [18] combined DFT calculations and HREELS experiments to prove the existence of

[4]Mechanism by Ullmann's Encyclopedia of Industrial Chemistry [6].

an oxametallacycle intermediate, using the reversibility of the reaction. Its vibrational presence in the infrared spectrophotometer had been previously recorded by Force and Bell [41]. This has been considered to be the common intermediate previously postulated.

The oxametallacycle is the most thermodynamically stable and kinetically accessible intermediate, which makes it a prime example of the Sabatier principle [2, 39, 42]. The predominate belief is that the oxametallacycle intermediate forms ethylene oxide or acetaldehyde. The latter is then readily combusted, generating the unselective pathway [42, 43].

Although some authors report otherwise [44], the general agreement is that ethylene adsorbs. Yet, some mechanisms do not have adsorbed ethylene participating in the reaction, conducing to its inhibiting nature at high partial pressures (site-blocking) [43]. However, it is thought that ethylene molecules are in continuous motion, adsorbing and desorbing rapidly [18].

Ethylene oxide has been reported to adsorb on oxygen-free and covered silver surfaces [45].

Several reports of the products' effect in the reaction scheme are contradictory. Metcalf and Harriott [21] consider water to inhibit both TOX and POX equally, while Liu et al. [46] believe it inhibits epoxidation and promotes combustion, decreasing the selectivity. The effect of the presence of ethylene oxide is more congruent, being widely stated that this species inhibits both TOX and POX [47, 48]. Carbon dioxide is said to inhibit combustion more strongly than increasing the EO selectivity [49, 50].

Generally, the rate-determining step under industrial conditions has been set as the dissociative chemisorption of oxygen [8, 18], although the same may not be applicable in other temperature and pressure ranges. In contrast, Grant and Lambert [32] reported the surface reaction as the rate-limiting step.

The dissociation of oxygen occurs in stepped sites since the activation energy is much lower (-15 kcal mol^{-1}) [18]. However, this barrier is coverage-dependent and will be decrease at lower coverages. Thus, low oxygen feeds promote the reaction, while simultaneously help ensure reaction safety (explosion limits).

Stegelmann et al. [2] have created a revolutionary microkinetic model for unpromoted silver with parameters obtained from transient surface science experiments in UHV and steady-state kinetics on single crystals. It reports the presence of two types of active sites: metallic silver sites and surface oxide sites (assuming that for every former, the latter are generated). Although this has not been proven, the authors suggest it is not of relevance to the overall scheme. It further describes the adsorption of oxygen from an oxide layer, which results in surface reconstruction: these events are corroborated by DFT and ab initio calculations and laboratory experiments [2].

Stegelmann et al.'s model is consistent with oxygen adsorbing more strongly on pre-oxidized surfaces [2, 12, 39, 44, 51, 52]. The limitation of the model is the under-prediction of activity below the oxygen partial pressure of 10 kPa [2]. This is, however, not an issue under industrial conditions. A poor fit of the oxygen concentration evolution with experimental data was also noted. This was accredited to background reactions involving oxygen [2].

Product inhibition was neglected in Stegelmann et al.'s model since only initial rates were considered [2]. Future analyses should include this variable. The model further shows that the size of the catalyst is of no relevance (if density of sites is changed accordingly) to determined rates within industrial reactors [2], accounting for its wide applicability. This mechanism was further reviewed in a subsequent article [39], where the transient kinetics were explored by adding two additional steps (using the subsurface oxygen reservoir theory).

Partopour and Dixon [43] have simulated the microkinetics proposed by Stegelmann et al. [2] using CatalyticFoam. The simulation ran under industrial conditions and the differences between using a lumped[5] and extended model were explored. The lumped model was found to be satisfactory during isothermal analysis, whilst thermal predictions were more prone to error over spatial coordinates (the length of the reactor). This led to the conclusion that the lumped model would be valid for short-length reactors. The major discrepancy

[5] The lumped model was developed using the quasi-equilibrium assumption to generate a LHHW-type rate law.

arose from the presence of radial profiles, which were not adequately described through the lumped model [43].

2.2.7 Modelling and optimisation

The optimisation and control of the selectivity in the ethylene epoxidation is of extreme importance since the loss of selectivity indicates combustion occurs at a higher extent. This triggers a larger heat release (combustion is more exothermic), and may lead to reaction runaway [7, 12]. It has long been stated that 1% increase in the selectivity would result in a profit increase of several millions every year [53]. This furthers the cause of optimisation as a driving force for safer and more profitable processes.

The main objective is to build a universal model (applicable in a large range of conditions) to better understand the activity and selectivity of the process [2]. Models with different degrees of detail may be developed; whether radial temperature and concentration profiles are considered, or division between solid and fluid phase and axial dispersion are relevant [10, 25, 54]. Nonetheless, it is common procedure to couple diffusion effects with parameter determination, making the two-dimensional heterogeneous model obsolete [25].

There have been recent attempts to tackle the present goal [7, 25], however the optimisation of an industrial ethylene oxide reactor has often been simplified. The latter is explained by the computational effort required to simultaneously simulate all occurring phenomena being too steep. Thus, it is standard practice to use lumped models such as explained by Partopour and Dixon [43], experimentally parameterised Langmuir–Hinshelwood rate-expressions [28, 30, 31, 55–58], or experimentally obtained power-laws that describe the behaviour of the reaction for a given range [7]. Furthermore, it is noteworthy that kinetic parameters estimation is not a trivial task, since the rate dependence of reactors is non-linear and software tend to find local minima [25] without the correct initialization.

Although Zhou and Yuan [25] simplified the kinetics, their modelling and optimisation method is still very relevant, since they considered two very important industrial occurrences: deactivation and promotion. Using a one-dimensional model and the Ergun expression for pressure drop, a dynamic optimisation was performed to optimise modifier concentration in the feed and bed temperature. All variables were not optimised at once, since it is infeasible to do so. Additionally, it has been noted that the improvement provided by changing all variables simultaneously is not significant compared to the optimal solution of one variable, with the remaining variables kept constant at adequate values.

The objective of Zhou and Yuan's optimisation was to maximise profit while keeping productivity constant so that operations downstream ran smoothly. Thus, the underlining objective was to maximize the selectivity and to minimize feed consumption. A time-horizon of 40 months yielded a comparison of the deactivation predictions for differing deactivation energies. Nevertheless, the analysis would have been improved with the presence of real deactivation data. Moreover, the results indicated that the optimal addition of EDC was strongly dependent on the thermal stability of the catalyst and the reaction rate, and not as impacted by the operating conditions [25].

Aryana et al. [7], similarly to Zhou and Yuan [25], used a lumped model and considered the important modifiers and deactivation effect. A one dimensional model was developed (no radial profiles considered) and optimisation was performed to the variables that were deemed preferable through the sensitivity analysis. External parameters were used, while the simulation was compared to industrial data, accounting for the model's validation. The deactivation expression adopted was the recent gPLE developed by Boskovic et al. [27].

The manipulated variables used in Aryana et al.'s study were the EDC content inserted in the feed, feed concentrations and the coolant temperature. The dynamic optimisation enabled a gradual increase of bed temperature (via oil temperature) to compensate for activity losses. As a second goal, a smooth transition from a stipulated low-production to high-production was optimised for a 2-hour period. The main conclusion

of this article was the inhibition caused by the presence of ethylene oxide in the feed [7].

Luo et al. [10] developed a hybrid model using Support Vector Regression (SVR), which uses historical plant data of reaction kinetics and deactivation, along with the process knowledge tool, to predict outlet composition, conversion, and selectivity based on inlet conditions (composition, temperature and pressure). The reactor model adopted was homogeneous, since the pore diffusion limitations have been incorporated in the kinetics. Axial dispersion was neglected due to thin tubes [10]. Zhou and Yuan's [25] model was adjusted.

According to Luo et al. [10], the model could be adapted for other plants, with the corresponding input of 2 years of monthly operating data. The model is also more robust when a wide range of plant capacities are covered; and stages of catalyst life, likewise.

Gan et al.'s [59] deactivation kinetics were used to develop the hybrid model, along with a LHHW-type expression for the rate of reactions (including moderator effects). The novelty added by this deactivation expression was the fixed form which has been converted to a dynamic expression using SVR's prior knowledge concept [10].

Luo et al.'s [10] model was validated by comparison to an ethylene oxide reactor in a petrochemical plant in China. The results showed that the deactivation rate prediction through SVR are appreciably more accurate than the conventional methods (less than 6% deviation).

3. Materials and Methods

To carry out the objective of this work it was necessary to benefit from a modelling tool capable of address the complexities of the process in question, which should, in the very least, include the option of a multitubular catalytic fixed bed reactor and a coolant. The general Process Modelling System (gPROMS) platform developed by Process Systems Enterprise (PSE) was chosen. As an equation-oriented software, it solves simultaneously the set of the equations presented in the model, contrasting with sequential solvers.

gPROMS ProcessBuilder holds the various instruments needed for this work: parameter estimation, model validation, global system analysis (GSA), and most consequential, an Advanced Model Library for Fixed-Bed Catalytic Reactors with custom modelling of kinetic reactions.

The advantage of gPROMS sets on its flexibility: the custom modelling functionality allows for the development of any conceivable model. Furthermore, the already defined models are easily adapted to the users needs and offer a wide range of functionalities not supplied by competing software.

gPROMS ProcessBuilder versions 1.3.1 and 1.4.0 were used.

3.1 AML:FBCR Library

The Advanced Model Library for Fixed-Bed Catalytic Reactors (AML:FBCR) was used to model the catalytic section, inert section, and the shell-side (cooling) of the reactor. It has a topology environment, where models can be selected and arranged into a flowsheet. High-fidelity catalytic models are provided, with adjustable features.

This library has two main branches: the catalyst bed and the catalyst pellet. The pellet branch offers the choice of distributed or lumped pellet models. The catalyst bed may be modelled as 1-dimensional reactor (axial distribution) or 2-dimensional (axial and radial distribution).

The models used in this work will be discussed briefly.

3.1.1 Lumped and Distributed Pellet Model

The lumped pellet model is the designation given to the pseudo-homogeneous model which considers internal mass or heat transfer limitations to be calculated by the effectiveness factor. The use of the lumped pellet is a simplification which should be used carefully, since its application is limited. Mostly it is used as a tool to identify possible internal heat and mass transfer limitations by comparison of the more exact distributed pellet model.

The distributed pellet, considers the diffusion of the species in the pellet. Although this approach is more accurate, the use of the lumped pellet will suffice for reactions which are rate-limited, yielding virtually identical results.

3.1.2 Fixed-Bed Section Model

The 1D fixed bed reactor model considers only the axial dimension along the bed. This simplification is widely applicable for reactors which have a large length/diameter ratio (which is standard in reactor design) [60]. When this occurs, the radial effects are insignificant. A technique used to validate this assumption is to compare temperature and composition profiles along the reactor using 1 or 2-dimensional reactors model and verify if there are accentuated deviation between the two.

3.1.3 Cooling System

Various pre-defined models for reactor cooling are offered by gPROMS ProcessBuilder. The following models are provided: boiling water cooling section, cooling compartment, cooling jacket, fired heater, fixed coolant (one or two dimensional) and pool boiling coolant.

The choice of model depends on several factors: the amount of information compiled about the performance and size of the coolant, the degree of accuracy needed, and the assumptions considered.

In this work, the fixed coolant was found adequate to simulate the cooling effect seen in the industry.

3.2 gML Basics Library

Other pre-defined models were used: source material and sink material. These are a part of the standard gML Basics library and enable the user to define a feed (pressure, temperature and flows) and the number and placement of the process' outlets (material sinks).

3.3 Multiflash

Multiflash (version 6.1), by Infochem/KBC, was used as the physical properties software. It is available as a Foreign Object for physical properties in gPROMS.

Equation of State (EOS) methods were used to obtain component's thermodynamic properties. Redlich-Kwong-Soave cubic EOS was selected since it is accurate enough to predict the properties of the reacting mixture at typical reaction conditions.

4. EO Reactor Models

The detailed modelling of a reactor involves compiling numerous phenomena to obtain a comprehensive model that will incorporate micro and macro scale effects. For this purpose, microkinetics were explored and related to external parameters (temperature, pressure, feed conditions, etc.) for a stronger understanding of the reactor's inner performance. The decision on which reactor flow model to apply is dependent on the reaction's nature, enthalpy and operating conditions, as well as the reactor's relative dimensions (length/height ratio).

Chapter Materials and Methods discussed the different options supplied by gPROMS to create models. In this chapter, the customised models added to the software, as well as the most relevant changes to the existing models are detailed.

4.1 Detailed Reaction Kinetics

Although the gPROMS reactors are coded to allow for user-defined kinetics, the template is designed for power-law or LHHW-type rate expressions. For this reason, a custom model (*kinetics_in_1D_bed_Stegelmann_microkinetics*) was created in order to enable the simulation of a multi-step reaction.

The reaction scheme presented by Stegelmann et al. [2, 39] was used in this work. As described previously, Stegelmann et al. [2, 39] developed a 17-step scheme for ethylene epoxidation which incorporates the two secondary (undesirable) reactions: ethylene and ethylene oxide combustion. Furthermore, it corroborates the predominate theory of an oxametallacycle intermediate for both selective and unselective reactions.

Table 4.1 shows the reaction steps included in *kinetics_in_1D_bed_Stegelmann_microkinetics*.

* represents the free actives sites available for reaction. The active specie considered in this model is the O*, an adsorbed dissociated oxygen. It acts as a secondary active site to which different species adsorb. Species may be adsorbed on * and O* sites, generating what Stegelmann et al. coined as *surface species*. These adsorbed species, in addition to the gaseous components, are the reactants/products of the reaction steps presented in Table 4.1.

Other advantages comprised by this mechanism are the incorporation of ethylene oxide isomerisation to acetaldehyde and the existence of two paths for obtaining combustion products.

To use the reactions steps in the model, the following rationale was used to describe the rate at which each step i takes place at temperature T (eq. 4.1).

$$r_i^T = k_i^{forw,\,T} \prod_l^{RR} \left(\frac{p_l^a}{P_{ref}} \cdot \theta_l^a \right) - k_i^{rev,\,T} \prod_l^{P} \left(\frac{p_l^b}{P_{ref}} \cdot \theta_l^b \right) \tag{4.1}$$

$$k_i^{j,\,T} = k_{0,\,i}^{j} \cdot e^{-\frac{E_i^j}{RT}} \tag{4.2}$$

Where r_i^T is the overall reaction rate for step i at temperature T, $k_{0,\,i}^{j}$ is the pre-exponential factor in the

Table 4.1: Stegelmann et al.'s Reaction Scheme for ethylene partial oxidation [2]

O_2 (g) + * ⇌ O_2*	Step 1
O_2* + * ⇌ 2 O*	Step 2
O_2 (g) + 2 O* ⇌ 2 O/O*	Step 3
C_2H_4 (g) + O* ⇌ C_2H_4/O*	Step 4
C_2H_4/O* + O/O* ⇌ CH_2CH_2O/O* + O*	Step 5
C_2H_4O (g) + O* ⇌ C_2H_4O/O*	Step 6
CH_2CH_2O/O* ⇌ C_2H_4O/O*	Step 7
CH_2CH_2O/O* ⇌ CH_3CHO/O*	Step 8
CH_3CHO/O* ⇌ CH_3CHO (g) + O*	Step 9
CH_3CHO/O* + 6 O* ⇌ 2 CO_2* + 4 OH* + *	Step 10
C_2H_4 (g) + * ⇌ C_2H_4*	Step 11
C_2H_4/O* + O* ⇌ CH_2CHOH/O* + *	Step 12
CH_2CHOH/O* + O* ⇌ CH_2CHO/O* + OH*	Step 13
CH_2CHO/O* + 5 O* ⇌ 2 CO_2* + 3 OH* + *	Step 14
2 OH* + ⇌ H_2O* + O*	Step 15
CO_2* + ⇌ CO_2 (g) + *	Step 16
H_2O* ⇌ H_2O (g) + *	Step 17

direction j (forward, reverse), $k_i^{j,T}$ is the rate constant, E_i^j is the activation energy, p_l is the partial pressure of component l, P_{ref} is the reference pressure, θ_k is the surface coverage of species k, RR and P represent reactants and products, respectively, and a and b represent the stoichiometric coefficient at which RR and P react/are produced, respectively.

The discretized expressions, which were written in the custom model (*kinetics_in_1D_bed_Stegelmann_microkinetics*), are summarized in Appendix A.

The surface coverage, θ_k, of the surface species k is the fraction of active sites (*) that have been occupied by the given species. As a result, the sum of coverages must be equal to 1 (eq. 4.3).

$$\sum_k \theta_k = 1 \tag{4.3}$$

This expression is included in the model with proper scaling. Depending on the weight given on the accuracy of the free sites, this expression may have identical multiplicators in both sides of the equation. The magnitude of the multiplicator determines the number of significant digits in the free sites.

To determine the coverages, the following mass balance was written:

$$\frac{\partial \theta_k}{\partial t} = \sum_k \left(\beta_1 \cdot r_{k\ is\ produced} - \beta_2 \cdot r_{k\ is\ consumed}\right) \tag{4.4}$$

where β_1 and β_2 are the stoichiometric coefficients of surface species k in the step it was produced and consumed, respectively.

In Appendix A, the rates that influence each coverage are identified. These are the equations that define the dynamics of the model. Additionally, the pre-exponential factors (k_0), activation energies (E) and reference

pressure (P_{ref}) obtained from literature [2] are also listed in Appendix A.

An additional parameter was defined, *Dynamics_Flag*, which enabled the accumulation for dynamic mode and disabled it for steady state. The parameter was set within the process entity, to allow the user to define if the simulation should be dynamic. *Dynamics_Flag* is a binary parameter, applied as a multiplicator to the accumulation term. For steady state simulations, there is no accumulation (*Dynamics_Flag* = 0), which simplifies the model, stipulating equalities between the rates of the steps that produce and consume a surface species (e.g. r_1 and r_2, eq. A.1, Appendix A). This is known as Quasi-Steady-State Assumption (QSSA).

Consequently, the rate of step 11 is 0 at steady state (eq. A.8, Appendix A), which means the forward and reverse reaction must be equal. Therefore, $C_2H_4^*$'s coverage is given by the partial pressure of ethylene.

There is an Arrhenius temperature dependence for the reaction constants (eq. 4.2). Therefore, the rates, and necessarily the surface coverages, are temperature dependent. Furthermore, the rates are a function of the partial pressures at a given point.

The reaction scheme, as explained previously, was written in the gPROMS language in a custom model created from scratch. Parameters which would later be estimated had to be defined as variables and assigned a value within the model.

When using the pre-defined kinetic model (*kinetics_in_1D*), the inputs are the stoichiometry of the reaction, the reaction rate, and the corresponding kinetic parameters. However, for the given work, *kinetics_in_1D* was adapted to call these inputs from the *kinetics_in_1D_bed_Stegelmann_microkinetics* outputs.

kinetics_in_1D_bed_Stegelmann_microkinetics had to be made compatible to the user-defined models, namely by including the array variables *RRate* and *nu*. The former is the rate at which a component is produced in a given reaction, and the latter is the stoichiometry of said reaction in respect to the existing components.

The use of elementary steps eliminates the concept of overall reactions between the gas species. Since mass balances in the catalyst pellet models consider only the gas phase components, reactions for production/consumption of all the gas components were defined independently as the sum of the reaction steps in which they intervene. *nu*'s default value was assigned as 0, and defined as 1 for the component consumed/produced in the "reaction".

$$RRate_{rr} = \phi \cdot \rho_* \cdot \sum_{i}^{\text{Step 17}} (\beta_{i,m} \cdot r_i) \tag{4.5}$$

$RRate_{rr}$ represents the rate of reaction rr, ϕ is the effectiveness factor, ρ_* is the density of active sites (mol kg^{-1}), r_i is the rate of step i and $\beta_{i,m}$ is the stoichiometric coefficient of component m in this reaction. Each reaction rate is associated with only one component, m:

$$nu_{rr,m} = 1 \tag{4.6}$$

The reactions and stoichiometric coefficients considered are in Appendix A.

At each point of the reactor, the overall rates of consumption/production of gaseous components are supplied to the reactor section model (higher level), which passes these details along (and other information, e.g. temperature, pressure) to various lower level reactor models. One of these models performs the reactor's mass balance, simultaneously communicating with the kinetics to provide and receive information necessary to produce solutions.

4.1.1 Model Formulation, Numerical Scaling and Protections

Model formulation is an important topic since this impacts the initialisation of the model and the search for the final solution. Namely, it eliminates very high gradients of certain variables (which hamper the solver's progress) by transforming the variable into its logarithm (and then using the exponent in the equations involving it).

Moreover, the model must secure that it will not fail if a variable becomes 0 in the initialisation. This is of real concern for equations that involve only variables as denominators in a fraction. The strategy adopted in these cases is to add a vestigial quantity to the denominator (10^{-100} or equivalent).

Variable scaling was investigated using different scaling factors. These variables need to be defined in units of measurements that give reasonable order of magnitude for non-zero values. The same principle may be applied to equation scaling.

Another limitation of numerical solvers consist in proceeding its iterations when variables are stuck at their bounds. This is often the reason of many failed simulations, namely for variables that have to be positive. This was the source of initial issues in solving the coverage distribution, since most of them hit the lower bound in initialisation.

One strategy used is loosening the bounds, i.e. setting the lower bound to a very small negative number, in the case of the coverages. This method must be posteriorly validated, by ensuring the variable did not converge to a negative value. In many cases, this technique is sufficient since it enables the solver the flexibility to proceed its calculations. Nonetheless, it was not the best method for the model in question.

The method used consists in applying a small numerical protection to a variable (e.g. to the surface coverages in the rate equations to ensure the reaction rates reach zero before the surface coverage reaches zero). The variable which is stuck at 0 is subtracted by a very small factor ϵ. Thus, the variable will increase in the negligible increment ϵ and cease to be stuck. This approach also requires validation: ϵ must be at least 2 orders of magnitude lower than the variable. Yet, if ϵ is too low, the simulation will most likely fail.

This technique has the constraint of not being easily applied to two variables which are multiplied by each other. In these cases, a signal filter[1] must be added posteriorly.

$$(\theta_k - \epsilon_k) \cdot (\theta_l - \epsilon_l) \cdot \ \mathrm{SGN}\left(\ 1 + \mathrm{SGN}\left[0.5 + \mathrm{SGN}(\theta_k - \epsilon_k)\right] + \mathrm{SGN}\left[0.5 + \mathrm{SGN}(\theta_l - \epsilon_l)\right] \ \right) \tag{4.7}$$

These protections were used and validated for the coverages.

4.1.2 Model Initialisation Procedure

Initialisation procedures (IPs) are used as a method to condition how the gPROMS platform initialises a model. This function becomes essential for complex models, where IPs may lead to quicker initialisations and a greater robustness of the models. The latter ensures that the model will initialise correctly for a wider range of initial conditions and model specifications. For the *kinetics_in_1D_bed_Stegelmann_microkinetics* model, this was an essential issue to be addressed. An adequate initial guess was required due to the degree of complexity of the kinetics.

In the gPROMS software, an initialisation procedure may be included in lower level models, such as the kinetics, by calling these in the high-level models. It may also be ignored for a simulation, if the user chooses to do so.

A possible IP tactic is to create *case* statements within the model. *Cases* are a gPROMS feature which work as a broader form of an *If Cycle*. *Cases* are defined with two or more branches (modes). A set of equations must be defined for each branch. The same variables must be present in the remaining branches.

[1] SGN, signal filter that produces -1 for a negative result, 1 for a positive one, and 0 for zero.

Additionally, the branches must maintain the number of equations. A default branch must be set which will be active in the absence of a contradictory statement.

The use of *cases* is versatile within the platform, being beneficial in schedules and IPs, among others. In an initialisation procedure, the employment of cases is effective. For instance, considering a reactor to be adiabatic at first (to perform the heat balances) and then proceeding to determine the heat transfer in isothermal flow. The initially selected branch would set the heat output to 0. The switch to the complex heat balance may be declared later within the initialisation procedure.

A similar approach was used. A case named *calculation_mode* was defined. For the *normal* mode the equations presented in section A.2, Appendix A were used. The other mode defined that, if in steady state (*dynamic_flag* = 0), the coverages would be set to 10^{-4} and, if in dynamic mode, then $\frac{\partial \theta}{\partial t} = 0$. In steady state, the initialisation gives the coverages an initial value, which is used to calculate the rate of each step. These rates are then used to recalculate the coverages, restarting the cycle. For dynamic simulation, the steady state solution is given as the initial point.

Furthermore, a complementary technique to ease the initialisation was used: a rate factor. The rate factor (f_R) was supplied in the dialogue box of the high-level (reactor) models. It may be interpreted as a measure of activity, since it is employed in the rate of the global reactions (eq. A.14 - A.19, Appendix A). As a default value it is set to 1. A similar parameter was defined for the step reactions (f_s) and included in the rate expressions (Appendix A, section A.1).

In the first steps of the IP both factors begin as 0. This causes the solver to generate a mass balance in the absence of reactions, to obtain a first estimate of what flows through the catalyst bed and exits at the sink material (outlet). Subsequently, f_s is increased to a very low number (10^{-5}), meaning that the calculations associated with each step have been activated, yet the steps have a very low activity (since $f_s \ll 1$), which causes lower rates. The gradual increase in activity is exceptionally useful for identifying runaway reactions. Since f_R is still 0, global reactions are turned off, i.e. there is no change in composition along the bed.

f_s is then reverted to its original value (1), rendering the steps in full activity. Finally, the rate factor is set to (10^{-5}), activating the composition gradients along the bed. The initialisation procedure ends with f_R being reverted to 1.

Once the full solution is obtained using the IP, the solution can be stored in a Saved Variable Set (SVS). The SVS can be used in subsequent simulations as initial guess for all the variables, skipping the IP.

4.2 Industrial Reactor Model

The initial phase of this work consisted in exploring the limitations and potential of the microkinetics proposed by Stegelmann et al. With this goal in mind, a model was set up to perform various sensitivity analysis. The results of this analysis would uncover which parameters to estimate in the final *Parameter Estimation*.

Furthermore, the same arrangement will be utilized in a final stage. That stage aims to explore if additional phenomena could be included in Stegelmann et al.'s [2] model (e.g. moderator effect, deactivation).

Previous works have aimed to simplify kinetics to rate expressions when simulating an EO reactor. Others focused on simulating only the kinetics, without the reactor environment. The simultaneous use of microkinetics and a high-fidelity reactor has the objective of identifying if the increasing complexity of the model is compensated by the increase of accuracy of the predictions.

In the preliminary sensitivity analysis, the use of generic industrial data enabled to determine if the results were within reasonable bounds. The reactor's feed conditions input in the pre-defined gPROMS ProcessBuilder reactor model are reported in Tables 4.2 and 4.3. Additionally, Table 4.4 shows the inserted reactor design specifications.

Table 4.2: Industrial reactor's feed specifications - Part I

Specification		Units
Inlet flow	100	ton h^{-1}
Inlet temperature	220	℃
Pressure	16	kg cm^{-2}

Table 4.3: Industrial reactor's feed specifications - Part II

Component	Feed Composition (%mol)
Nitrogen	2%
Argon	5%
Oxygen	6%
Methane	60%
Ethylene	25%
Carbon dioxide	2%
VCM	4 ppm

Fig. 4.1 shows the gPROMS ProcessBuilder environment developed to make the *Preliminary Analysis* and the *Model Extensions*. The set-up consisted of a simplified assembly of a catalytic industrial reactor. The innovation of this work sets on the application of microkinetics within a predefined reactor model. Two 1D fixed-bed sections models were used for the flowsheeting: a catalyst bed (*Catalyst_1*) and an inert bed (*Inert_1*). Two fixed coolants were also used, one connected to each fixed-bed section.

Table 4.4: Typical industrial reactor's design specifications

	Catalyst Section	Inert Section	Units
Section length	10	1	m
Bed radius	20		mm
Number of tubes	2000		
Catalyst mass per tube	11	-	kg
Bed porosity	-	0.6	
Catalyst pellet shape	Hollow cylinder	-	
Pellet radius	4	-	mm
Pellet length	7	-	mm
Pellet hollow radius	2.75	-	mm
Tube wall thickness	2.5		mm

The KPIs were shown in the topology for a fast output of the most relevant aspects of the simulation.

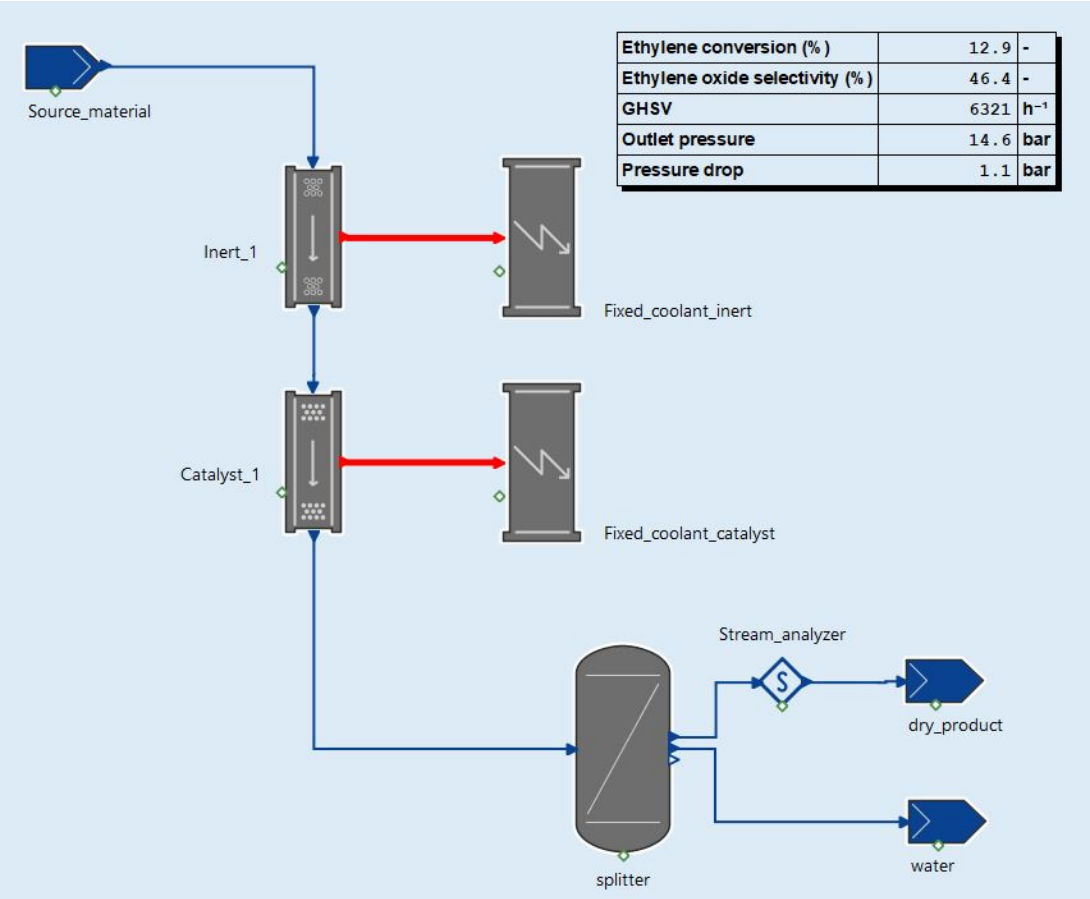

Figure 4.1: Industrial EO reactor set-up in the gPROMS ProcessBuilder

The sizing of the inert and catalyst section also used typical values for EO production. The fixed coolants used a linear temperature profile, with the expected drop in temperature. A splitter unit was added to the flowsheet to remove the water from the reactor's outlet since the literature data available usually refer to a dry product. The stream analyzer detailed extra information of said stream.

The kinetics model used for this analysis was *kinetics_in_1D_bed_Stegelmann_microkinetics*.

4.2.1 Key Performance Indicators

Key Performance Indicators (KPIs) were defined for a better analysis of the performance of the reactor. Namely, ethylene conversion and EO selectivity:

$$\text{Conversion (\%)} = \frac{F_{\text{ethylene, inlet}} - F_{\text{ethylene, outlet}}}{F_{\text{ethylene, inlet}}} \tag{4.8}$$

$$\text{EO Selectivity (\%)} = \frac{F_{\text{EO, outlet}} - F_{\text{EO, inlet}}}{F_{\text{ethylene, inlet}} - F_{\text{ethylene, outlet}}} \tag{4.9}$$

where F represents the molar flow.

Note that the selectivity expression is valid, since the production of ethylene oxide through ethylene epoxidation is 1:1 stoichiometry reaction.

4.2.2 Discretisation Settings for the Distributed Tube Models

The AML:FBCR pre-defined catalyst section models require a selection of the *Numerics* to solve the differential equations. A setting must be selected for each domain. Depending on the complexity of the

selected model the domains may vary and accumulate: axial, radial and radial_pellet.

Since the finite difference discretization is used in the pre-defined reactor models, a distribution of grid points must be selected. The default mode is a uniform grid, which only requires the input of the amount of nodes. The grid will then be uniformly divided, generating a normalized domain (0 to 1).

The default mode is sufficient for many applications. However, for the current situation, an logarithmic transformation was found to be better suited. This places higher density of nodes towards the initial section of the reactor, dispersing the remaining throughout the final section. This type of transformation is helpful when there are significant changes towards the beginning of the domain, while the end remains virtually unchanged.

When ploting the temperature and composition profiles, it was found that the beginning points were the most essential, and therefore had to be modelled with greater precision.

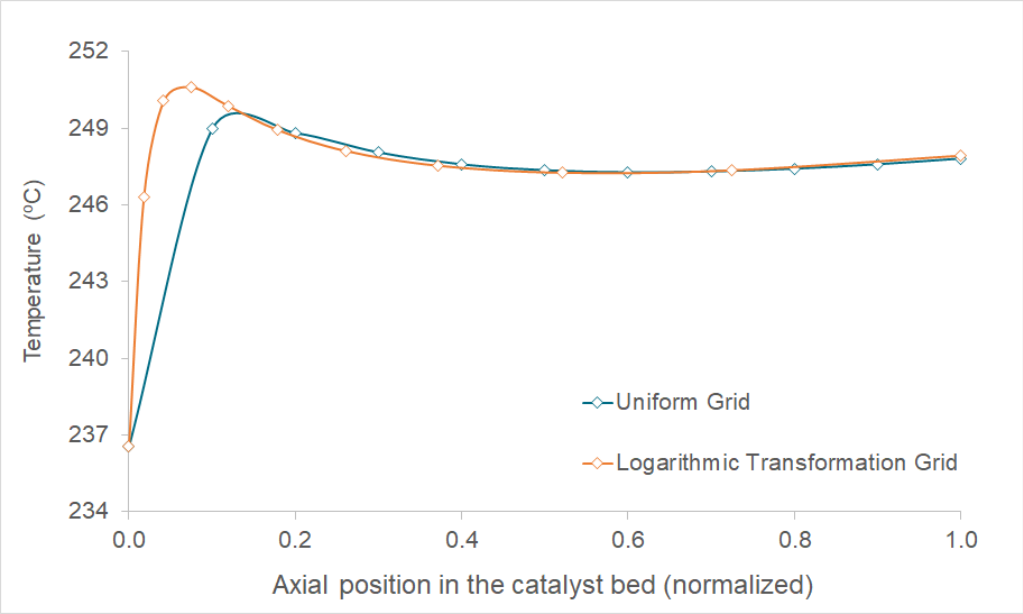

Figure 4.2: Grid domain distribution comparison: Temperature profile

By observing Fig. 4.2 the effects of choosing the correct grid are made evident. With the same amount of points, the quality of the simulation can be severely elevated by considering thoroughly where these nodes are most needed. In the case of Fig. 4.2, the sharp increase in temperature observed in the beginning of the catalyst bed requires special attention.

Modelling the correct profiles (temperature, composition, pressure, etc) impacts the extent to which certain reactions take place. Inherently, this affects the overall output of the process as well.

Table 4.5: Grid domain distribution comparison: KPIs

KPI	Uniform Grid	Logarithmic Transformation Grid
Ethylene Conversion	11.20%	11.04%
EO Selectivity	78.07%	78.14%

Table 4.5 shows the difference between the KPIs predicted by the model simulations using the two different sets of grid points. The difference is not significant, meaning the two are interchangeable for preliminary calculations. Nonetheless, when optimisation of reacting conditions or predicting disturbances is necessary (safety concerns), the difference between the two may be pivotal. It can be the difference between predicting

the outlet product to be within specification or not. Furthermore, depending on the reacting conditions, the influence of the grid chosen may become vital in ensuring the quality of the simulations.

4.3 Laboratory Reactor Model

The data used in the parameter estimation was obtained in a laboratory reactor[2]. Various experiments were carried out with different feeds, and operating temperatures and pressures. The set-up is detailed in the scheme below (Fig. 4.3).

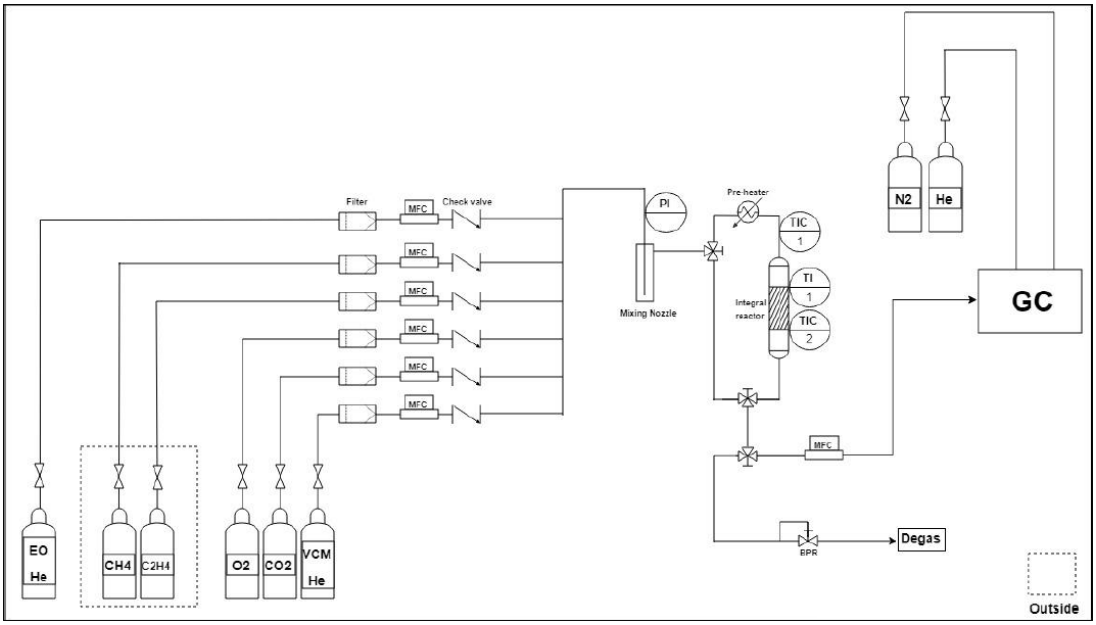

Figure 4.3: Experimental set-up scheme [61]

These experimental laboratory trials have previously been used and described in a greater extent in Sarrafi's thesis [61].

The experiments had six feeds which were monitored using mass flow controllers (MFC) [61]. As may be observed in Fig. 4.3, the outlet compositions were determined by gas chromatography (GC). A MFC was also assembled before the gas chromatography to ensure it was not subjected to high pressures [61].

Impurities in the feeds were removed using filters placed before the Mass Flow Controllers. The various feeds were pre-mixed using a nozzle before being introduced in the reactor. Downstream of the nozzle, there was also-premixing provided by electric heating with the same set-point as the reactor's furnace [61].

The pressure of the reactor was monitored using a pressure transducer placed at the inlet. The target pressure was controlled by the operator that manually changes the back pressure controller [61].

Some experiments were done in the presence of the product in the feed to observe its inhibiting effect. Trials in the presence of the moderator, VCM, were also conducted to measure its effect. The VCM carrier was the inert helium. The other inert used in the reacting mixture was methane.

The reactor itself was scaled-down from industry. In contrast with a plant reactor, there was no fluid used to cool the reactor. It was substituted by a furnace which would heat the miniature reactor to the desired reacting temperature.

The set-point of the furnace (Fig. 4.4) may have not been achieved in the duration of the experiment. Furthermore, the reactions that took place within the reactor generated temperature profiles along the bed, rendering the set-point to be merely a reference value.

[2]Courtesy of Petkim Petrokimya Holding A.Ş.

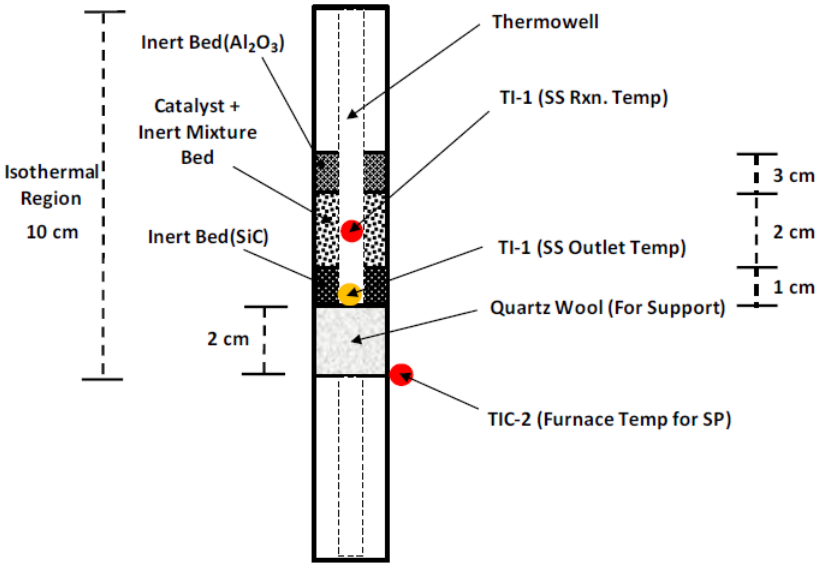

Figure 4.4: Catalyst bed used for the laboratory experiments scheme [61]

Measurement of the temperature along the bed were conducted through thermocouples (TI) as may be observed in Fig. 4.4. TI-1 was placed in the thermowell to fix its location to the center of catalyst until steady state was achieved. Afterwards, the thermocouple slid upwards and downwards to measure bed temperatures at different points [61]. A layer of inert (silicon carbide) was placed at the outlet so that the TI-1 could read temperature in the full extent of the catalyst section [61]. The kinetic model, however, used just the center measurement of the catalyst bed, referred to as *Bed Temperature at 10 mm*.

The lumped pellet model was used for this sequence of parameter estimations, since the size of the catalyst particles ensure no internal heat and mass limitations. The use of the simpler lumped pellet model was preferable for quicker estimations. The experiments were performed at near isothermal conditions, aiming to eliminate temperature gradients in the axial direction of the reactor. This was decisive in obtaining scale-invariant parameters.

Table 4.6: Laboratory reactor's design specifications [61]

	Catalyst Section	Units
Section length	20	mm
Bed radius	4.5	mm
Thermowell radius	1.5	mm
Number of tubes	1	
Catalyst pellet shape	sphere	
Pellet radius	110	µm
Pellet bulk density	3272.6	kg m^{-3}
Pellet heat capacity	913.42	J kg^{-1} K^{-1}
Pellet conductivity	1	W m^{-1} K^{-1}
Pellet porosity	0.4289	
Inert bulk density	2500	kg m^{-3}
Tube wall thickness	2	mm

Table 4.6 shows the specifications used for the pre-defined reactor model within the gPROMS platform.

Table 4.7: Catalyst loadings considered in the parameter estimations [61]

Catalyst Loading	Mass of Catalyst (g)	Experiments	Total Duration (h)
1	0.1	27	131.5
2	0.1	6	36
3	0.1	25	295
4	0.2	51	522
6	0.2	5	81.5
7	0.2	46	685.5

The experiments were divided into different catalyst loading. Catalyst loadings could differ in the amount of mass of catalyst used in the reactor (Table 4.7). Furthermore, each catalyst loading had a different start-of-run activity.

Table 4.8: Description of the experiments considered in the parameter estimations [61]

Experiment	Relative Pressure (kg cm^{-2})	Furnace Setpoint Temperature (℃)	Feed Composition (%mol) (*)					
			C_2H_4	O_2	CO_2	EO	VCM	CH_4
1_1	0	219	22.74	5.77	4.14	0	0	63.08
1_2	0	237	22.74	5.77	4.14	0	0	63.08
1_3	0	255	22.74	5.77	4.14	0	0	63.08
2_1	0	219	66.6	1.81	2.1	0	0	29.49
2_2	0	219	66.6	23.04	6.18	0	0	4.18
2_3	0	219	25.68	1.81	6.18	0	0	66.33
2_4	0	219	8.53	23.04	2.1	0	0	66.33
2_5	0	219	35.18	14.28	4.28	0	0	46.26
2_6	0	255	66.6	1.81	6.18	0	0	25.41
3_1	0	255	29.76	1.81	2.10	0	0	66.33
3_2	0	255	26.95	23.04	6.18	0	0	43.83
3_3	0	255	7.13	23.04	4.39	0	0	65.44
4_1	0	237	22.74	5.77	4.14	0	0	63.08
4_2	0	219	22.74	5.77	4.14	0	0	63.08
4_3	0	250	22.74	5.77	4.14	0	0	63.08
6_1	0	237	22.75	5.77	4.14	0	0	57.34
6_3	0	237	22.75	5.77	0	0	0	57.34
6_5	0	237	22.75	5.77	4.14	0	0	57.34
7_1	0	237	22.75	5.77	4.14	0	0	57.34
7_27	0	237	22.75	5.77	4.14	0	0	57.34
7_46	0	237	22.75	5.77	4.14	0	0	57.34

(*) Balance with Helium

Each catalyst loading was used for multiple experiments. These could vary in the feed composition, the furnace set-point temperature or the pressure. The full list of experiments is listed in Sarrafi's thesis [61]. Table 4.8 shows a subset of experiments used in the *Parameter Estimation* of this work. The experiments were identified using the following nomenclature: *catalyst loading_experiment number*.

The experiments' feed composition was defined for each trial and are shown in Table 4.8. These have been calculated by defining the standard volumetric flow of the various feeds shown in Fig. 4.3. The remaining component in the feed is helium, an inert used to carry small quantities of the EO and VCM.

The experiments measured the temperature along the bed and the outlet dry composition. The latter was obtained by gas chromatography and focused on the five following components: methane, ethylene, oxygen, ethylene oxide and carbon dioxide. The Orsat composition has subsequently been submitted to a data reconciliation process, where the outlet of methane was adjusted to ensure carbon balance. The methane outlet composition measurement was then disregarded for the present parameter estimations. The other four components were used as targets for the parameter estimation.

Although the experiments were considered dynamic when defining a *Performed Experiment* in the gPROMS environment, for the current experiments this definition was rather imprecise. The measurements for each experiment were obtained after the reactor stabilized for the current conditions. Thus, the most accurate approach would be to define these experiments as a series of steady state points spread out in time.

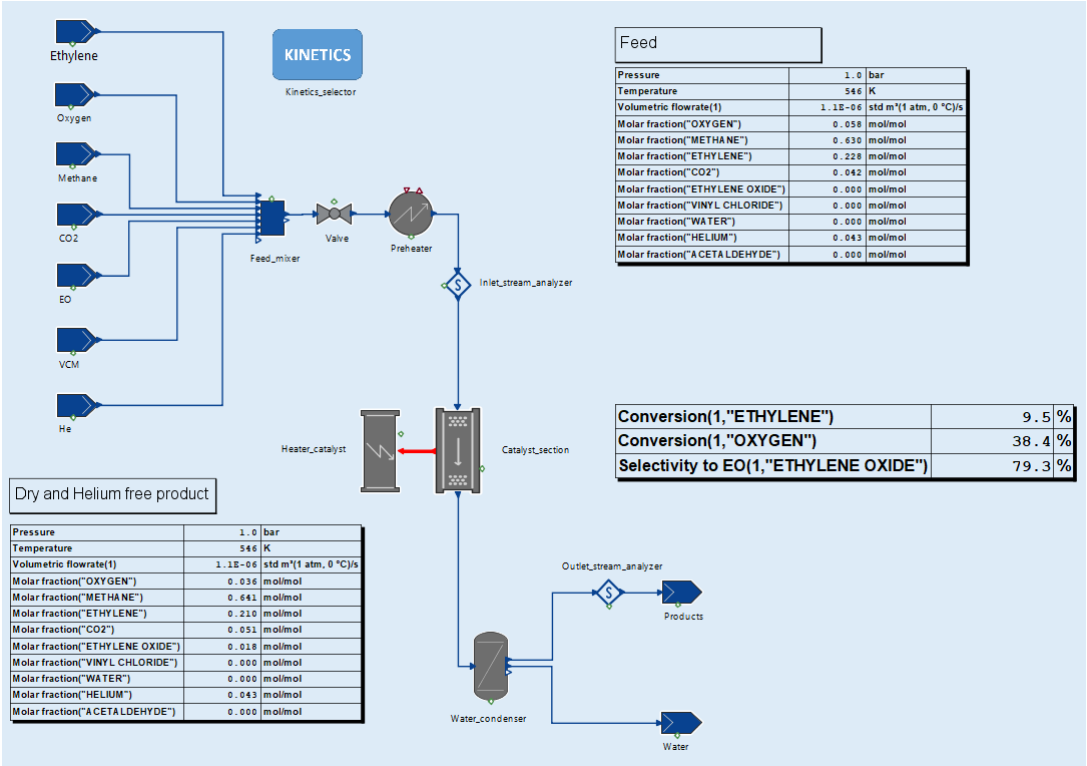

Figure 4.5: Experimental set-up in the gPROMS ProcessBuilder used in the parameter estimation

Fig. 4.5 shows the gPROMS ProcessBuilder flowsheet created to resemble the experiment conditions and set-up. It included various models, namely, the Stegelmann et al.'s [2] microkinetics custom model. The corresponding *Process* was then used for the parameter estimations.

The controls defined in the gPROMS platform were the variables from the originally defined *Process*, which may change for each experiment. The controls used for the Performed Experiments in the gPROMS environment were the following:

(a) Time invariant variables

- Catalyst loading
- Mass of catalyst
- Relative pressure
- EO/He and VCM/He inlet standard volumetric flow

(b) Piecewise constant variables

- Bed temperature at 10 mm
- Remaining components' inlet standard volumetric flow

The measurements used for the Performed Experiments in the gPROMS environment were the following:

(c) Measurements

- Outlet dry composition of ethylene
- Outlet dry composition of oxygen
- Outlet dry composition of EO
- Outlet dry composition of carbon dioxide

The measurements were taken every 0.5 hours. Depending on the quality of the data reconciliation, the outlet dry composition measurements were included in the parameter estimation.

Thus, the objective of the parameter estimations was to meet the target outlet composition, knowing the inlet constraints as well as the temperature at a specific point of the reactor's bed (conditioning the temperature profile).

5. Surface Reaction Microkinetics

The selected reaction scheme was proposed by Stegelmann et al. [2] and has been described in chapter *4. EO Reactor Models*.

The work done with the proposed reaction scheme may be divided into two parts: a sensitivity analysis to the potential and limitations of the model and a parameter estimation. The sensitivity analysis enabled to identify the parameters which are most suitable for the parameter estimation and provided a deeper understanding of the model's operation.

5.1 Preliminary Analysis

The reaction scheme proposed by Stegelmann et al. [2] aims to detail all the steps that the reactants undertake to become the products observed in EO production. However, it must be noted that not all the steps considered within the scheme are elementary. This is the case for steps 10 and 14. Due to absence of additional insight on the workings of the mechanism, the authors considered these simplified steps, which are, therefore, void of scientific veracity.

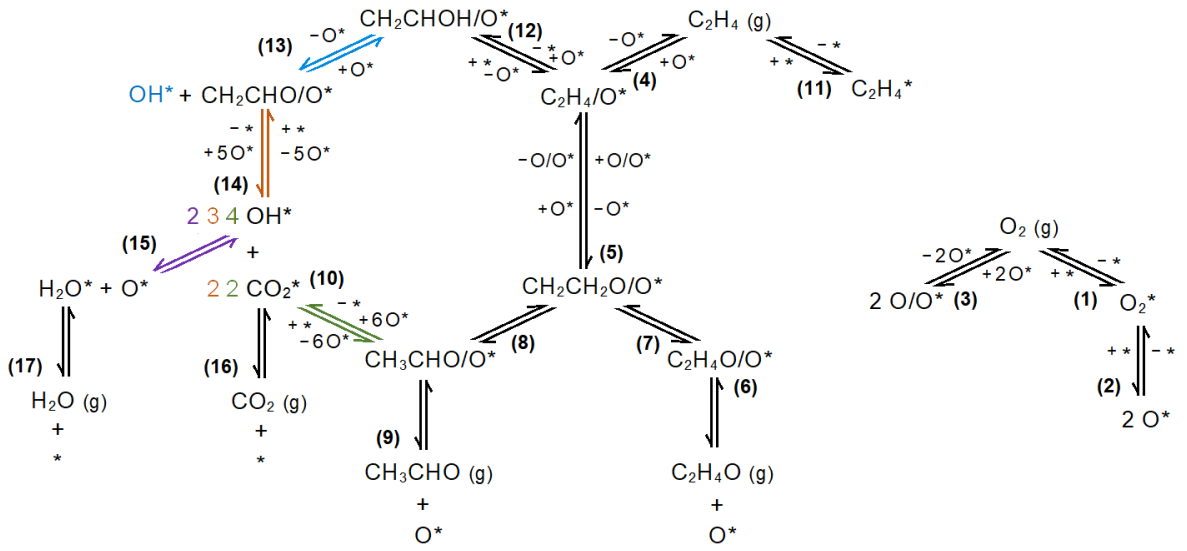

Figure 5.1: Schematic representation of the multi-step mechanism[1]

The product (lower right corner, Fig. 5.1) is consumed through reaction 6. Stegelmann et al. [2] have defined the reaction as an adsorption on oxide sites (O*). Thus, the desorption (i.e. production) of the desired product is the reverse reaction, hence the negative rates observed for this step.

[1] The colours mark the stoichiometry and species that intervene in a step. The numbering is done through brackets and placed next to the forward direction of the corresponding step.

This representation underlines how ethylene oxide production and ethylene oxide combustion may have the same oxametallacycle intermediate (CH_2CH_2O/O^*). As mentioned previously, this common intermediate has been supported by many articles [32, 62–65]. The ratio between the equilibrium constants for steps 7 and 8 would, therefore, be decisive in determining the relevancy of EO combustion.

In addition to ethylene oxide combustion there is a second route to CO_2 and water production (steps 12-14). These steps represent ethylene combustion, which is less meaningful for the current mechanism. Interestingly, authors Partapour and Dixon [43] found these steps insignificant to the extent that they eliminated them completely to create a simplified model. Preliminary simulations in this work reported that less than 25% of the CO_2 produced (using Stegelmann et al.'s [2] literature kinetic parameters) was done so through ethylene combustion.

It is important to emphasise that the O* species is used in an overwhelming amount of steps. Thus, its effect on the overall scheme is harder to grasp using this visual aid. The steps for the formation of this species (from oxygen) are presented separately, since they impact too many other steps, and would render the analysis of the scheme to be extremely complicated.

The isomerisation of the product to acetaldehyde (step 8) was included in the reaction scheme by the authors. The path of the isomerisation uses the oxametallacycle intermediate. Reports of this species in the data have not shown significant levels, rendering this step possibly unnecessary.

This model suggests that, although ethylene adsorbs on the free sites (step 11), this process inhibits the overall desired reaction. In contrast, the adsorption in oxide sites (step 4) is favourable. The arrangement is consistent with literature, since it is known that ethylene absorbs more strongly on silver which has previously been exposed to oxygen [44, 51, 52, 62, 63].

The majority of the model parameters were determined, by the authors [2], through surface science experiments and auxiliary calculations, conferring them physical meaning. However, these experiments were performed on single unpromoted crystals, rending its extrapolation to industrial catalyst dubious. Furthermore, the validation that Stegelmann et al. [2] performed used initial rates which do not account for the product inhibition effect to the extent which it occurs industrially.

Thus, the scope of this work is to provide an enhanced model, adapted to industrial catalysts and conditions.

5.1.1 Rate-Determining Step

In a complex reaction scheme, as the one that is considered throughout this work, the notion of rate-determining step is not absolute. The controlling step can (and does) vary for different ranges of temperature, pressure, etc. In fact, Campbell [66] discussed extensively what he deemed to be the best method to establish a rate-determining step (RDS): defining degrees of rate control. The degrees of rate control are calculated as the change in rate of an elementary step caused by the Arrhenius forward reaction constant of each step (while the rest remain unchanged). Partopour and Dixon [43] used this method to isolate steps 2, 5, 7 and 8 as the rate-limiting steps for the adopted reaction scheme.

In contrast, Stegelmann et al. [2] added step 13 to the lot. These authors identify steps 2 and 5 as the activity defining reactions, whereas steps 7 and 8 define selectivity. Step 5 is considered more significant at higher oxygen content and/or lower temperature.

Moreover, steps 12 to 14 (ethylene combustion) are considered only relevant at low pressures, which are not used for industrial production of ethylene oxide. Thus, Stegelmann et al. [2] concluded that step 2 is the RDS within industrial working conditions.

In this work, a different approach was used to evaluate the importance of the various steps. Namely, identifying which reactions (within the industrial conditions) were fast (close to or in equilibrium) and which were slow.

The approach to equilibrium APE of a given step *s* is calculated using the following expression:

$$\text{APE} = \frac{\text{Forward Rate (s)}}{\text{Reverse Rate (s)}} \tag{5.1}$$

A step which is at equilibrium will have a unity APE. If, however, the ratio is higher than 1, the step proceeds in the forward direction. For ratios lower than 1 the step goes in the reverse direction.

A simulation was run for the the previously described flowsheet (section *4.2. Industrial Reactor Model*) using a lumped pellet model for the catalyst and 1D reactor model. It was found that step 11 is at equilibrium throughout the bed and that steps 10 and 14 are irreversible.

Table 5.1: Approach to equilibrium at the axial normalized position 0.3 of the catalyst bed

Step 1	Step 2	Step 3	Step 4	Step 5	Step 6
1.002	2 x 10^5	1.1	1.000002	1 x 10^9	0.99999

Step 7	Step 8	Step 9	Step 10	Step 11	Step 12
6	1 x 10^{19}	1.000002	Infinity	1	1.0000004

Step 13	Step 14	Step 15	Step 16	Step 17
9 x 10^{13}	Infinity	1.06	1.000006	1.000001

Furthermore, steps 1, 4, 6, 9, 12, 16 and 17 were found to be virtually in equilibrium (APE extremely close to 1). Steps 2, 5, 8 and 13 have exceptionally high APEs which indicates that these reactions are markedly shifted towards the forward direction.

Step 3 does not stray far from equilibrium yet still has a revealing driving force:

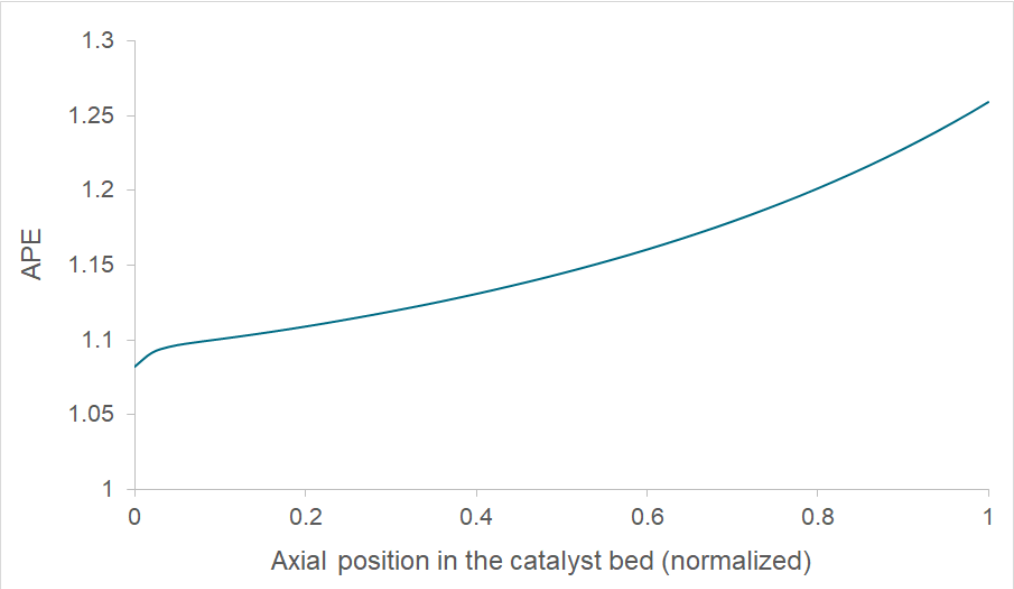

Figure 5.2: Approach to equilibrium along the bed for Step 3

Fig. 5.2 shows an interesting occurrence: the APE increases for step 3 along the catalyst bed. Two distinct effects create theses conditions: a decreasing coverage of O/O* species and a decreasing equilibrium

constant. The decrease in equilibrium constant is consistent with the decreasing temperature profile along the bed. The decreasing of O/O* coverage can be accredited to most of the oxygen (limiting reactant) having already been consumed.

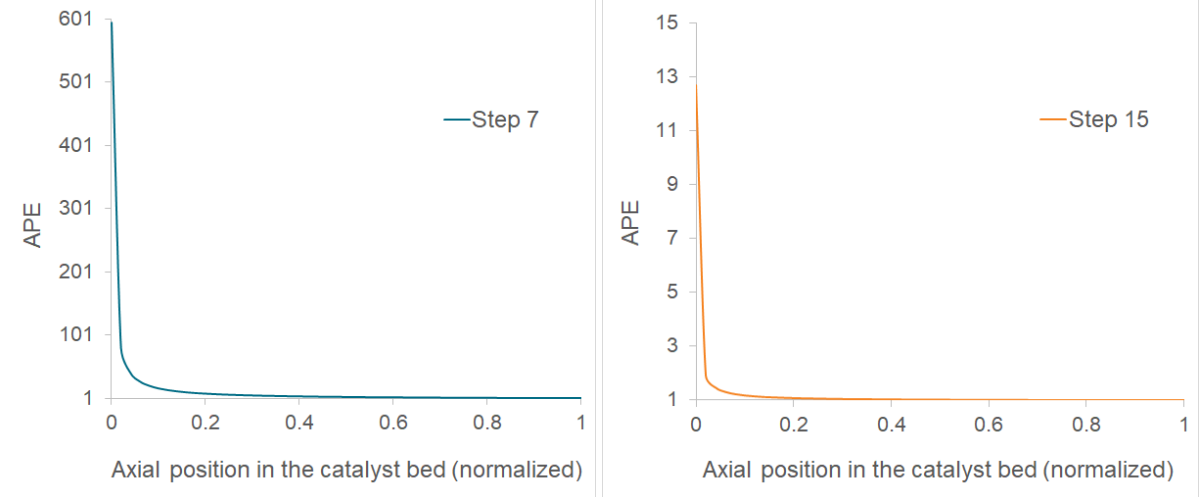

Figure 5.3: Approach to equilibrium along the bed for Steps 7 and 15

Steps 7 and 15 start out nearly irreversible and progressively advance towards equilibrium. The steps begin almost irreversible since the feed to the reactor considered in this simulation contains no water or ethylene oxide. Once these products are produced, even if in vestigial quantities, the driving force to generate more of them decreases markedly. Since carbon dioxide is included in the feed, the same is not reported for this product.

The steps which are shifted towards the products side, yet not completely irreversible, are singled out as the RDS (steps 2, 5, 8 and 13). Steps 7 (most significantly) and 15 also report this shift for the initial length of the reactor. This analysis is compatible with Stegelmann et al.'s [2] as well as Partopour and Dixon's [43] views.

Stegelmann et al. [2] had identified step 7 as a decisive step. This work agrees with this conclusion for the most part. As may be seen in Fig. 5.3, this step is far from equilibrium in the beginning of the reactor and therefore rate-limiting at that point. These are the conditions observed in Stegelmann et al.'s paper, since there is absence of EO and therefore no product inhibition. However, this work focuses further on the posterior occurrence: the quality of the mechanism in the presence of ethylene oxide (and other products). The accurate modelling of the reactions mechanism under these conditions is crucial, since EO concentration in the reaction mixture increases along the reactor.

5.1.2 Validity of Model Parameters

Developing the detailed model required certain assumptions that must be verified when applying it. Firstly, it is relevant to note that the model parameters (Arrhenius pre-exponential factors and activation energies) for the various steps were also taken from different sources, which may lead to some discrepancy.

Furthermore, there are some steps for which the values of rate constant were just selected. This is the case of step 10. Empirical data suggests that this step is irreversible and, therefore, a large pre-exponential factor for this forward constant was selected by Stegelmann et al. [2]: 2 x 10^{20} s^{-1}. However, it is unknown how large this value should really be and if the wrong value selection would affect the overall reaction scheme.

For this purpose, a sensitivity analysis was performed to assess how a change in $k_{0,10}^{forw}$ would affect the conversion and/or selectivity (Figure B.1, Appendix B). It was found that the selected value was appropriate to model the reaction scheme, since it did not affect either of the KPIs, even in an uncertainty of over 5 orders

of magnitude. Values below 1 x 10^{15} s^{-1} are not relevant for this analysis, since below this value the reaction can no longer be considered fast (the reverse reaction rate will be comparable to the forward reaction rate, due to a reverse pre-exponential factor of 5.3 x 10^{13} s^{-1}).

Moreover, the path outlined by the authors for ethylene total oxidation is merely speculative. Various equally relevant intermediates besides vinyl alcohol could be considered (e.g. formate, acetate). The aim of the authors was solely to provide a pathway which would explain the low pressure trends observed in experiments. However, without proper tuning, ethylene combustion could interfere with the quality of the model predictions.

The values adopted for these steps (12 to 14) have been selected by the authors to "reproduce experimental effects". The goal was to have a irreversible step 14, a rate-determining step 13 (hydrogen stripping) and a fast equilibrium as step 12. The parameters were selected accordingly.

The article also mentions that it is reasonable to assume that the activation energy for ethylene, EO, carbon dioxide and water's adsorption to be 0. This assumption should be examined under experimental data.

Steps 7 and 8 are also source of uncertainty; Stegelmann et al. [2] fitted theses two adsorption constants to reproduce the sticking probability of the oxametallacycle, the combustion of ethylene oxide and the selectivity on Ag(111). Since the foundation for the current work is industrial application, which uses promoted catalysts, it is natural that the fitted pre-expoentials are not adequate. Therefore, it was necessary to adapt these model parameters.

The simulation of the reaction scheme using the article's parameters yielded approximately the selectivity (52%) reported for unpromoted and unmoderated catalyst: 55% [2, 24]. This points to the model being adequate for an unpromoted and unmoderated catalyst, as expected.

To conclude, the kinetic parameters used for step 5 were also obtained from fitting. The author's fitting used Arrhenius plots for Ag(111) [67], which culminates in the previous concerns.

5.1.3 Site Density

The site density (ρ_*) is a variable that plays a significant role in the current reaction scheme. It is a measure of activity that impacts all global reactions (section A.3, Appendix A).

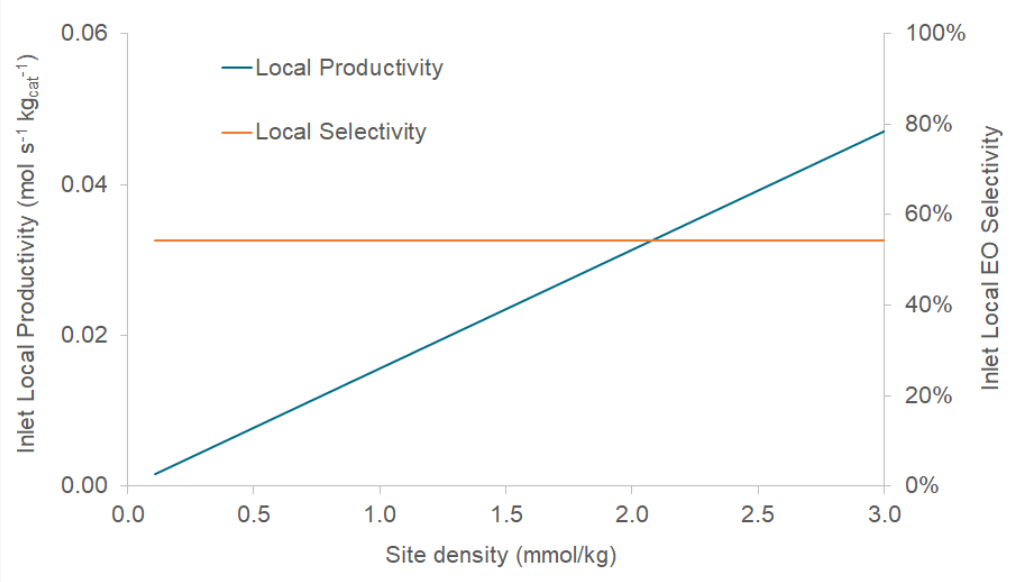

Figure 5.4: Influence of site density on ethylene conversion and EO selectivity: Stand-alone kinetics

This variable represents the amount of available active sites (silver particles) for adsorption. When simulating the stand-alone[2] kinetics, the results are intuitive. Fig. 5.4 shows the inlet local productivity and EO selectivity. Since there is no change in composition in this type of simulations the overall conversion and selectivity cannot be calculated. However, these KPIs are capable of demonstrating the desired effect.

Firstly, the local productivity (surrogate for the conversion) increases linearly with site density. This is expected, since the section A.3 shows ρ_* as a multiplicator for all of the global rates (including ethylene consumption). Secondly, there is no impact on selectivity due to the change in site density. This is consistent with none of the global rates (EO or carbon dioxide) having a higher order than 1 in respect to site density.

However, when inspecting the site density's performance in a real reactor (Fig 5.5) the trends are quite distinct.

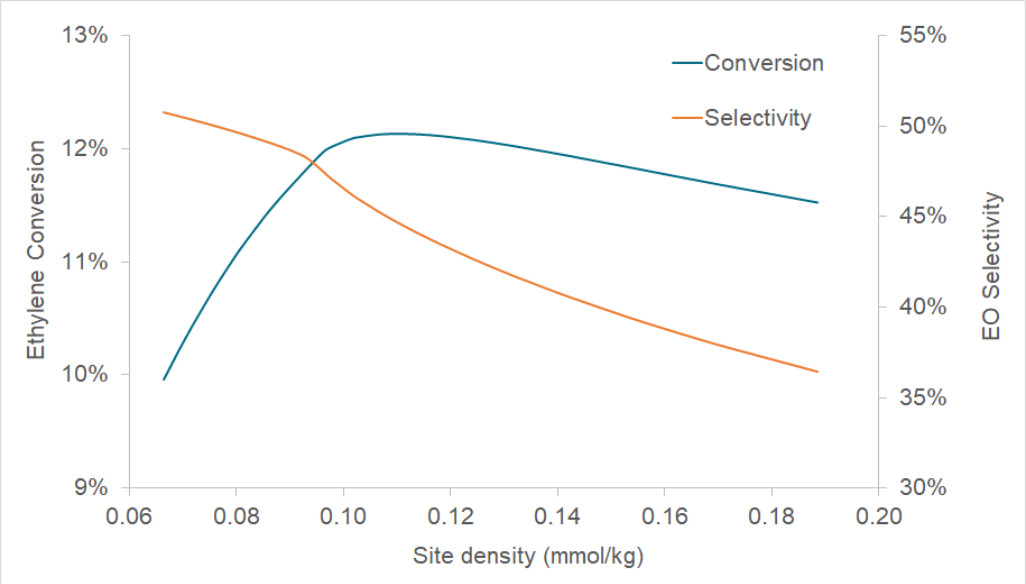

Figure 5.5: Influence of site density on ethylene conversion and EO selectivity: Industrial reactor

Firstly, there is a peak in the conversion, pointing to an optimal site density if the KPI is to be maximised. The presence of a maximum indicates that the conversion increased swiftly with this variable, until a limiting factor detained further growth. When examining the results of the simulation, this factor was isolated as the limited local availability of oxygen.

Thus, it is concluded that for some values of site density, the consumption of oxygen in the initial section of the reactor is too steep and will hinder the overall yield of the reactor by delivering oxygen deficient reacting mixture to the ensuing grid point.

Furthermore, there is a most undesirable impact in the selectivity: a non-negligible decrease. This is also a result of the combustion products being more readily desorbed from active sites than EO. The trade-off between increased conversion and non-decreased selectivity is a precarious balance. The study of this variable is concluded to be crucial for the optimisation of the process' efficiency.

A similar analysis was performed on the reacting temperature. To change the reacting temperature the best variable to vary is the coolant inlet temperature. In Appendix B, Fig. B.2 shows the effects of this analysis. As becomes evident from observing Fig. B.2, the trends for the conversion and selectivity are identical to Fig. 5.5, and the same conclusions may be drawn.

[2] Simulating the reaction kinetics with no composition, pressure or temperature change along the catalyst bed.

5.1.4 Selectivity

An important aspect of the sensitivity analysis is to ascertain if the model could reach the selectivities observed for the promoted catalysts by changing the lowest number of parameters possible. As mentioned previously, the ratio of step 7 to 8 is decisive in determining the selectivity. Furthermore, changing these variables is fairly justified, since they were obtained from fitting on Ag(111).

$\text{Ratio}_{7/8}$ was defined as the ratio between steps 7 and 8 equilibrium adsorption constants.

$$\text{Ratio}_{7/8} = \frac{K_{ads,\,7}}{K_{ads,\,8}} \tag{5.2}$$

$\text{Ratio}_{7/8}$ was defined as the ratio between steps 7 and 8 equilibrium adsorption constants.

The conversion was kept constant to isolate the effect of the ratio increase on the selectivity. The constant conversion was obtained by varying site density accordingly. The values required to keep the conversion at 11.5% are presented in the graph as well.

When performing this analysis without the constant conversion, the values of conversion plummet to 0. Due to the lack of converted ethylene, the denominator in the selectivity expression (eq. 4.9) decreases markedly, creating an artificial increase in selectivity. Maintaining constant conversion is thus crucial for this analysis.

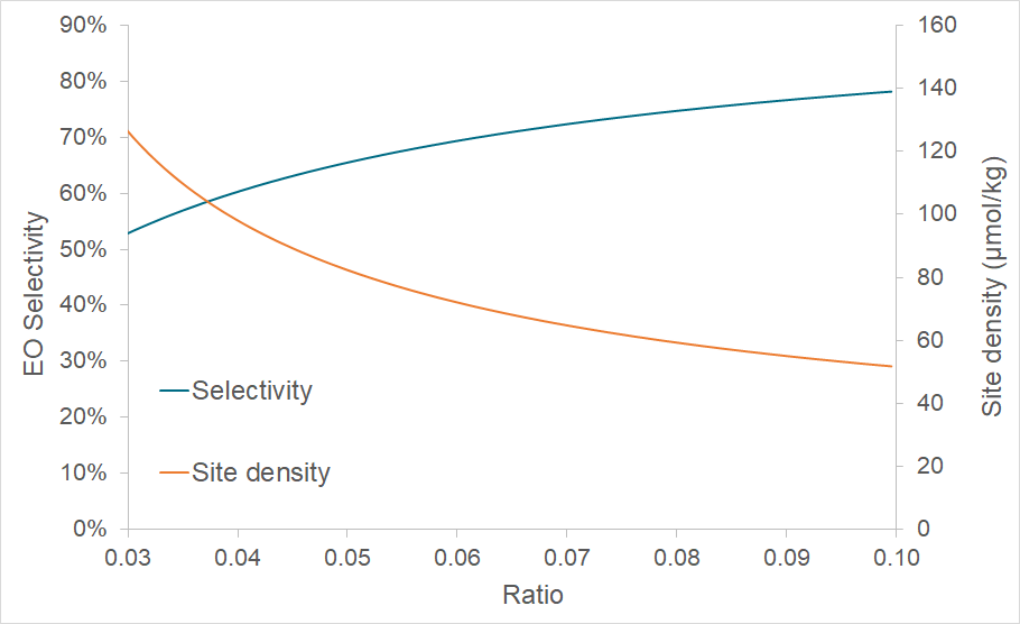

Figure 5.6: Increase in EO selectivity with $\text{Ratio}_{7/8}$ variation at constant ethylene conversion

Fig. 5.6 shows it is possible to reach 70-80 % selectivity (in agreement with literature [22]), thus proving the potential for the model to predict selectivities for promoted catalysts in a posterior stage.

5.2 Parameter Estimation

After ensuring that the kinetic scheme developed by Stegelmann et al. [2] would be capable of predicting reasonable values for the KPIs, outlet compositions, temperatures, and pressures, it was necessary to test the quality of the model against experimental data. Petkim Petrokimya Holding A.Ş. has provided a series of experimental laboratory trials in which different reaction conditions were tested.

Since the catalysts used in these experiments had different activities from the catalysts used to determine the parameters proposed by Stegelmann et al. [2] it was necessary to adapt the model to the current activity

and selectivity. As was observed previously, model parameters, such as steps 7 and 8 pre-exponential factors, were selected to fit the selectivity on Ag(111). Furthermore, the density of active sites is also particular to the catalyst as it is a measure of its activity. These parameters must be estimated prior to model validation for a coherent comparison.

The set-up used for this objective has been detailed in the *Laboratory Reactor Model* section. To facilitate the parameter estimation, a change in variables was performed. The pre-exponential terms were substituted by constants at a reference temperature which was set as 525 K (the furnace set-point for multiple trials). The new parameters were determined using the original ones and the following expression:

$$k_i^{j,T_{ref}} = k_{0,i}^{j} \cdot e^{-\frac{E_i^j}{RT_{ref}}} \tag{5.3}$$

in which $k_i^{j,T_{ref}}$ is step i's new constant in the direction j (forward, backward) and E_i^j is the activation energy for step i in direction j.

In the model, the term to calculate the kinetic constant of a reaction rate, at a given temperature T ($k_i^{j,T}$), was replaced with the following term:

$$k_i^{j,T} = k_i^{j,T_{ref}} \cdot e^{-\frac{E_i^j}{R}\cdot\left(\frac{1}{T}-\frac{1}{T_{ref}}\right)} \tag{5.4}$$

This change in variables produces mathematically identical solutions. However, it smooths the parameter estimation. Using the reference temperature reduces the correlation between the rate constant and its activation energy, which facilitates the solver's search for optimal values.

5.2.1 Parameter Estimation Runs: I. Identifying Key Variables

The first run of the parameter estimation used experiments of identical feed and operating pressures with different furnace set-point temperatures and mass of catalyst as differentiators. Eleven experiments (1_1-1_3, 4_1-4_3, 6_1, 6_5, 7_1, 7_27, and 7_46) were used to conduct the parameter estimation from four distinct catalyst loadings.

A preliminary parameter estimation was carried out to determine how the model parameters would suit the provided data, only adjusting the site density. The value obtained was (675 ± 3) x 10^{-6} mol kg^{-1}.

To underline some relevant effects of the parameter estimation, the KPIs were calculated using the experimental measurements and were monitored in the model predictions.

Catalyst loading 1 presented in Fig. 5.7 shows that the site density adjustment was enough to ensure quality predictions of the ethylene conversion for 230.5℃. Although the modelled predictions were satisfactory for lower temperatures (230.5℃), they strayed significantly at higher ones.

The differentiating factor between the three experiments of catalyst loading 1 was the furnace temperature setpoint (Table 4.8), as may be observed in Fig. 5.7's plot. It was therefore implied that the temperature dependence of the model is not accurately tuned. This points to a poor selection of activation energies in the model, namely for the step that defines ethylene conversion.

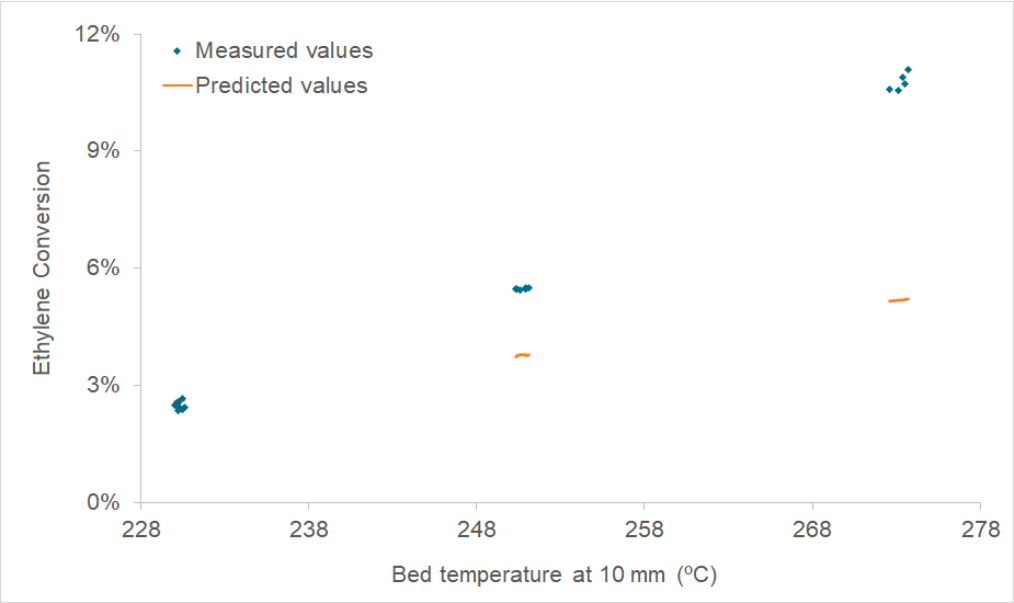

Figure 5.7: Catalyst loading 1's measured and predicted (Run I) ethylene conversion as a function of the bed temperature

Fig. 5.8 presents the measured and predicted ethylene conversion at the same temperature (230.5℃) for two distinct catalyst loadings. The only difference between the two being the mass of catalyst in each loading. The controls of the parameter estimation were instructed to change this variable (mass of catalyst) accordingly.

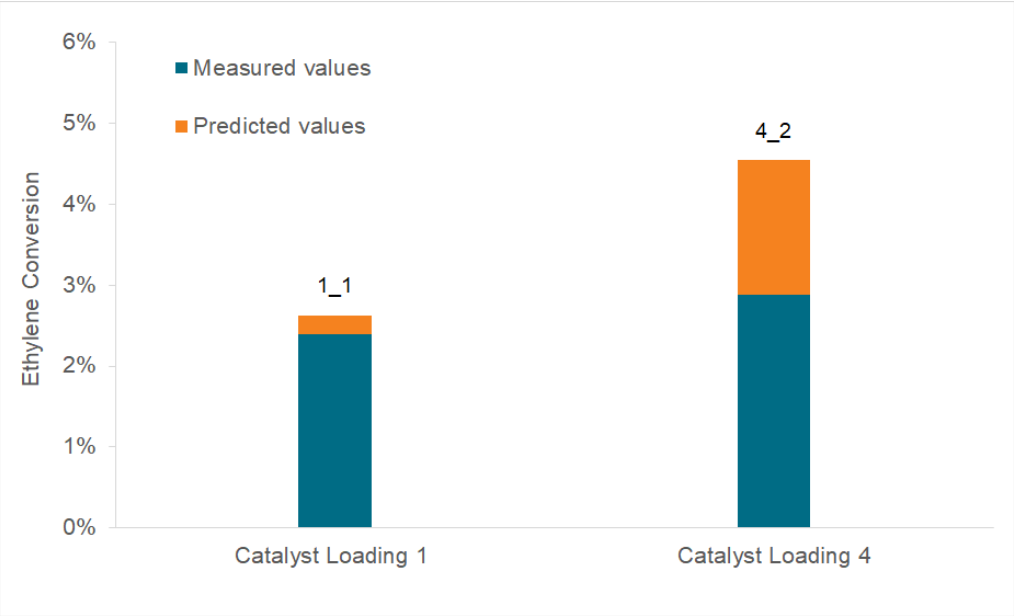

Figure 5.8: Catalyst loading 1 and 4's measured and predicted (Run I) oxygen conversion at 230.5℃

Fig. 5.8 emphasises the need for a catalyst reference activity, since the model prediction for catalyst loading 4 is subpar. As mentioned previously, each catalyst loading had a different start-of-run activity. These have been stressed by Fig. 5.8.

The usefulness of this parameter arises from the non-uniformity of the catalyst batches created. The activity varies (but not substantially) between batches. By establishing a reference batch, the quality of the activation of the remaining can be analysed by comparison. Reference activities higher than 1 translate into

a better activation. The latter concept will henceforth be referred to as catalyst reference activity ($\alpha_{ref}^{\rho_*}$), and will be employed in the model generating the site density variable:

$$\rho_* = \rho_{*,0} \cdot \alpha_{ref}^{\rho_*} \tag{5.5}$$

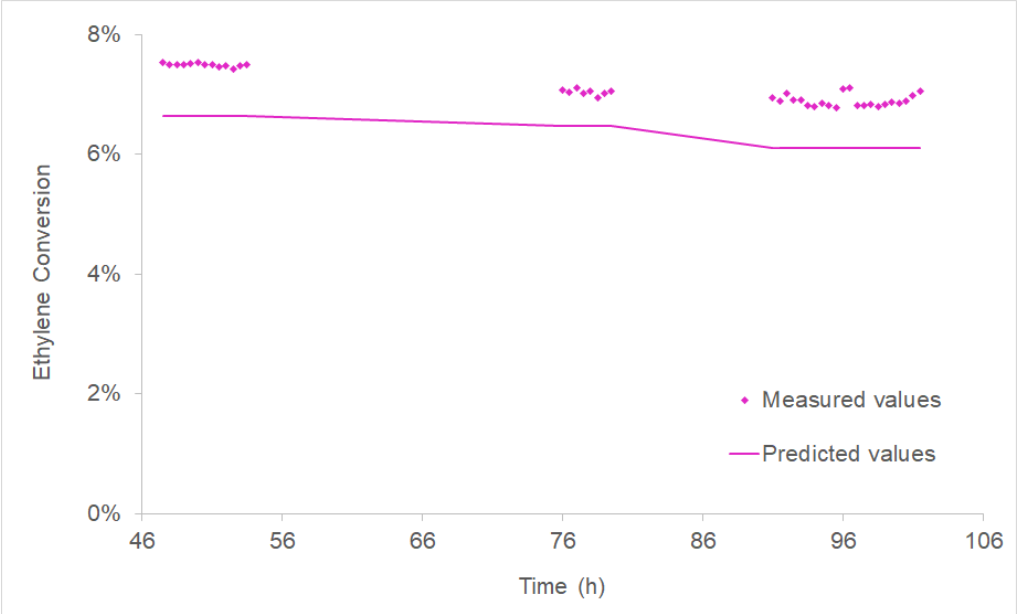

Figure 5.9: Catalyst loading 7's measured and predicted (Run I) ethylene conversion as a function of time

A third conclusion is drawn from Fig. 5.9: the activity of the catalyst is a function of time. Catalyst loading 7's used experiments (shown in Fig. 5.9) all had the same furnace temperature set-point. Nonetheless, the same temperature was not achieved in all the trials[3]. The deactivation of the catalyst is therefore evident in Fig. 5.9. This conclusion is not surprising since the protuberant deactivation of the α-alumina supported catalyst has been referred previously in this work.

The following plot predicts the oxygen conversion for different bed temperatures using the first catalyst loading. It is clear, once more, by observing the plot (Fig. 5.10) that the temperature dependence is not correctly modelled. However, in this plot, the 251 ℃ temperature is the best modelled one, in contrast with what was seen in Fig. 5.7.

The oxygen conversion is a measure of the selectivity of the process since more oxygen is consumed in the combustion than in the epoxidation (6 times more). Although, experiment 1_1's ethylene conversion predictions (Fig. 5.7) are very accurate, the same cannot be reported for oxygen conversion (Fig. 5.10), which indicates that the selectivity of the model, prior to adjustment, is too low for low temperatures (experiment 1_1: 230.5 ℃) and too high for high temperatures (experiment 1_3: 273.3 ℃).

This points to a poor selection of activation energies in the model, for Step 7 and/or 8, which have been put into question in subsection *5.1.2. Validity of Model Parameters*.

[3] Experiment 7_1: 255.2 ℃; Experiment 7_27: 253.3 ℃; Experiment 7_46: 249 ℃;

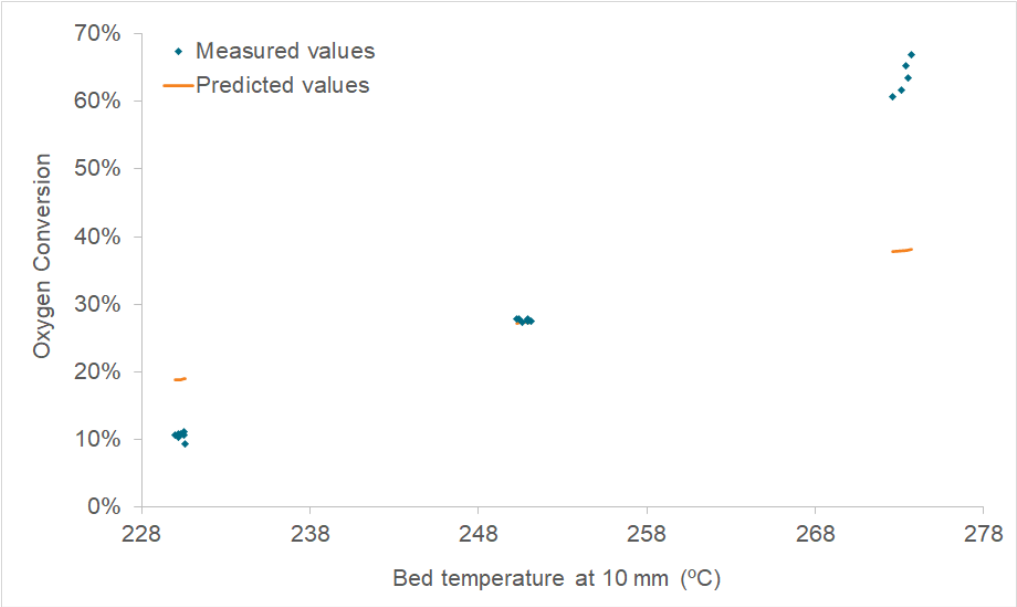

Figure 5.10: Catalyst loading 1's measured and predicted (Run I) oxygen conversion as a function of the bed temperature

5.2.2 Parameter Estimation Runs: II. Catalyst Start-of-Run Activity

Following the preliminary parameter estimation, some of the parameters regarded as necessary to be estimated in the prior analysis were included. The mentioned catalyst reference activity ($\alpha_{ref}^{\rho_*}$) for steps 4, 6 and 7 were added to the site density. The catalyst reference activity for the first loading was set as 1, leaving the remaining three to be freely estimated.

For this parameter estimation only experiments[4] with the same target furnace temperature were included (which excludes 4 of the previous 11 experiments). Since the temperature dependence is not tackled at this stage it was considered preferable to use runs at similar temperatures.

The results obtained are presented below.

Table 5.2: Parameter estimation - Run II

Model Parameter	Estimated Value	Standard Deviation
$\rho_{*,0}$ (mol kg^{-1})	103 x 10^{-5}	± 2 x 10^{-5}
$\alpha_{ref,4}^{\rho_*}$	0.39	± 0.01
$\alpha_{ref,6}^{\rho_*}$	0.45	± 0.01
$\alpha_{ref,7}^{\rho_*}$	0.52	± 0.01

Estimating parameters in parts is a useful approach for complex models, for it is efficacious in obtaining adequate initial points for the subsequent estimations, which is a matter of the utmost importance.

Fig. 5.11 shows that the new parameter estimation was successful in obtaining a more congruent result for ethylene conversion than previously. The measured deviation from the model (which is not meaningful) is distributed between all the catalyst loadings, contrasting with the results observed in Fig. 5.8. Furthermore, unlike *Run I*, the measured values exceed the predictions.

[4] Run II experiments: 1_2, 4_1, 6_1, 6_5, 7_1, 7_27, and 7_46

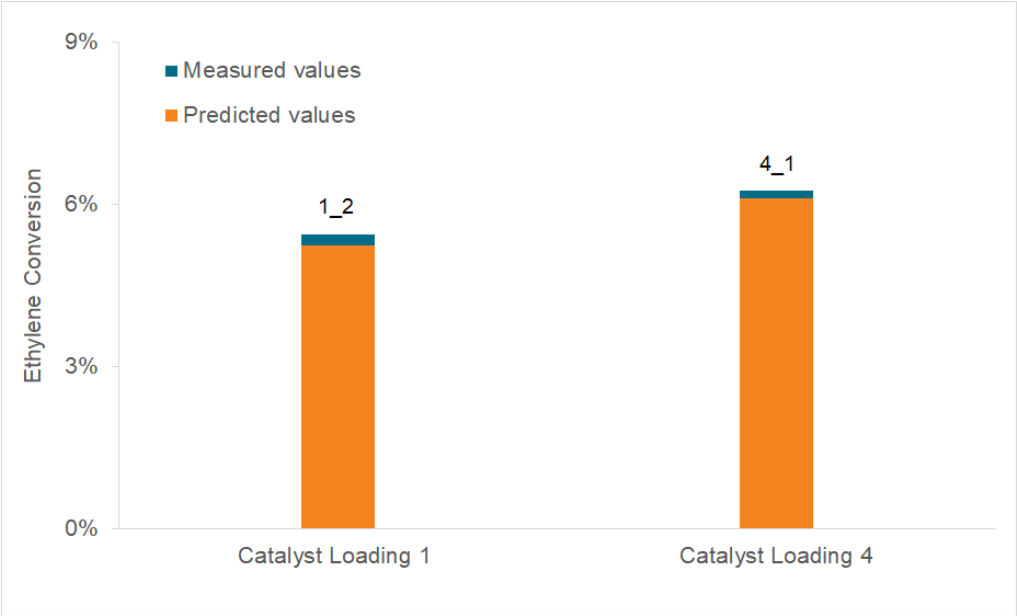

Figure 5.11: Catalyst loading 1 and 4's measured and predicted (Run II) ethylene conversion at 250.9℃ and 253.8℃, respectively

5.2.3 Parameter Estimation Runs: III. Model Selectivity

Four conclusions were drawn from the results of *Run I* : the ethylene conversion temperature dependence, the ethylene conversion time dependence (catalyst deactivation) and the selectivity temperature dependence must be estimated; along with adding the catalyst reference activity array variable. The latter was tackled in *Run II* which corroborated that the catalyst reference activity was a needed adjustment.

The experiments outlined in *Run I* were used, being that they have similar feeds. Yet, catalyst loading 7 was excluded because catalyst deactivation must be determined when there is already a better understanding of the surface reaction kinetics.

Steps 7 and 8 were determined to be crucial to model the selectivity correctly. Furthermore, the authors of the proposed scheme [2] have fitted the values of these steps' kinetic parameters to Ag(111). Thus, to ensure quality predictions for a promoted catalyst, the adsorption constants and activation barriers must be adjusted for these steps.

The purpose of this estimation was to adjust adsorption constants and activation barriers. Therefore the reverse reaction were maintained constant (minimizing the number of estimated parameters).

The model proposed by Stegelmann et al. [2] uses activation energies obtained from statistical thermodynamic treatment. To maintain the enthalpies, the activation energy of the reverse step must then be changed accordingly. In the model, the assignment of the reverse activation energies were replaced with the following expression:

$$E^{rev}_{Step\,i} = E^{forw}_{Step\,i} - \Delta H_{Step\,i} \tag{5.6}$$

where $\Delta H_{Step\,i}$ represents the difference between the literature's forward and reverse activation energy of step *i*.

Table 5.3: Parameter estimation - Run III

Model Parameter	Estimated Value	Standard Deviation
$\rho_{*,0}$ (mol kg^{-1})	93 x 10^{-5}	± 1 x 10^{-5}
$\alpha_{ref,4}^{\rho_*}$	0.76	± 0.02
$\alpha_{ref,6}^{\rho_*}$	0.50	± 0.02
$k_7^{forw,\,T_{ref}}$ (s^{-1})	232 x 10^{1}	± 6 x 10^{1}
E_7^{forw} (kJ mol^{-1})	138	± 3

Preliminary estimations using kinetic parameters of both steps 7 and 8 showed a very high correlation between theses two (0.997). To avoid obtaining parameters with a standard deviation that exceeds the order of magnitude of the value in question, only one of these steps will be used. The result of the parameter estimation was a series of reasonable values, estimated within a tight confidence interval as may be analysed in Table 5.3.

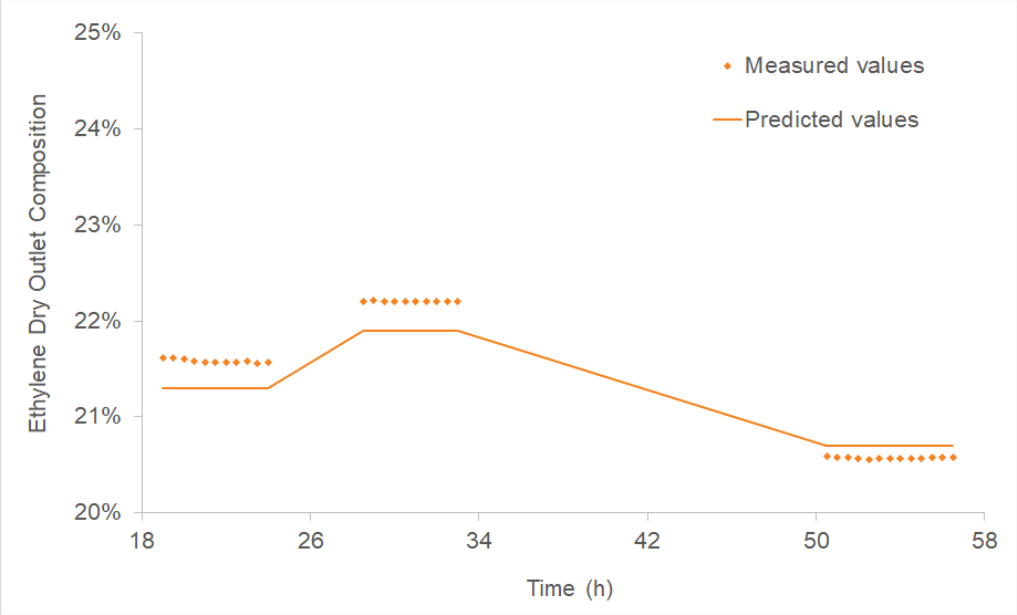

Figure 5.12: Catalyst loading 4's measured and predicted (Run III) ethylene dry outlet composition

Fig. 5.12 shows that both experiment 4_1 and 4_2 underpredict the composition of ethylene (i.e. over-predict the ethylene conversion). It may be observed that using the site density and the catalyst reference activity has been successful in obtaining reasonable predictions. However, the conversion predictions vary in quality at different temperatures.

Thus, the following hypothesis is suggested: E_7^{forw} is not sufficient to model the temperature dependence of the model. This theory is based on the following: E_7^{forw} is a parameter mainly used to tweak the selectivity's temperature dependence, and, although it does influence conversion, a second parameter is needed to adjust the conversion temperature dependence. The previous remarks are further empahsied by Fig. 5.13. Catalyst loading 1 shows a significant deviation for the third experiment (1_3) which occurs at higher temperature (Table 4.8).

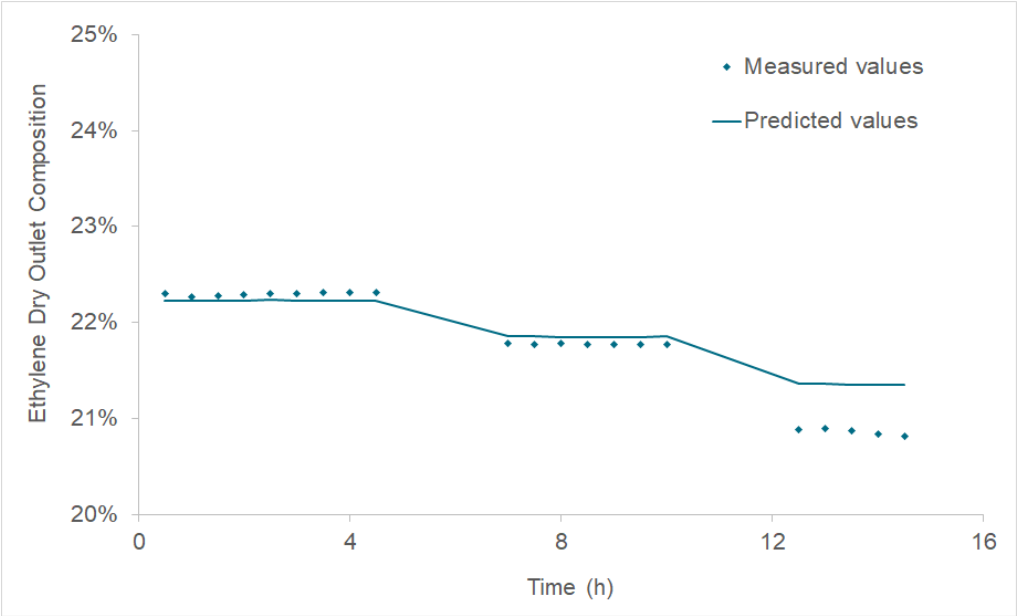

Figure 5.13: Catalyst loading 1's measured and predicted (Run III) ethylene dry outlet composition

Since site density is a measure of activity, it impacts all global reactions (section A.3, Appendix A), hence the need to identify a measure of activity which will have a more pronounced effect in the ethylene conversion. As was underlined in subsection *5.1.3. Site Density*, the effects of this variable do not have a linear impact in the KPIs. These contradictory influences hamper the search for an optimal solution. Furthermore, the experimental data showed a need to match the temperature dependence. This points to the necessity of including the activation energy of the step which limits the conversion.

As was identified in the preliminary sensitivity analysis, step 2 is the decisive step for determining the conversion. Thus, $k_2^{forw,\,T_{ref}}$ and E_2^{forw} were included in the next estimation. To avoid correlations with the former mentioned, the site density was removed from the parameters to be estimated.

5.2.4 Parameter Estimation Runs: IV. Model Temperature Dependence

Analysis of the preliminary parameter estimations (which used both step 7 and 8 kinetic constants at T_{ref}) mentioned in the previous part, led to believe that the solver aims to remove the ethylene oxide combustion route (step 8) to obtain better predictions. This was concluded when $k_8^{forw,\,T_{ref}}$ reached near 0 values.

This occurred when there was a high correlation between steps 7 and 8. Thus, in order not to form hasty conclusions, three scenarios were outlined to determine if a simplified model would be better in describing the process: the original model, a model that eliminates the ethylene combustion route and a model that eliminates the ethylene oxide combustion route (Fig. 5.14). Identical parameter estimations were then performed with different values of site density since its value had to be fixed throughout the estimation.

The best scenario was selected based on the objective function value. The *Model Validation* in gPROMS is based on the Maximum Likelihood formulation. The aim of the solver is to determine values which maximise the probability of the model predicting the experiment measurements, i.e. minimize the objective function.

For all the different values of site density tested[5], the model which removed the ethylene oxide combustion route performed the best (showing significantly lower objective function values). This disparity between quality of the site densities had been identified in subsection *5.1.3. Site Density*. The presence of an optimal value for this variable when simulated within a reactor model limits its choice.

[5] 0.3, 0.4, 0.5, 0.6, 0.65, 0.7, and 0.8 mmol kg^{-1}

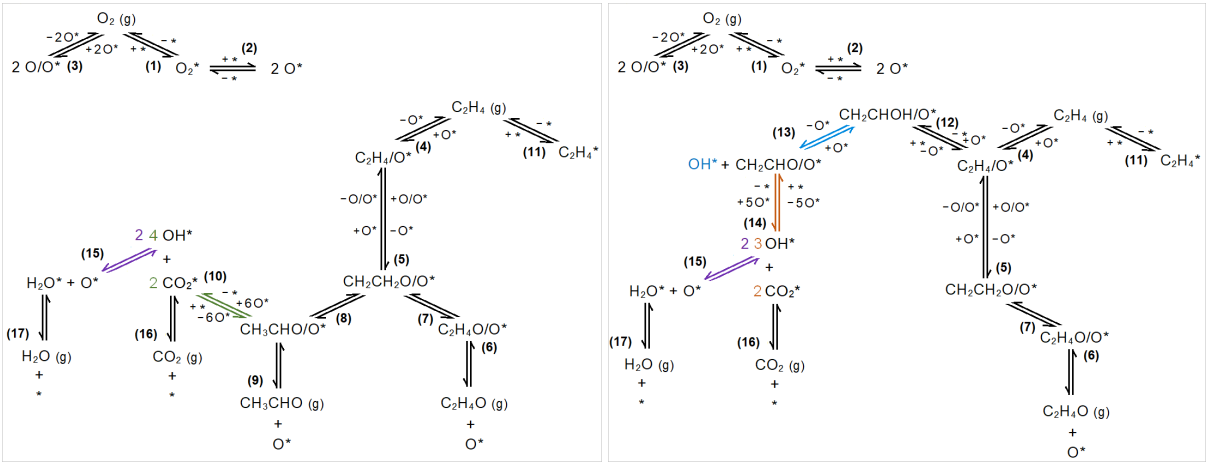

Figure 5.14: Simplified reaction schemes: ethylene combustion (left) and ethylene oxide combustion (right) route removed

The original model displayed the second best objective functions, rendering the model that eliminates the ethylene combustion as the worst scenario. These results point to an interesting theory: ethylene oxide combustion is not relevant under the current conditions. The *Literature Review* (chapter 2) had alluded to the negligible nature of this path [6, 15]. Furthermore, it corroborates that the solver was, in fact, aiming to remove this route in the preliminary estimations.

The best case obtained was the estimation with no ethylene oxide combustion with $\rho_{*,0}$ fixed at 0.6 mmol kg^{-1}. The corresponding parameters estimated are presented in Table 5.4.

Table 5.4: Parameter estimation - Run IV

Model Parameter	Estimated Value	Standard Deviation
$\alpha_{ref,4}^{\rho_*}$	0.579	± 0.008
$\alpha_{ref,6}^{\rho_*}$	0.67	± 0.01
$k_2^{forw,\,T_{ref}}$ (s^{-1})	85 x 10^5	± 5 x 10^5
$k_7^{forw,\,T_{ref}}$ (s^{-1})	17.7	± 0.7
E_2^{forw} (kJ mol^{-1})	197	± 8
E_7^{forw} (kJ mol^{-1})	69	± 5

Fig. 5.15 underlines how the parameter estimation was enhanced with the addition of E_2^{forw}. The quality of the fit is highlighted by the graph which shows precise predictions for ethylene outlet composition, and necessarily the ethylene conversion. These quality predictions are observable regardless of the reacting temperature.

Fig. 5.16 accentuates yet another positive trait of this parameter estimation: matching the selectivity. By accurately predicting the outlet of both dry products, the new parameters prove to be successful in matching the selectivity. Being that the conversion has been also found satisfactory, it may be concluded that these parameters are adequate for an industrial catalyst.

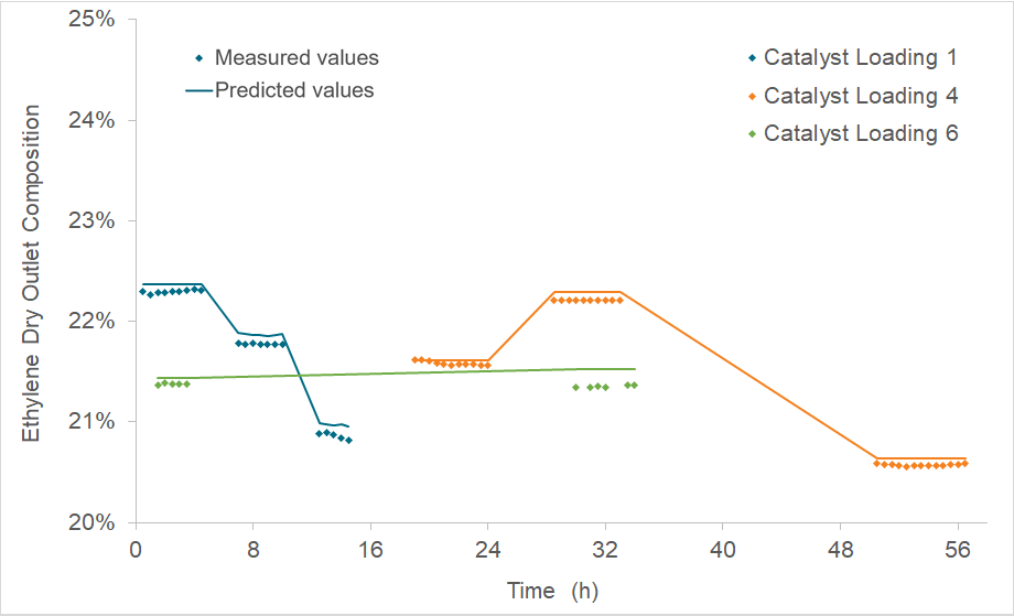

Figure 5.15: Catalyst loading 1, 4 and 6's measured and predicted (Run IV) ethylene dry outlet composition

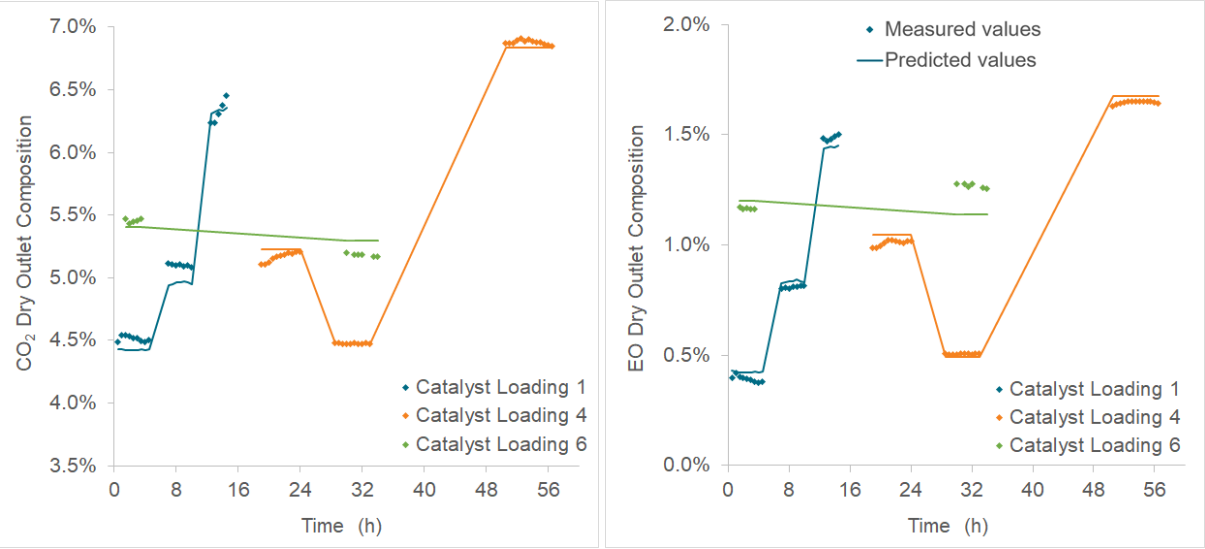

Figure 5.16: Catalyst loading 1, 4 and 6's measured and predicted (Run IV) carbon dioxide and ethylene oxide dry outlet composition

5.2.5 Parameter Estimation Runs: V. Model Validation

This stage aimed to validate the previously obtained parameters. New experiments (not used in the previous estimations) were introduced. The objective was to observe how these parameters perform in matching new conditions.

Unlike the previous experiments, these experiments have different feed composition. The last estimations only handled similar feeds at various temperatures. The added experiments would ascertain if the newly parameterized model were sufficiently robust to handle different compositions. The added experiments were the following: 2_1-2_6, 3_1-3_3 and 6_3.

Although it would be preferable to not further estimate parameters, the use of new catalyst loadings required the estimation of their respective catalyst reference activity (Table 5.5).

Table 5.5: Parameter estimation - Run V

Model Parameter	Estimated Value	Standard Deviation
$\alpha^{\rho_*}_{ref,2}$	1.02	± 0.02
$\alpha^{\rho_*}_{ref,3}$	0.77	± 0.01

The enhanced model was able to accurately describe the reactor's conversion for the new experiments, as may be observed in Fig. 5.17. Unfortunately, experiment 3_3 showed no measurements which withstood the data reconciliation quality test and, therefore, was excluded.

Matching the outlet ethylene is an easier target than the carbon dioxide. The inlet of ethylene is large (~20 mol%) and its conversion is low, rendering the outlet value of molar flow also high. The prediction error is, therefore, readily diluted.

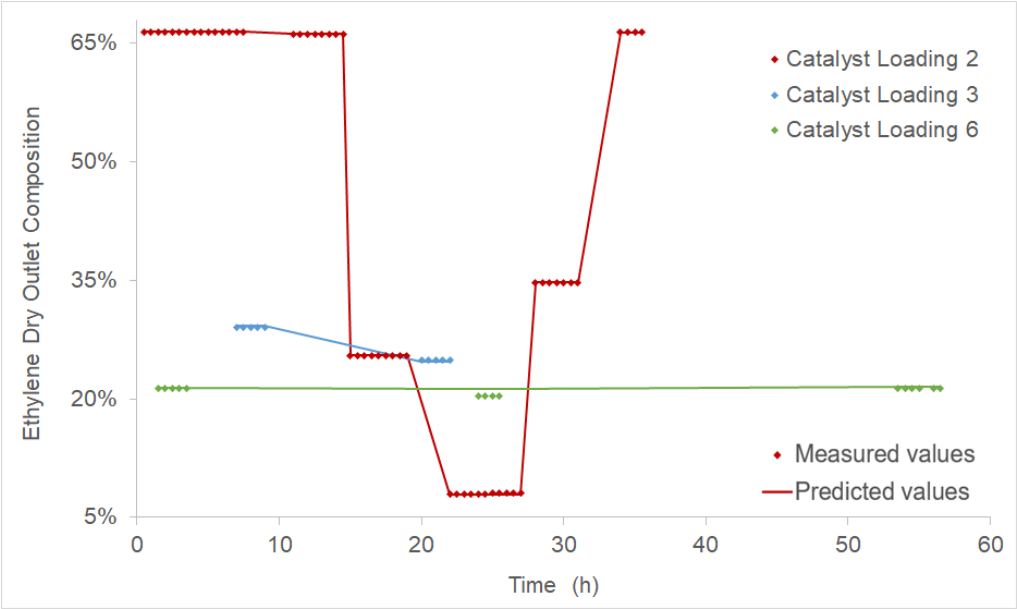

Figure 5.17: Catalyst loading 2, 3 and 6's measured and predicted (Run V) ethylene dry outlet composition

However, the results did not achieve the desired goal for the selectivity. The predictions for the two products EO and carbon dioxide were unsatisfactory, as may be observed in Fig. 5.18.

This parameter estimation was performed once again, unfixing the parameters estimated in *Run IV*. Although this did improve the fit, the fact remained that these parameters are unsuited to describe the current reaction scheme universally.

The newly paramterized reaction scheme is not without its success. It is precise in matching reacting conditions for a wide range of temperatures and will perform commendably for feeds similar to shown in Table 5.6.

Table 5.6: Standard feed composition (%mol) for the simplified model

C_2H_4	O_2	CO_2	EO	VCM	CH_4
22.74	5.77	4.14	0	0	63.08

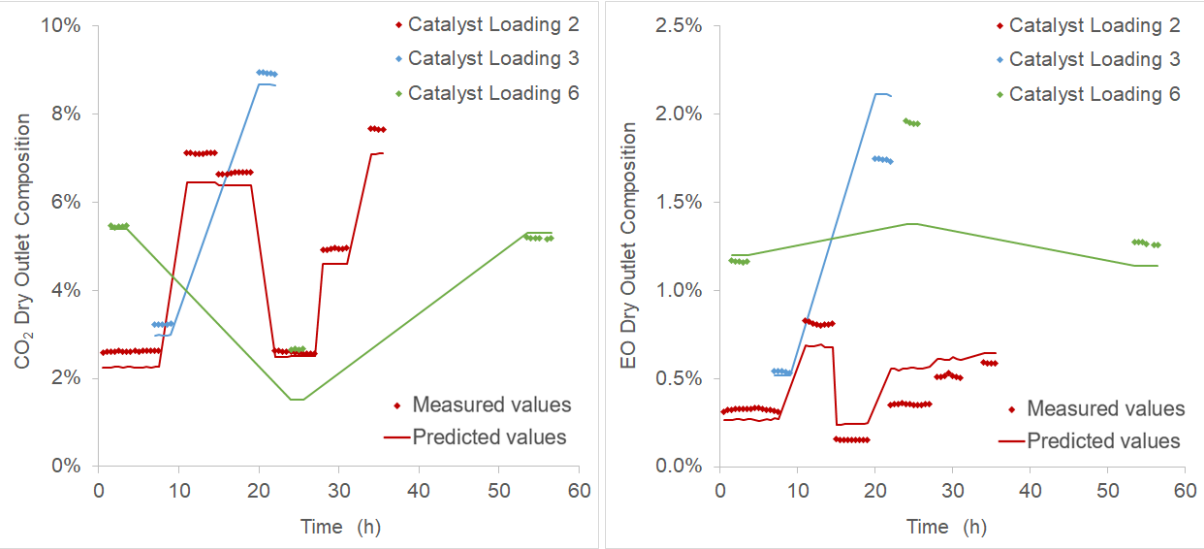

Figure 5.18: Catalyst loading 2, 3 and 6's measured and predicted (Run V) carbon dioxide and ethylene oxide dry outlet composition

The model will presumably work adequately if the feed is similar. The essential point is maintaining similar partial pressures of the reactants and products. The composition of the inert components is irrelevant if these are maintained, as well as the addition of new inert substances.

The simplified model developed so far is not unlike a rate expression deduced based on adsorption formulations. Its limited applicability indicates it describes solely a branch of a much more complex scheme.

To identify the reason for which this model worked so distinguishably for the first set of experiments, it was necessary to inspect which were the effects which had the most influence on the selectivity (since this was the distressing factor). When analysing the various simulations of the experiments, two elements were singled out as the major contributor: temperature and ethylene oxide presence (throughout the reactor).

Temperature plays a role in changing the equilibrium adsorption constants of the various steps, rendering some steps more relevant than others in certain temperature ranges. This is done so through the activation energies (forward and reverse) which condition the temperature dependence of the model.

The second predominate factor is the ethylene oxide presence. Although none of the experiments used have EO in the feed, this component, being the desired product, is naturally produced along the reactor. And as this product is generated, its combustion becomes steadily more significant.

Intuitively, the latter would have been even more noticeable for feeds which included EO. Yet, it must be stressed that the first set of experiments worked for the simplified model not because EO combustion was not substantial, but because this effect had been included in the former (temperature).

With the coupling of ethylene oxide combustion in the temperature dependence of the simplified model, the determined activation energies are simply apparent activation energies, and void their original meaning. This theory is underlined by Fig 5.19 which shows two experiments (1_1 and 2_5) which display the same measured temperature (~504 K).

The fit for the experiment 1_1 is nearly perfect since it was used for the estimation of the parameters in *Run IV*. Experiment 2_5 is matched less accurately because this simplified model uses temperature as the modelling strategy for the selectivity. Thus, two identical temperatures will predict the same carbon dioxide production (if the feed is identical and considering the same reference activity). Due to the catalyst reference activity, the predictions for two experiments would never be identical, unless this value were to be 1[6].

[6]However, the $\alpha_{ref,2}^{\rho_*}$ is 1.02, which is virtually 1 ($\alpha_{ref,2}^{\rho_*} = 1$).

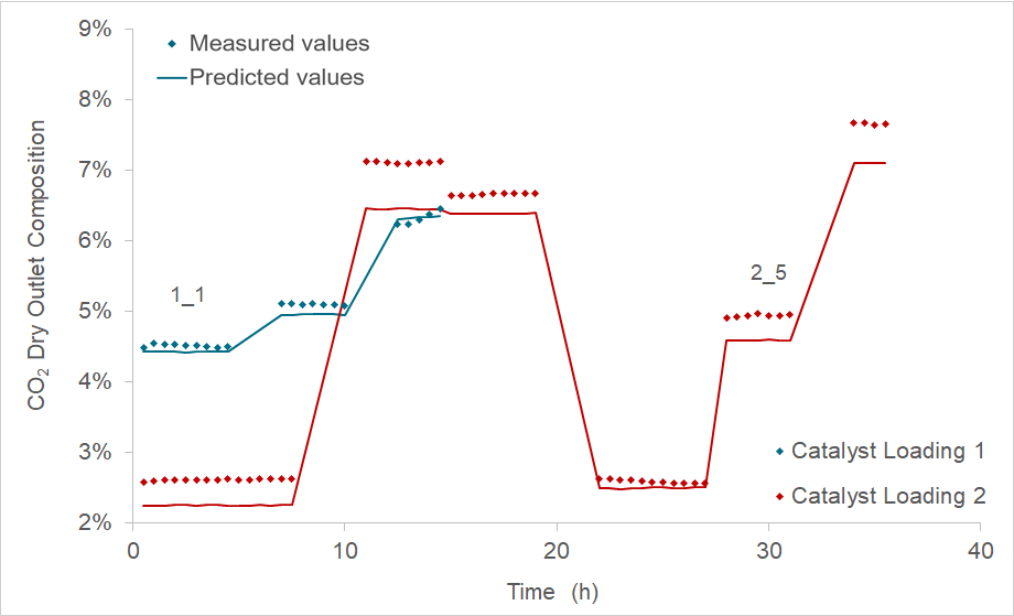

Figure 5.19: Catalyst loading 1 and 2's measured and predicted (Run V) carbon dioxide dry outlet composition

When moving on to different feeds, the decoupling of both effects became a requirement. And thus, the quest for restoring the universality of the model is the subject of the next subsection.

5.2.6 Parameter Estimation Runs: VI. Model Adjustments

Returning to the original model, the following strategy was applied: the steps identified as RDS were estimated (only the forward parameters). This approach had the disadvantage of the substantial amount of parameters it entailed. However it eliminated estimation of parameters that would not have a significant impact on the overall scheme. Due to the overall amount and nature of the parameters, the existence of correlations and, consequentially, the low confidence of the estimated parameters was expected.

A preliminary parameter estimation identified another issue: some experiments which matched conversion would under/overpredict both products. This led to a supplementary review of the data reconciliation. Using constant inert flow as a calculation basis, it was found that a few experiments did not conserve the carbon balance. For these experiments, it is impossible to single out which of the compositions is most reliable.

Two measures were taken to remediate this issue. Firstly, experiments with a relative change in carbon flow superior to 2.1% were removed from the estimation pool. Secondly, the parameter estimations begun to only use EO and carbon dioxide dry outlet composition as targets. Although oxygen and ethylene were still included for monitoring purposes, their variance was set as at a very high value, ensuring these measurements would not impact the parameters estimated. The following experiments were removed: 2_2, 2_6 and 6_1.

In theory, EO and carbon dioxide's compositions are sufficient to infer the remaining two (since the feed composition is known, and considering there are no unknown side reactions). Furthermore, the variance model stipulated for the two products was tightened to ensure more precise predictions.

Table 5.7 confirms the suspected drawback of this approach: there is low confidence in the values estimated.

Table 5.7: Parameter estimation - Run VI

Model Parameter	Estimated Value	Standard Deviation
$\alpha_{ref,2}^{\rho_*}$	1.51	± 0.05
$\alpha_{ref,3}^{\rho_*}$	0.98	± 0.03
$\alpha_{ref,4}^{\rho_*}$	0.549	± 0.005
$\alpha_{ref,6}^{\rho_*}$	1.16	± 0.08
$k_2^{forw,\,T_{ref}}$ (s^{-1})	6 x 10^7	± 10 x 10^7
$k_5^{forw,\,T_{ref}}$ (s^{-1})	1153	± 2
$k_7^{forw,\,T_{ref}}$ (s^{-1})	0.7	± 2
$k_8^{forw,\,T_{ref}}$ (s^{-1})	0.2	± 2
$k_{13}^{forw,\,T_{ref}}$ (s^{-1})	19	± 2 x 10^4
E_2^{forw} (kJ mol^{-1})	390	± 2000
E_5^{forw} (kJ mol^{-1})	383	± 50
E_7^{forw} (kJ mol^{-1})	14	± 8
E_8^{forw} (kJ mol^{-1})	98	± 10
E_{13}^{forw} (kJ mol^{-1})	70	± 900

Once again, the conversion fit is very accurate (Fig. 5.20). This had already been reported for the last parameter estimation phase. However, maintaining the quality of the fit for this KPI is important in ensuring the new parameters are at least equally capable.

The advantage of this method sets upon its grasp on the selectivity. Contrasting with the previous estimation, the dry outlet composition predictions of ethylene oxide and carbon dioxide (Fig. 5.21) are almost a perfect match.

The improvement is most visible on the carbon dioxide composition, which is predicted with near perfect accuracy. In respect to the EO predictions, it must be underlined that the axis of the graph shows a much more confined range, for which the deviations shown are lower than the 0.1% magnitude (irrelevant). Thus, it may be concluded that both products are predicted extremely well, confirming the success of this final estimation phase.

Furthermore, the CO_2 produced by ethylene combustion as a percentage of the total produced CO_2 was defined. This performance indicator was used to investigate the case study presented in *Run V*, experiments 1_1 and 2_5. It was found that for experiment 1_1, the CO_2 produced through ethylene total oxidation varied from 55% to 60% (along the bed). For experiment 2_5, ethylene total oxidation only accounted for 45 to 48% of the CO_2 produced.

The use of the new model provides an explanation for the different measurements reported for these two experiments. It points to experiment 1_1's feed composition being a region in which ethylene combustion is predominant. The same is not applicable to experiment 2_5.

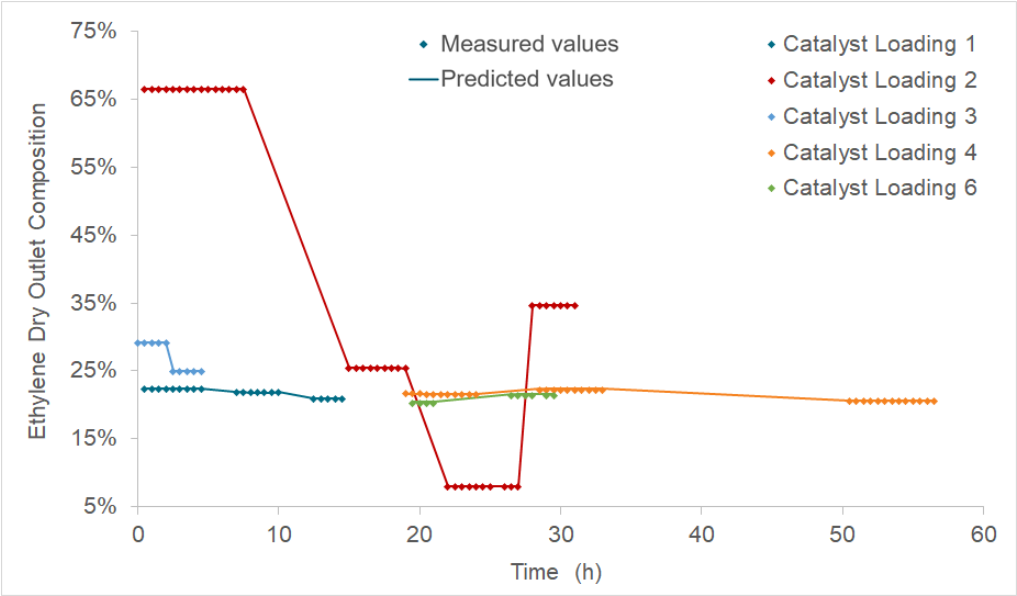

Figure 5.20: Catalyst loading 1, 2, 3, 4 and 6's measured and predicted (Run VI) ethylene dry outlet composition

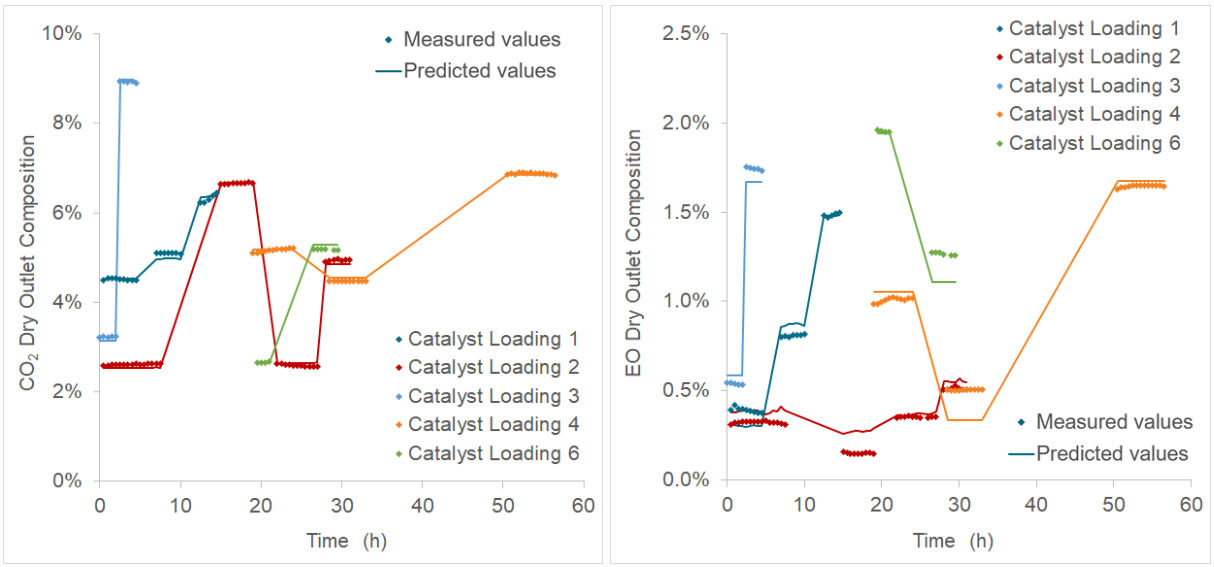

Figure 5.21: Catalyst loading 1, 2, 3, 4 and 6's measured and predicted (Run VI) carbon dioxide and ethylene oxide dry outlet composition

Moreover, since the percentage of CO_2 produced from ethylene oxide is established, it is possible to quantify the increase in the selectivity that would be observed if ethylene oxide combustion were to be totally inhibited.

The summary of the parameter estimations is provided by Table 5.8.

Table 5.8: Parameter estimation - Summary

Run	Estimated Parameters			Experiments Considered
	$\rho_{*,\,0}$ [a]	α^{ρ_*} [b]	$k^{forw,\,T_{ref}}$ E^{forw} [c]	
I	yes			1_1-1_3, 4_1-4_3, 6_1, 6_5, 7_1, 7_27, 7_46
II	yes	4, 6, 7		1_2, 4_1, 6_1, 6_5, 7_1, 7_27, 7_46
III	yes	4, 6	7	1_1-1_3, 4_1-4_3, 6_1, 6_5
IV		4, 6	2, 7	1_1-1_3, 4_1-4_3, 6_1, 6_5
V		2, 3		1_1-1_3, 2_1-2_6, 3_1, 3_2, 4_1-4_3, 6_1, 6_3, 6_5
VI		2, 3, 4, 6	2, 5, 7, 8, 13	1_1-1_3, 2_1, 2_3-2_5, 3_1, 3_2, 4_1-4_3, 6_3, 6_5

[a] Included site density in the estimation
[b] Catalyst reference activity's loading number
[c] Forward activation energy and constant at T_{ref}'s step number

6. Model Extensions

In this section, the potential to extend Stegelmann et al.'s [2] model beyond the current scope is explored.

This work focuses on applying detailed surface science deduced kinetics within the complex environment that is a multitubular reactor. The advantages of this reaction scheme successfully modelling the reactor's outlet are numerous. These advantages expand further if the model is considered universally applicable.

The benefits of creating this platform include the possibility of optimising the reactor's feed or operating conditions or even changing the process (due to safety concerns or others). It could also be useful in a control strategy, by predicting the effect of specific disturbances with high fidelity.

The applications listed are serviceable within an industrial setting. It then became apparent that enhancing the model with other developments that are indispensable in a plant would be an imperative augmentation. Particularly, since a model without these alterations would be unsuitable for most of the former applications.

The present considerations encompass the moderator effect and the catalyst deactivation. The original literature scheme was used as starting point.

6.1 Moderator Effect

This section aims to include the effect of a moderator/modifier in the scheme proposed by Stegelmann et. al. [2]. The *Literature Review* (chapter 2) briefly explained the role of these moderators in EO production. Nowadays, the use of chlorine-base modifiers is fairly widespread. It may be stated that rare are the cases which do not use this strategy to increase overall yield from the raw materials and render the process more profitable. Being a crucial aspect in reactor's performance and optimisation, this factor must be considered in the scheme.

These compounds are not considered promoters, since they do, in fact, inhibit the reaction (lower conversion) [68–70]. Yet, they are added consistently to reactor's inlets, due to their ability to increase the selectivity to the 90% threshold[1] [71]. These chlorine compounds (VCM, EDC, etc) are added in vestigial amounts to the streams (few ppm), and still have a substantial impact [14, 71].

As a case study, Vinyl Chloride (VCM) was studied.

The goal of this work was to insert this effect as a physical phenomenon (non-empirical) to maintain consistency with the overall tone of the scheme. However, as was underlined in chapter *2. Literature Review*, there is no universal agreement in the scientific community of how the modifiers operate.

The possible mechanisms in which VCM may operate and are simultaneously applicable to the current surface reaction mechanism can be divided into two branches: adsorption and Ag-bonding.

6.1.1 Competitive Adsorption

Competitive adsorption was the first option examined. Chemical adsorption of VCM on an active site is a realistic scenario. Inhibition through chemisorption is a common reaction scheme contribution.

[1] Valid for promoted catalysts which show a 80% selectivity before this addition [22, 24].

In the current mechanism, it is the case for ethylene, which adsorbs on free active sites (*). C_2H_4* may be seen as a suppressor, since it is not an active species and it does not generates an active species; it merely occupies free sites, thus limiting their availability.

Since the presence of VCM is said to both increase the selectivity and decrease conversion, the purpose was to find an adsorption that met these two goals. The most potential was accommodated by the oxide sites (O*). The incorporation of a step 18 (shown below) would represent the adsorption of the moderator on the vacant oxide sites.

$$\text{VCM (g)} + \text{O*} \rightleftharpoons \text{VCM/O*} \tag{6.1}$$

Adsorption on the oxide sites causes the coverage of O* to decrease by generating a new surface species, VCM/O*. By analysing the reaction scheme (Fig. 5.1), it may be observed that the decrease in O* coverage decreases step 4, which is the reaction that defines the consumption of ethylene (since step 11 is ate equilibrium), thus achieving the first goal.

Another observation is that steps 10 and 14 are highly dependent on O* coverage, consuming 6 and 5 O*, respectively. These two reactions are the steps which produce the adsorbed combustion products (CO_2* and H_2O*). Therefore, decreasing these steps increases the selectivity by inhibiting the combustion reactions.

Furthermore, steps 12 and 13 are also inhibited (in a lower extent) by the decrease of oxide coverage. These steps (along with step 14), form the path for ethylene combustion, which is an unwanted side reaction, increasing once more the selectivity. Finally, the low coverage of oxides would promote the desorption of ethylene oxide (since it produces a vacant O*), also increasing the selectivity.

Different adsorption constants and activation energies for the reaction shown as step 18 were tested. These were performed under a Global Systems Analysis (GSA). The GSA entity in the gPROMS enables two different options: sensitivity analysis and uncertainty analysis.

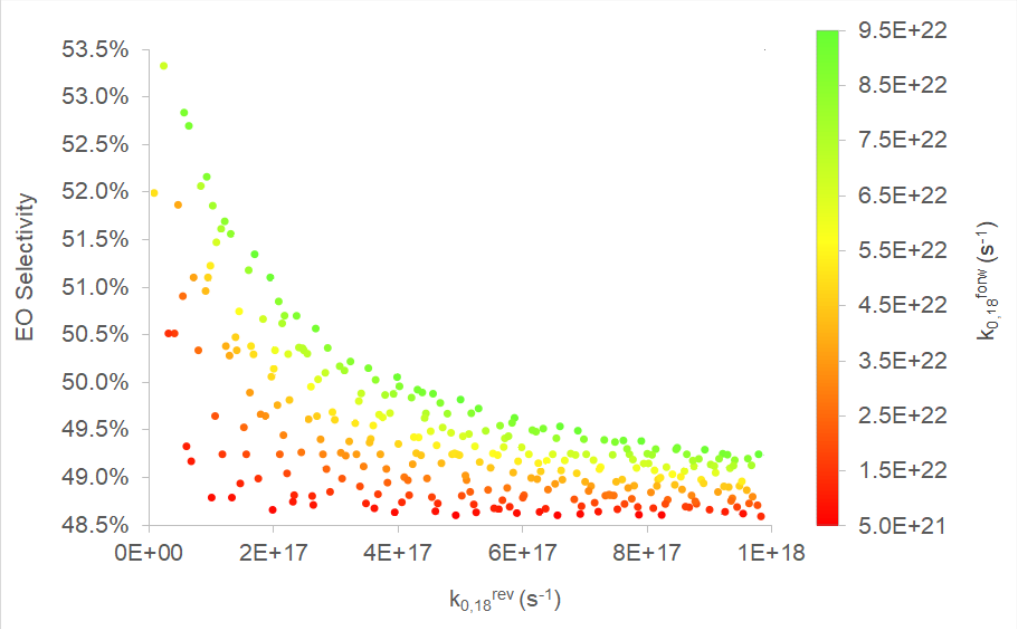

Figure 6.1: Step 18's pre-exponential constants GSA on the EO selectivity

After choosing which variable(s) are to be varied (*factors*), the *responses* must also be selected (variables whose factor's influence is to be observed). A random uniform distribution within the variable bounds may be selected. Additionally, discrete sets may be chosen, as well as other distributions.

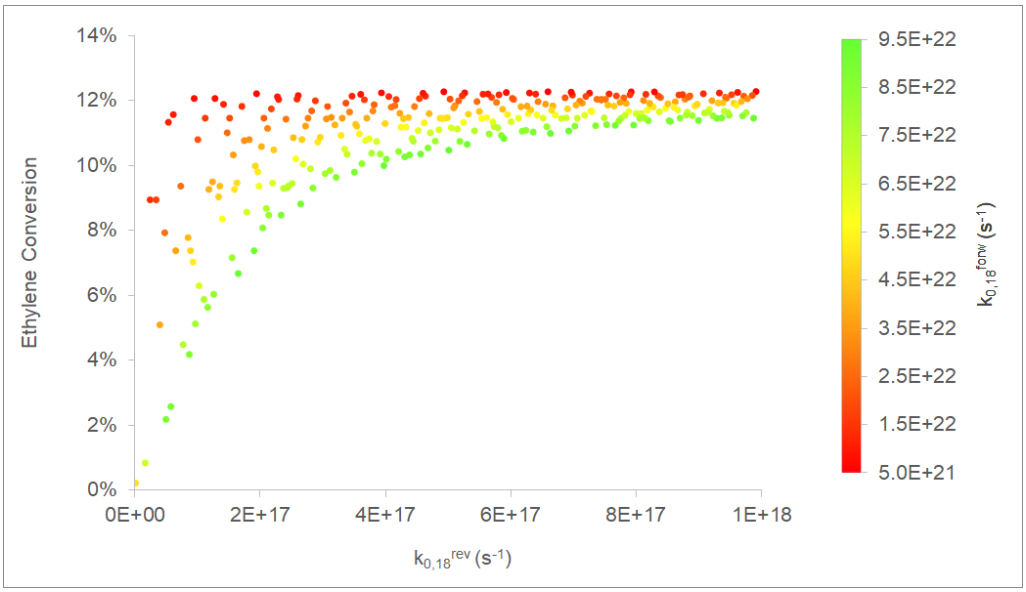

Figure 6.2: Step 18's pre-exponential constants GSA on the ethylene conversion

The tested constants are visible in Fig. 6.1 and 6.2. Although the proposed adsorption gathered all the conditions, the simulations were not satisfactory. The simulations showed that lowering the O* coverage had a much more severe impact on ethylene conversion than on EO selectivity. It was observed that the conversion reached values below 1% before any real change in the selectivity could be registered. Even so, the values of selectivity were still far below what was expected.

At this level of low conversion, artificial increases in the selectivity may be reported, caused by a denominator which approaches 0. Furthermore, industrial values report selectivity increasing to 90% (for promoted catalysts), while the conversion remains in the 7-15% window [71]. When analysing the results, several factors were outlined.

Step 4 is determined solely by the availability of oxide sites, since there is an excess of ethylene present. This is closely related to oxygen being the limiting reactant and explains the denoting change in the conversion.

Secondly, steps 10 and 14 are not actually dependent on the availability of oxide sites, hence the sharp decrease in these steps being unachievable. The reason for which these steps do not depend on O* availability was later allocated to their irreversible nature. This attribute has been discussed in greater depth in subsection *5.1.2. Validity of Model Parameters*. Markedly high forward constants (in the 10^{20} s^{-1} order of magnitude) have been set for these steps, rendering them virtually irreversible.

Other adsorptions were attempted as well. Specifically on free active sites (*), or on unwanted intermediates (e.g. CH_2CHOH/O^*, CH_2CHO/O^*). However, for theses alternatives, there were lower expectations, since none of them had the potential of changing so many steps in the same direction, as had the O*.

Although unsuccessful, the simulation of VCM adsorbing on oxide sites breeds interesting questions. Namely, is the path drawn by the authors for ethylene combustion the best approach? Surely, it is fairly adequate to describe the surface reactions. But, the work done with the surface reaction suggests that the crucial point of the original mechanism is that it included both the path of ethylene and ethylene oxide combustion.

However, perhaps if the correct ethylene combustion intermediates were to be determined (and the reaction parameters accordingly), the oxide sites adsorption would most certainly be an adequate solution to the moderator effect. Nevertheless, one must also consider the alternative that the original reaction scheme proposed by Stegelmann et al. [2] is, in fact, correct. In this note, the best approach is to move on to the

Ag-bonding phenomenon.

6.1.2 Ag-Bonding

In this approach, VCM works as a surrogate for subsurface oxygen, providing the silver-oxygen (atomic) intermediate the electrophilic character that promotes epoxidation. This theory has been proposed by literature [8, 15, 16, 18].

The alternative step 18 is presented by eq. 6.2. It should be emphasised that this is not an adsorption on a free site.

$$\text{VCM (g)} + * \rightleftharpoons \text{VCM}* \tag{6.2}$$

Incorporating the electrophilic effect provided by the VCM is more trying. In theory, VCM-Ag bonding would promote some steps and inhibit others. The proposed effect is simple in theory, but too complex to apply at this stage.

The premise is that all the steps which involve * in the original scheme, develop a twin step, identical to the originals, but using VCM*. These steps would have different temperature dependence and rate constants. The challenge is presented by this astronomical amount of new parameters suggested by this proposal: 18 new steps (17 twins and the step presented by eq. 6.2) with 4 sets of parameters each (forward and reverse activation energies and pre-exponential constants).

To apply this proposal at this stage would result in a highly-empirical model, since the number of added parameters is hefty, with no known constraints. It remains as a suggestion that will be further detailed in chapter *8. Future Work*.

6.2 Catalyst Deactivation

The model had to be adapted to support the loss of activity with time. This concept is known as the catalyst's deactivation and, as mentioned previously, is a decisive consideration in sizing a reactor.

The deactivation of a catalyst may have various causes. Poisoning or deposition on the surface of the catalyst, changes in oxidation state of the catalyst's metals and sintering, are common examples [72]. Although all the previous types of decay may impact the present catalyst, the latter is the most predominant effect [73, 74]. For this reason, a sintering instigated deactivation was added to the model.

It would be interesting to model deactivation considering all the previous effects. For example, acetylene has been reported to poison the EO catalyst [72, 75], and thus its feed content must be monitored. However, to isolate each one, extensive data regarding experiments with different feed composition, feed impurities, temperatures, among other factors would be needed.

Including all the effects would add numerous parameters to an already substantial number of parameters required to tune the deactivation kinetics. Thus, the outcome would be a highly-empirical model, brought upon by an excessive amount of parameters to be fitted. Thus, the solution was to focus solely on sintering.

Sintering is a temperature activated phenomenon, which promotes the formation of particle clusters, decreasing metal dispersion in the catalyst. The Ag/α-alumina catalyst is exposed continuously to very high temperatures for a prolonged period of time in the ethylene oxide production process, hence the sintering effect being prominent.

An advantage of using a detailed model is, once again, highlighted by this situation. In other models deactivation would be included directly into the rate expression(s). Although this would be computationally

less demanding, the oversimplification rids the expression of what could be an opportunity to allocate scientific meaning to parameters.

In the present case, the loss of dispersion (caused by sintering) may be allocated to the parameter site density. Since this model parameter represents the number of free active sites available to adsorb (*), these will naturally decrease in number (of availability) if the clusters prevent molecules from contacting with all the metal particles.

A standard gPLE, proposed by Bartholomew [76], was used:

$$\frac{\partial \alpha}{\partial t} = k_d(\alpha - \alpha_{terminal})^m \tag{6.3}$$

$$k_d = k_{d,0} e^{-\frac{E_d}{R}\cdot(\frac{1}{T}-\frac{1}{T_{ref}})} \tag{6.4}$$

in which α represents the catalyst activity, $\alpha_{terminal}$ is the terminal activity, k_d is the deactivation kinetic constant (which follows a standard Arrhenius temperature dependence, eq. 6.4), and m is the deactivation rate order.

As one may observe, this expression accounts for the deactivation being a temperature promoted occurrence. Higher temperatures result in higher deactivation rates which is compatible with sintering. This expression has another important factor: terminal activity. Contrary to reality, many deactivation expressions consider that the activity of the catalyst can reach 0. This expression, however, considers an end-of-life activity. An activity to which the decaying catalyst tends, observed for industrial catalysts [27, 73]. Nevertheless, even with a residual activity, the loss of efficiency of the process is notorious, hence the frequent replacement of catalyst (2 years for highly selective catalysts [6]) adopted by plants.

More complex expressions have been attempted, in which the microkinetics of particle sintering were modelled. The application of this model in EO production had limited success [74].

By applying the previous expression to the site density, a new variable is generated:

$$\rho_* = \rho_{*,0} \cdot \alpha^{\rho_*} \tag{6.5}$$

Interestingly, a wide number of implications are drawn from the previous expression. For once, the site density becomes a distributed variable, since α^{ρ_*} is temperature-dependent, and temperature varies along the bed. Secondly, at time 0 the activity of the catalyst is defined using the scalar $\rho_{*,0}$ and the $\alpha_{t=0}^{\rho_*}$. The latter has been formerly introduced as the catalyst reference activity ($\alpha_{ref}^{\rho_*}$).

Once deactivation had been inserted in the model, preliminary values had to be given to the new parameters. Three sets of parameters proposed by Zhou and Yuan [25] were tested (Table 6.1). The value of m was fixed as 2 for this is the most common deactivation rate order and simultaneously the one used in Zhou and Yuan's article [25].

Table 6.1: Zhou and Yuan's [25] proposed deactivation kinetics

Option	$k_{d,0}$ (months^{-1})	E_d (kJ mol^{-1})	$\alpha_{terminal}$
A	4 x 10^{11}	120	0.3
B	4 x 10^{7}	80	0.3
C	2 x 10^{3}	40	0.3

Upon simulation testing, all three options were considered unviable since the decay was too rapid (Fig. C.1, Appendix C). The standards for the speed of decay were set using the article in question [25].

It is not entirely surprising that these parameter values would not be suited for the given model, since they were initially determined for deactivation rates applied to global rate expressions. In detailed kinetics, changes in key parameters (as is this case of site density) have a very significant impact in the overall scheme, as had been reported in subsection *5.1.3. Site Density*. These sensitive parameters must therefore deactivate very gradually.

To continue the sensitivity analysis on the model's potential extension (deactivation), the site density deactivation constant pre-exponential factor ($k_{d,0}^{\rho_*}$) was fixed with option A's value and possible values for $E_d^{\rho_*}$ were examined. The method to find a feasible $E_d^{\rho_*}$, was set in comparison with the deactivation article [25]. The article showed the increase in coolant temperature with time. Increasing coolant temperature is a commonly employed strategy in plants to maintain the conversion as the catalyst deactivates progressively.

In Zhou and Yuan's paper, it is stated that the coolant must increase approximately 35℃ in 4 years to compensate for the loss in activity. Thus, a simulation was run which used constant conversion, and replaced this degree of freedom with the inlet temperature of the coolant. The activation energy that yielded the decay corresponding to a 35℃ in 4 years was then determined.

The value obtained was 155 kJ mol^{-1}. In Appendix C the graph which show that this activation energy follows the desired trend may be observed (Fig. C.2). The values outlined for the parameters are simply preliminary values to evaluate the model's capabilities.

An analysis on the effects of this deactivation energy to the KPIs was also performed. This analysis used constant coolant temperature (Fig. 6.3).

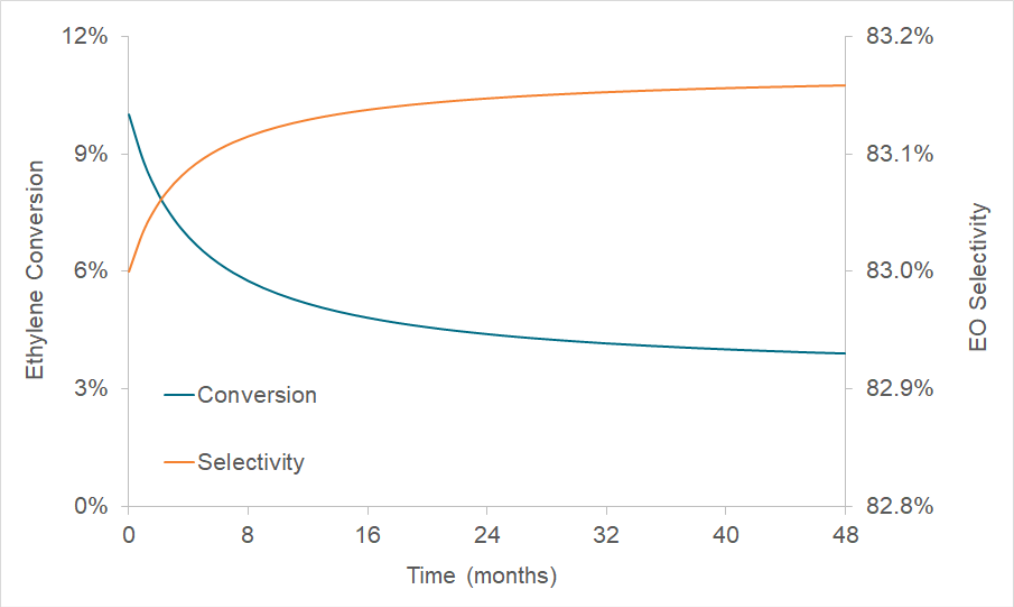

Figure 6.3: Change in the conversion and selectivity due to site density deactivation using $k_{d,0}^{\rho_*}$ = 4 x 10^{11} months^{-1} and $E_d^{\rho_*}$ = 155 kJ mol^{-1}

There is a visible decrease in conversion, as intended. Its trend is within expected, for it reaches the 5% deactivation barrier. Most importantly, there is only a residual change in the selectivity (increases slightly, approximately 0.15 pp). Reports on the deactivation having a discernible effect on the selectivity have been seen throughout literature [27, 72, 73]. Ergo, the need for a second handle (that will tune the selectivity) arises. A parameter estimation phase would uncover if this second handle is truly required, or if this residual effect is considered sufficient. Nevertheless, the handle should be set in place in case it might be needed.

The expression used in eq. 6.3 was used once more, in this instance to deactivate the combustion reaction via step 8. It has been previously mentioned (subsection *5.1.4.Selectivity*) that the ratio between the reaction rate for steps 7 and 8 is crucial in defining the selectivity.

In this note, deactivating the isomer branching (steps 7 and 8) intends to enhance the selectivity in the decaying catalyst.

$$r_8 = r_{8,0} \cdot \alpha^{comb} \tag{6.6}$$

Three deactivation energies (using similar values to the ones obtained for site density deactivation) were tested for the present deactivation. The pre-exponential factor for the combustion deactivation was set to the same value as the site density's.

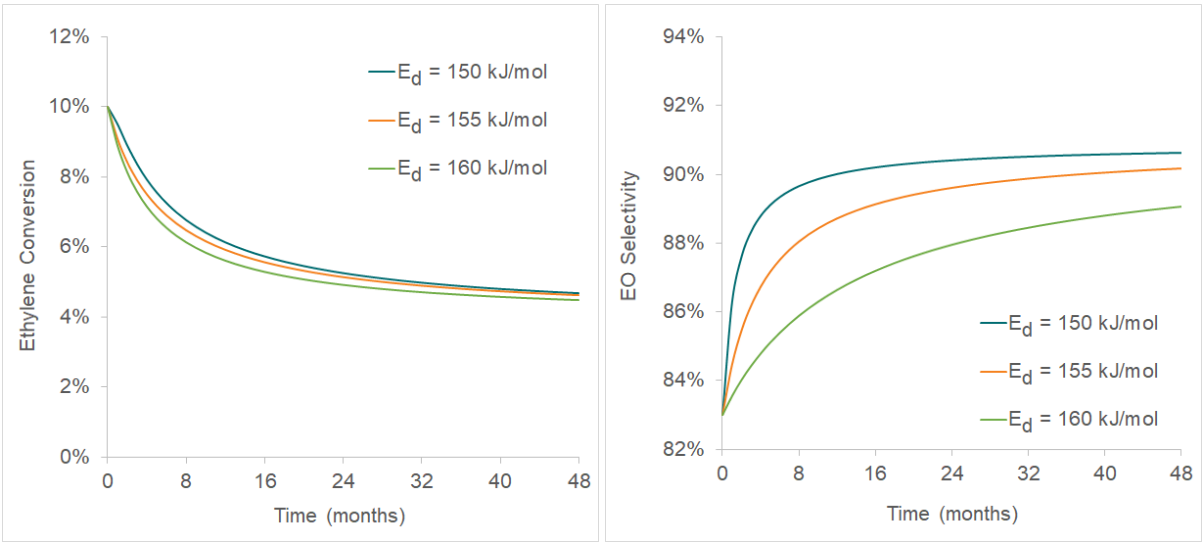

Figure 6.4: Change in the conversion and selectivity due to combustion deactivation using $k_{d,0}^{comb}$ = 4 x 10^{11} months^{-1} and E_d^{comb} = 150, 155 and 160 kJ mol^{-1}

The simulation results (Fig. 6.4) show positive outcomes, which may be observed firstly on the conversion. The conversion graph shows a nearly identical behaviour for the various deactivation activation energies tested. Thus, it may be reported that the handle selected for the selectivity deactivation will not have a significant influence on the conversion; which facilitates the tuning of these parameters since there is little internal interference.

The second observation uses the selectivity graph as visual aid. It is possible to identify that the activation energies shown have all marked impacts on the present KPI. Yet, they all follow utterly distinct trends to which the catalyst reaches its terminal selectivity.

Both these observations lead to the conclusion that if a handle on the selectivity is considered advantageous, the proposed strategy is successful in adapting to a plethora of deactivation trends. Furthermore, these two handles may be easily employed, demanding merely experimental data.

7. Conclusions

Ethylene oxide is a product with a growing market demand. Its potential stems from its wide applicability, since it is an intermediate for the production of many other chemicals. Its main derivative is ethylene glycol. Ethylene oxide is obtained through ethylene partial oxidation (epoxidation), and has as side products the total oxidation outputs, carbon dioxide and water.

Modelling is a potent and extremely versatile tool. It enables the sizing of equipment, the optimisation of conditions, and the creation of control strategies. Particular attention must be given to modelling the reactor, since this is often the core of a process. Most reactor modelling approaches have focused on fluid dynamics. Indeed this has been the major tactic for ethylene epoxidation [7, 43, 77, 78]. Fluid dynamics are essential for the prediction of the reactor's non-ideal behaviour. Yet, there are other equally important matters which should not to be overlooked. This work sheds light on this issue by using microkinetics to describe the reactions that take place within the reactor.

Rate expressions based on Langmuir-Hinshelwood formulations, power-laws or equivalents are the usual treatment for the reaction kinetics. This approach is sufficient for many reactions. However, due to its complexity, catalytic partial oxidation reaction modelling is improved by the use of microkinetics. This has previously been proven with methanol partial oxidation [1].

A mechanism for ethylene epoxidation was selected from literature. The reaction scheme was proposed by Stegelmann et al. [2]. The kinetics were tested in a stand-alone environment and then transferred into more complex setting.

The microkinetics were simulated within gPROMS ProcessBuilder, using the Advanced Model Library for Fixed-Bed Catalytic Reactors. Both the catalyst pellet distributed and lumped model were tested. The lumped model was considered sufficient for the majority of the analysis. These approximations reduced the computational demand of the model, with negligible decrease in precision of the model predictions.

A flowsheet was assembled to resemble an industrial reactor set-up, additionally using coolants and an inert bed. The flowsheet was used to carry out a sensitivity analysis. The aim was to address the limitations and potential of the model. These limitations/potential were measured by evaluating if the model could obtain values of the selectivity and conversion observed in the industry. Additionally, the corresponding trends were examined for their viability.

The simulation of the reaction scheme with literature parameters showed a 52% EO selectivity. This value was found consistent, since it is similar to the value registered for unpromoted catalysts in the absence of moderators (55%) [2, 24]. Subsequently, it was proven that typical selectivity values for promoted catalysts are achievable using this reaction scheme simply by tweaking $\text{Ratio}_{7/8}$. For example, by changing this ratio from 0.03 to 0.082, a 75% EO selectivity is reached (23 percentage points higher than the unpromoted catalyst), while maintaining a constant conversion by adjusting site density to 59 µmol.

An analysis of the site density and the reacting temperature showed there were optimal values to maximize the conversion. However, operating at the optimal point may not be the best scenario, since selectivity must be accounted into the optimization of the reactor's performance. Using literature parameters, the optimal site density and temperature were determined as 111 µmol and 258℃, respectively. Furthermore, one additional

constraint must be taken to account when selecting the operating reacting temperature: the reacting mixture must remain outside the flammability limits, as a safety measure. The site density is equally implicated in the latter statement.

The sensitivity analysis culminated in determining the rate-limiting steps in Stegelmann et al.'s model [2]: 2, 5, 7, 8 and 13. This observation was then corroborated by literature [43].

The next stage was a parameter estimation, in which the RDSs played a decisive role. It was performed using experimental data provided by Petkim Petrokimya Holding A.Ş.. The aim of these estimations was to obtain a model adapted to industrial catalysts.

The original model was fitted using pure silver. To meet the specifications of an industrial setting, the model was reparameterised using a promoted silver dispersed in α-alumina catalyst. The parameter estimation's Run IV obtained a simplified model which removed the ethylene oxide combustion route. $\alpha_{ref,4}^{\rho_*}$, $\alpha_{ref,6}^{\rho_*}$, $k_2^{forw,\,T_{ref}}$, $k_7^{forw,\,T_{ref}}$, E_2^{forw}, and E_7^{forw} were estimated successfully, with a tight confidence interval (Table 5.4). However, Run V showed that the simplified model was only applicable to a particular feed specification, predicting accurately for a wide range of temperatures. The added catalyst loadings' outputs were predicted less accurately (different feed), yielding an objective function of 2445.39.

Run VI estimated E^{forw} and $k^{forw,\,T_{ref}}$ for all the rate-limiting steps: 2, 5, 7, 8, and 13. The $\alpha_{ref}^{\rho_*}$ for catalyst loadings 2, 3, 4, and 6 were also estimated (Table 5.7). The outcome was a overall better prediction for the various loadings, obtaining a substantially smaller objective function, 268.07[1]. The improvement is specially visible for the EO dry outlet; for example, for catalyst loading 2, the standard deviation decreased from 0.2% (Run V) to 0.1% (Run VI).

Equally important was to introduce other effects to the model which are ubiquitous in the industry. For this purpose, the last phase of this work investigated feasible extensions to the current model. Firstly, the moderator effect was considered of the utmost relevance. Moderators are being added to the feed to improve the overall yield in ethylene oxide, hence the need to include this effect in the enhanced model. A discussion on conceivable approaches to incorporate this phenomenon was completed. Competitive adsorption and Ag-bonding were selected as the most feasible options.

Studying the implementation of catalyst deactivation in the model equally suited the objective of obtaining a comprehensive industrial reactor model, since deactivation is a source of concern in this process. Deactivation is commonly balanced with coolant temperature elevation to maintain equal conversion in time. These efforts are a short-term solution, to extend catalyst lifetime before replacement becomes imperative. A deactivation expression was developed for the current microkinetic model. A sensitivity analysis was performed to test the quality of the incorporated effect. The deactivation was inserted in the model with success, and viable kinetic parameters were suggested using generic data. The site density deactivation was found reasonable when using $k_{d,0}^{\rho_*}$ = 4 x 10^{11} months^{-1} and $E_d^{\rho_*}$ = 155 kJ mol^{-1}. These values were selected to reproduce the Zhou and Yuan's [25] observed 35℃ coolant temperature increase in 48 months. These parameters correspond to a drop in conversion from 10% to 4% and negligible change in EO selectivity at constant coolant temperature.

Values for the combustion deactivation were tested to observe if different trends are achievable for the selectivity using distinct E_d^{comb} values (150, 155 and 160 kJ mol^{-1}), with $k_{d,0}^{comb}$ = 4 x 10^{11} months^{-1}. EO selectivities of 91%, 90%, and 89% were obtained (respectively) at the end of the 48-month time horizon. The contribution of the combustion deactivation on the conversion decrease was considered negligible compared to the site density's. The main conclusion was that these three combustion deactivation activation energies produce very different plots, thus demonstrating that the selectivity trends from future data are attainable.

Overall the goal of this work was completed. Microkinetics were simulated within a high-fidelity reactor model. Several conclusions were drawn from the various simulations. Moreover, the model was enhanced to meet the specifications of the industrial production of ethylene oxide.

[1] Note that this value should not be directly compared to Run V's value because three experiments were removed and the variance model was tightened.

8. Future Work

The current work has advanced the knowledge of the ethylene epoxidation reaction scheme. This has proved to be a potent advantage in modelling of this process. Nonetheless, there are many related complementary studies which would benefit the scientific community.

8.1 Surface Reaction Microkinetics

This work adapted Stegelmann et al.'s model [2] to be applicable to an industrial catalyst and conditions. This adaptation was established through parameter estimations using experimental data. Validation of these estimated parameters with other experimental trials would prove the quality of the enhanced model. This had been the objective of *Run V* of the *Parameter Estimation*, yet the explained concerns prevented from achieving this goal.

Adding trials which co-feed EO in the absence of ethylene to the parameter estimation would also help verify the extent of the ethylene oxide combustion, and its corresponding contribution to the CO_2 and water production. This would further validate the estimated parameters.

Additionally, to obtain a clear idea of the ethylene combustion route, supplementary experiments could be performed to trace intermediates. This would substantiate the outlined route or supply an alternative viable explanation. If an alternative route is outlined, the kinetic parameters should be determined using the original method elaborated by Stegelmann et al. [2], statistical thermodynamics using gas molecules and adsorbates.

In the *Preliminary Analysis*, the scheme was tested within a multitubular catalytic fixed bed reactor. That section was successful in discriminating the potential and limitations of the model. Given that the parameters have now been refined, it would be intriguing to test their quality against industrial data. With industrial data of the component and temperature profiles, a comparison could be made between the performance of the detailed kinetics against the conventional rate-expression models. Although these models work adequately to predict the KPIs, presumably, the current model would match profiles in a much higher quality. It would be advisable to test this assumption.

By attesting the superiority of the detailed kinetics (in comparison to rate expressions), this analysis would value the microkinetics despite its complexity-driven disadvantages.

Once the proposed parameters are validated, this reaction scheme could be used to optimise the reactor's performance (temperature, pressure, feed composition, etc.) or to elaborate a control scheme.

8.2 Moderator Effect

Future work with this model could consist in testing the Ag-bonding theory for VCM moderation. The starting point for determining the sets of parameters is suggested to be the values of the original model. Preferably, more data on surface science could be collected to prove/disprove this theory, along with possible intermediates and adsorption enthalpy values, before entering this stage.

Van Hoof et al. and other authors [68, 79, 80] have recently discovered (through STEM analysis) the importance of the size and shape of the silver particles in the epoxidation reaction. This fact had also previously been underlined in section *6.2. Catalyst Deactivation* of this work. Furthermore, they account for VCM's effects as suppressor of void formation. These vacant sites (voids) had been created by oxygen adsorption on the external surface and on grain boundaries.

Van Hoof et al. [79] surface science input suggest that VCM is a poison. Thus, this work proposes that employing the moderator effect may be a combined project with the catalyst deactivation. The VCM poisoning would then be reversible deactivation, to be applied to the site density. Thus, it would be preferable to create a more complex formulation of the site density variable, to account for shape and size of silver particles.

Upon validating the proposed model extensions, this model could be used to optimise the reactor's performance. This could include finding the optimal quantity of moderator to add to the reactor's feed. Literature reports the existence of an optimal value for the moderator in the feed [69, 70, 73], dependent on the moderator coverage of the catalyst's surface.

8.3 Catalyst Deactivation

Catalyst deactivation was one of the proposed model extensions. It was demonstrated that the reaction scheme had the ability to incorporate this effect in a non-empirical form.

Although the deactivation expressions were tested within the reactor model environment, it would be interesting to obtain the correct parameterised expressions through experimental data. A first approach could consist in applying the presented expressions to the experiments considered in the *Parameter Estimation* and conclude if the fit could be improved by inserting catalyst deactivation. The estimations should begin by using merely site density deactivation, and only add the combustion deactivation if the selectivity trends are seen to be notably modelled worse than the conversion.

In future studies, numerous lengthy experiments, which cover a wide range of temperatures, would be required to perfect the tuning of the deactivation temperature dependence. From the quality of the fit, interesting illations could be drawn. Namely, whether the proposed deactivation expressions are qualified to model the catalyst's decay, or if other aspects have an acute impact in deactivation as well.

As was mentioned previously, changes in oxidation state can lead to catalyst decay. Due to the oxidizing environment that the catalyst is exposed to daily (oxygen rich media), this may be a relevant effect to consider [73, 81]. This hypothesis may be authenticated by exposing the catalyst to different ranges of oxygen composition. If both the moderator effect (discussed previously) and the two deactivation handles incorporated in the reaction mechanism are not sufficient to predict the reactor's outlet, then it may be concluded that other forms of reconstruction of the catalyst surface have occurred.

Moreover, due to the uncertainty of how the moderator interferes with the surface reaction, the catalyst undergoing changes due to its presence is a valid possibility [72, 75, 82]. This last theory may be tested by exposing the catalyst to varying degrees of moderator content in the feed, using also experiments of different duration. If both the moderator effect (discussed previously) and the two deactivation handles incorporated in the reaction mechanism are not sufficient to predict the reactor's outlet, then it may be concluded that the decay of the catalyst is also promoted by the presence of moderators.

References

[1] A. Andreasen, H. Lynggaard, C. Stegelmann, and P. Stoltze, "Simplified kinetic models of methanol oxidation on silver," *Applied Catalysis A: General*, vol. 289, no. 2, pp. 267–273, Aug. 2005.

[2] C. Stegelmann, N. C. Schiødt, C. T. Campbell, and P. Stoltze, "Microkinetic modeling of ethylene oxidation over silver," *Journal of Catalysis*, vol. 221, no. 2, pp. 630–649, Jan. 2004.

[3] L. Schmidt, M. Huff, and S. S. Bharadwaj, "Catalytic Partial Oxidation Reactions and Reactors," *Chemical Engineering Science*, vol. 49, no. 24, pp. 3981–3994, Dec. 1994.

[4] A. Nagy and G. Mestl, "High temperature partial oxidation reactions over silver catalysts," *Applied Catalysis A: General*, vol. 188, no. 1-2, pp. 337–353, Nov. 1999.

[5] G. Eigenberger, "Fixed-Bed Reactors," in *Ullmann's Encyclopedia of Industrial Chemistry*, 6th ed. Wiley, Jun. 2000.

[6] S. Rebsdat and D. Mayer, "Ethylene oxide," in *Ullmann's Encyclopedia of Industrial Chemistry*, 7th ed. Wiley, Oct. 2011.

[7] S. Aryana, M. Ahmadi, V. Gomes, J. Romagnoli, and K. Ngian, "Modelling and Optimisation of an Industrial Ethylene Oxide Reactor," *Chemical Product and Process Modeling*, vol. 4, no. 1, Jan. 2009.

[8] O. Deutschmann, H. Knözinger, K. Kochloefl, and T. Turek, "Heterogeneous Catalysis and Solid Catalysts, 3. Industrial Applications," in *Ullmann's Encyclopedia of Industrial Chemistry*, 7th ed. Wiley, Oct. 2011.

[9] "Chemical Economics Handbook," IHS Markit, Tech. Rep., October 2018.

[10] N. Luo, W. Du, Z. Ye, and F. Qian, "Development of a Hybrid Model for Industrial Ethylene Oxide Reactor," *Industrial & Engineering Chemistry Research*, vol. 51, no. 19, p. 6926–6932, May 2012.

[11] H. H. Kung, "Kinetic model of the epoxidation of ethylene," *Chemical Engineering Communications*, vol. 118, no. 1, pp. 17–24, Nov. 1992.

[12] P. Borman and K. R. Westerterp, "An Experimental Study of the Kinetics of the Selective Oxidation of Ethene over a Silver on α-Alumina Catalyst," *Industrial & Engineering Chemistry Research*, vol. 34, no. 1, pp. 49–58, Jan. 1995.

[13] D. W. Green and R. H. Perry, *Perry's Chemical Engineers' Handbook*, 8th ed. McGraw-Hill, 2008.

[14] A. Eliyas, L. Petrov, and D. Shopov, "Ethylene oxide oxidation over a supported silver catalyst: II. Kinetics of inhibited oxidation," *Applied Catalysis*, vol. 41, pp. 39–52, Jul. 1988.

[15] T. C. Rocha, M. Hävecker, A. Knop-Gericke, and R. Schlögl, "Promoters in heterogeneous catalysis: The role of Cl on ethylene epoxidation over Ag," *Journal of Catalysis*, vol. 312, pp. 12–16, Jan. 2014.

[16] C. Chen, J. Harris, and A. Bhan, "Kinetics of Ethylene Epoxidation on a Promoted Ag/α-Al_2O_3 Catalyst-The Effects of Product and Chloride Co-Feeds on Rates and Selectivity," *Chemistry - A European Journal*, vol. 24, no. 47, pp. 12 405–12 415, Apr. 2018.

[17] M. Özbek, I. Onal, and R. van Santen, "Chlorine and Caesium Promotion of Silver Ethylene Epoxidation Catalysts," *ChemCatChem*, vol. 5, no. 2, pp. 443–451, Feb. 2013.

[18] S. Linic and M. Barteau, "Construction of a reaction coordinate and a microkinetic model for ethylene epoxidation on silver from DFT calculations and surface science experiments," *Journal of Catalysis*, vol. 214, no. 2, pp. 200–212, Mar. 2003.

[19] N. W. Cant and W. K. Hall, "Catalytic oxidation: VI. Oxidation of labeled olefins over silver," *Journal of Catalysis*, vol. 52, no. 1, pp. 81–94, Mar. 1978.

[20] H. Nakatsuji, K. Takahashi, and Z. Hu, "Electron transfer and back-transfer in the partial oxidation of ethylene on an Ag surface: dipped adcluster model study," *Chemical Physics Letters*, vol. 277, no. 5-6, pp. 551–557, Oct. 1997.

[21] P. D. Klugherz and P. Harriott, "Kinetics of ethylene oxidation on a supported silver catalyst," *AIChE Journal*, vol. 17, no. 4, pp. 856–866, Jul. 1971.

[22] D. M. Minahan, G. B. Hoflund, W. S. Epling, and D. W. Schoenfeld, "Study of Cs-Promoted, α-Alumina-Supported Silver, Ethylene Epoxidation Catalysts: III. Characterization of Cs-Promoted and Nonpromoted Catalysts," *Journal of Catalysis*, vol. 168, no. 2, pp. 393–399, Jan. 1997.

[23] M. C. N. A. de Carvalho, F. Passos, and M. Schmal, "Study of the active phase of silver catalysts for ethylene epoxidation," *Journal of Catalysis*, vol. 248, no. 1, pp. 124–129, May 2007.

[24] M. Özbek and R. van Santen, "The Mechanism of Ethylene Epoxidation," *Catalysis Letters*, vol. 143, no. 2, p. 131–141, 02 2013.

[25] X. Zhou and W. Yuan, "Optimization of the fixed-bed reactor for ethylene epoxidation," *Chemical Engineering and Processing*, vol. 44, no. 10, pp. 1098–1107, Oct. 2005.

[26] M. Özbek, I. Onal, and R. van Santen, "Ethylene Epoxidation Catalyzed by Silver Oxide," *ChemCatChem*, vol. 3, no. 1, pp. 150–153, 10 2011.

[27] G. Boskovic, N. Dropka, D. Wolf, A. Brückner, and M. Baerns, "Deactivation kinetics of Ag/Al_2O_3 catalyst for ethylene epoxidation," *Journal of Catalysis*, vol. 226, no. 2, pp. 334–342, Sep. 2004.

[28] J. T. Salmi, M. Roche, J. H. Carucci, K. Eränen, and D. Murzin, "Ethylene oxide - Kinetics and mechanism," *Current Opinion in Chemical Engineering*, vol. 1, no. 3, p. 321–327, Aug. 2012.

[29] Y. Jun, D. Jingfa, Y. Xiaohong, and Z. Shi, "Rhenium as a Promoter for Ethylene Epoxidation," *Applied Catalysis A: General*, vol. 92, no. 2, pp. 73–80, Dec. 1992.

[30] E. P. S. Schouten, P. Borman, and K. R. Westerterp, "Determination of the kinetics of ethene epoxidation," *Chemical Engineering and Processing*, vol. 35, no. 1, pp. 43–55, Jan. 1996.

[31] E. P. S. Schouten, P. Borman, and K. R. Westerterp, "Influence of reaction products on the selective oxidation of ethene," *Chemical Engineering and Processing: Process Intensification*, vol. 35, no. 2, pp. 107–120, Mar. 1996.

[32] R. B. Grant and R. Lambert, "A single crystal study of the silver-catalysed selective oxidation and total oxidation of ethylene," *Journal of Catalysis*, vol. 92, no. 2, pp. 364–375, Apr. 1985.

[33] V. I. Bukhtiyarov, A. I. Nizovskii, H. Bluhm, M. Hävecker, E. Kleimenov, A. Knop-Gericke, and R. Schlögl, "Combined in situ XPS and PTRMS study of ethylene epoxidation over silve," *Journal of Catalysis*, vol. 238, no. 2, pp. 260–269, Mar. 2006.

[34] R. A. van Santen and H. P. C. E. Kuipers, "The mechanism of ethylene epoxidation," *Advances in Catalysis*, vol. 35, pp. 265–321, Jan. 1987.

[35] C. Backx, J. Moolhuysen, P. Geenen, and R. A. van Santen, "Reactivity of oxygen adsorbed on silver powder in the epoxidation of ethylene," *Journal of Catalysis*, vol. 72, no. 2, pp. 364–368, Dec. 1981.

[36] R. A. van Santen and C. P. M. Groot, "The mechanism of ethylene epoxidation," *Journal of Catalysis*, vol. 98, no. 2, pp. 530 – 539, Apr. 1986.

[37] T. E. Jones, R. Wyrwich, S. Böcklein, E. A. Carbonio, M. T. Greiner, A. Y. Klyushin, W. Moritz, A. Locatelli, T. O. Menteş, M. A. Niño, A. Knop-Gericke, R. Schlögl, S. Günther, J. Wintterlin, and S. Piccinin, "The Selective Species in Ethylene Epoxidation on Silver," *ACS Catalysis*, vol. 8, no. 5, pp. 3844–3852, Mar. 2018.

[38] N. Kenge, S. Pitale, and K. Joshi, "The nature of electrophilic oxygen: Insights from periodic density functional theory investigations," *Surface Science*, vol. 679, pp. 188–195, Jan. 2019.

[39] C. Stegelmann and P. Stoltze, "Microkinetic analysis of transient ethylene oxidation experiments on silver," *Journal of Catalysis*, vol. 226, no. 1, pp. 129–137, Aug. 2004.

[40] K. C. Waugh and M. Hague, "The detailed kinetics and mechanism of ethylene epoxidation on an oxidised Ag/α-Al_2O_3 catalyst," *Catalysis Today*, vol. 157, no. 1, pp. 44–48, Nov. 2010.

[41] E. L. Force and A. T. Bell, "The relationship of adsorbed species observed by infrared spectroscopy to the mechanism of ethylene oxidation over silver," *Journal of Catalysis*, vol. 40, no. 3, pp. 356–371, Dec. 1975.

[42] A. Lukaski and M. Barteau, "Investigation of Ethylene Oxide on Clean and Oxygen-Covered Ag(110) Surfaces," *Catalysis Letters*, vol. 128, no. 1, pp. 9–17, Jan. 2009.

[43] B. Partopour and A. Dixon, "Resolved-particle Fixed Bed CFD with Microkinetics for Ethylene Oxidation," *AIChE Journal*, vol. 63, no. 1, pp. 87–94, Jan. 2017.

[44] E. L. Force and A. T. Bell, "Infrared spectra of adsorbed species present during the oxidation of ethylene over silver," *Journal of Catalysis*, vol. 38, no. 1, pp. 440–460, Jun. 1975.

[45] B. Krüger and G. Benndorf, "Ethylene and ethylene-oxide adsorption on Ag(110)," *Surface Science*, vol. 178, no. 1-3, pp. 704–715, Dec. 1986.

[46] W. Liu, A. Eliyas, and L. Petrov, "Influence of feed water vapour on the selective oxidation of ethylene over silver catalyst," *Applied Catalysis*, vol. 61, no. 1-3, pp. 265–274, May 1990.

[47] M. Stoukides and S. Pavlou, "Ethylene oxidation on silver catalysts: Effect of ethylene oxide and of external transfer limitations," *Chemical Engineering Communications*, vol. 44, no. 1-6, pp. 53–74, Jun. 1986.

[48] P. L.Metcalf and P. Harriott, "Kinetics of Silver-Catalyzed Ethylene Oxidation," *Industrial & Engineering Chemistry Process Design and Development*, vol. 11, no. 4, pp. 478–484, Oct. 1972.

[49] A. Eliyas and L. Petrov, "Modelling of the inhibiting effect of carbon dioxide on the selective oxidation of ethene over silver catalyst," *Applied Catalysis*, vol. 62, no. 1, pp. 11–21, Jun. 1990.

[50] R. B. Grant, C. A. J. Harbach, R. Lambert, and S. A. Tan, "Alkali metal, chlorine and other promoters in the silver-catalysed selective oxidation of ethylene," *Journal of the Chemical Society Faraday Transactions 1*, vol. 83, no. 7, pp. 2035–2046, Jan. 1987.

[51] D. Stacchiola, G. Wu, M. Kaltchev, and W. Tysoe, "A reflection–absorption infrared spectroscopic study of the adsorption of ethylene and ethylene oxide on oxygen-covered Ag(111)," *Surface Science*, vol. 486, no. 1, pp. 9–23, Jul. 2001.

[52] B. Krüger and G. Benndorf, "Ethylene and ethylene-oxide adsorption on Ag(110)," *Surface Science*, vol. 178, no. 1, pp. 704–715, Dec. 1986.

[53] M. Shima and H. Takada, "Silver catalyst for production of ethylene oxide, method for production thereof, and method for production of ethylene oxide," Patent 6 153 556, Dec. 28, 2000.

[54] Froment, Bischoff, and D. Wilde, *Chemical Reactor Analysis and Design*, 3rd ed. John Wiley & Sons, 2011.

[55] D. Lafarga, M. A. Al-Juaied, C. M. Bondy, and A. Varma, "Ethylene Epoxidation on Ag-Cs/α-Al_2O_3 Catalyst: Experimental Results and Strategy for Kinetic Parameter Determination," *Industrial & Engineering Chemistry Research*, vol. 39, pp. 2148–2156, Jul. 2000.

[56] Z. Nawaz, "Heterogeneous Reactor Modeling of Industrial Multi-Tubular Packed Bed Ethylene Oxide Reactor using Aspen Custom Modeler," *Chemical Engineering & Technology*, vol. 39, no. 10, May 2016.

[57] L. Petrov, A. Eliyas, and D. Shopov, "Kinetics of ethylene oxidation over a silver catalyst in the presence of dichloroethane," *Applied Catalysis*, vol. 24, no. 1-2, pp. 145–161, Jul. 1986.

[58] V. Russo, T. Kilpiö, J. H. Carucci, M. Di Serio, and J. T. Salmi, "Modeling of microreactors for ethylene epoxidation and total oxidation," *Chemical Engineering Science*, vol. 134, pp. 563–571, Jun. 2015.

[59] L. Gan, H. Wang, B. Zhu, M. Xu, and Z. Wang, "Global kinetics and deactivation of silver catalyst for ethylene oxide synthesis," *Huagong Xuebao/Journal of Chemical Industry and Engineering (China)*, vol. 52, no. 11, pp. 969–973, Nov. 2001.

[60] J. Sauer, N. Dahmen, and E. Henrich, "Tubular Plug Flow Reactors," in *Ullmann's Encyclopedia of Industrial Chemistry*, 7th ed. Wiley, Oct. 2011, p. 3.

[61] Ş. Sarrafi, "Development of Kinetic Model for Industrial Ethylene Oxide Catalyst by Using Model-Targeted Experimentation Approach," Master of Science in Chemical Engineering, Graduate School of Engineering and Sciences of Izmir Institute of Technology, May 2019.

[62] C. T. Campbell and M. T. Paffett, "Model studies of ethylene epoxidation catalyzed by the Ag(110) surface," *Surface Science*, vol. 139, no. 2-3, pp. 396–416, Apr. 1984.

[63] C. T. Campbell and M. T. Paffett, "The role of chlorine promoters in catalytic ethylene epoxidation over the Ag(110) surface," *Applications of Surface Science*, vol. 19, no. 1, pp. 28–42, Nov. 1984.

[64] C. T. Campbell and B. E. Koel, "Chlorine promotion of selective ethylene oxidation over Ag(110): Kinetics and mechanism," *Journal of Catalysis*, vol. 92, no. 2, pp. 272–283, Apr. 1985.

[65] C. T. Campbell, "Chlorine promoters in selective ethylene epoxidation over Ag(111): A comparison with Ag(110)," *Journal of Catalysis*, vol. 99, no. 1, pp. 28–38, May 1986.

[66] C. T. Campbell, "Finding the Rate-Determining Step in a Mechanism: Comparing De Donder Relations with the "Degree of Rate Control"," *Journal of Catalysis*, vol. 204, no. 2, pp. 520–524, Jan. 2001.

[67] C. T. Campbell, "The selective epoxidation of ethylene catalyzed by Ag(111): A comparison with Ag(110)," *Journal of Catalysis*, vol. 94, no. 2, pp. 436–444, Aug. 1985.

[68] E. Hermans, "Caesium and chlorine promotion in the silver particle size dependency and of the ethylene epoxidation," Master of Science in Chemical Engineering, Eindhoven University of Technology, Jan. 2018.

[69] J. Harris and A. Bhan, "Moderation of chlorine coverage and ethylene epoxidation kinetics via ethane oxychlorination over promoted Ag/α-Al_2O_3," *Journal of Catalysis*, vol. 367, pp. 62–71, Nov. 2018.

[70] D. Kamenski, N. V. Kulkova, and D. Bonchev, "A study of chloride moderated silver catalyst," *Reaction Kinetics and Catalysis Letters*, vol. 7, no. 4, pp. 481–485, Dec. 1977.

[71] H. E. Al-Ahmadi and A. S. Padia, "Epoxidation on process with added moderator," Patent 9 221 774, Dec. 29, 2015.

[72] M. Argyle and C. Bartholomew, "Heterogeneous Catalyst Deactivation and Regeneration: A Review," *Catalysts*, vol. 5, no. 1, pp. 145–269, Mar. 2015.

[73] G. Boskovic, D. Wolf, A. Brückner, and M. Baerns, "Deactivation of a commercial catalyst in the epoxidation of ethylene to ethylene oxide—basis for accelerated testing," *Journal of Catalysis*, vol. 224, no. 1, pp. 187–196, May 2004.

[74] X. Zhou and W. Yuan, "Modeling silver catalyst sintering and epoxidation selectivity evolution in ethylene oxidation," *Chemical Engineering Science*, vol. 59, no. 8-9, pp. 1723–1731, Apr. 2004.

[75] H. F. Rase, "Ethylene - Ethylene Oxide," in *Handbook of Commercial Catalysts: Heterogeneous Catalysts*, 1st ed. CRC Press, 2000, pp. 256–260.

[76] C. H. Bartholomew, "Mechanisms of catalyst deactivation," *Applied Catalysis A: General*, vol. 212, no. 1, pp. 17–60, Apr. 2001.

[77] K. Alhumaizi and A. Abahussain, "Analysis and Simulation of Cross-Flow Reactor for Ethylene Epoxidation," *Chemical Product and Process Modeling*, vol. 2, no. 1, pp. 1934–2659, Jan. 2007.

[78] L. Chen, H. Liu, C. Ge, L. Lv, and Q. Xia, "CFD analysis of ethylene epoxidation in a packed-bed membrane reactor," *Journal of Beijing University of Chemical Technology (Natural Science Edition)*, vol. 44, no. 1, pp. 7–12, Jan. 2017.

[79] A. J. F. van Hoof, I. Filot, H. Friedrich, and E. J. M. Hensen, "Reversible Restructuring of Silver Particles during Ethylene Epoxidation," *ACS Catalysis*, vol. 8, no. 12, p. 11794–11800, Nov. 2018.

[80] P. Christopher and S. Linic, "Shape- and Size-Specific Chemistry of Ag Nanostructures in Catalytic Ethylene Epoxidation," *ChemCatChem*, vol. 2, no. 1, pp. 78–83, Jan. 2010.

[81] M. L. Zheludkevich, A. G. Gusakov, A. G. Voropaev, A. A. Vecher, E. N. Kozyrski, and S. A. Raspopov, "Oxidation of Silver by Atomic Oxygen," *Oxidation of Metals*, vol. 61, no. 1-2, p. 39–48, Feb. 2004.

[82] K. Kumbilieva, L. Petrov, Y. Alhamed, and A. Alzahrani, "Reaction Mechanism and Deactivation Modes of Heterogeneous Catalytic Systems," *Chinese Journal of Catalysis*, vol. 32, no. 3-4, p. 387–404, Apr. 2011.

Appendix A: Stegelmann et al.'s Model

A.1 Reaction rates expressions for each step [2]

$$
\begin{aligned}
r_1^T &= f_s \cdot \left(k_1^{forw,\,T} \frac{p_{O_2}}{P_{ref}} \cdot \theta_* - k_1^{rev,\,T} \theta_{O_2^*} \right) \\
r_2^T &= f_s \cdot \left(k_2^{forw,\,T} \theta_{O_2^*} \cdot \theta_* - k_2^{rev,\,T} \theta_{O^*}^2 \right) \\
r_3^T &= f_s \cdot \left(k_3^{forw,\,T} \frac{p_{O_2}}{P_{ref}} \cdot \theta_{O^*}^2 - k_3^{rev,\,T} \theta_{O/O^*}^2 \right) \\
r_4^T &= f_s \cdot \left(k_4^{forw,\,T} \frac{p_{C_2H_4}}{P_{ref}} \cdot \theta_{O^*} - k_4^{rev,\,T} \theta_{C_2H_4/O^*} \right) \\
r_5^T &= f_s \cdot \left(k_5^{forw,\,T} \theta_{C_2H_4/O^*} \cdot \theta_{O/O^*} - k_5^{rev,\,T} \theta_{CH_2CH_2O/O^*} \cdot \theta_{O^*} \right) \\
r_6^T &= f_s \cdot \left(k_6^{forw,\,T} \frac{p_{C_2H_4O}}{P_{ref}} \cdot \theta_{O^*} - k_6^{rev,\,T} \theta_{C_2H_4O/O^*} \right) \\
r_7^T &= f_s \cdot \left(k_7^{forw,\,T} \theta_{CH_2CH_2O/O^*} - k_7^{rev,\,T} \theta_{C_2H_4O/O^*} \right) \\
r_8^T &= f_s \cdot \left(k_8^{forw,\,T} \theta_{CH_2CH_2O/O^*} - k_8^{rev,\,T} \theta_{CH_3CHO/O^*} \right) \\
r_9^T &= f_s \cdot \left(k_9^{forw,\,T} \theta_{CH_3CHO/O^*} - k_9^{rev,\,T} \frac{p_{CH_3CHO/O}}{P_{ref}} \cdot \theta_{O^*} \right) \\
r_{10}^T &= f_s \cdot \left(k_{10}^{forw,\,T} \theta_{CH_3CHO/O^*} \cdot \theta_{O^*}^6 - k_{10}^{rev,\,T} \theta_{CO_2^*}^2 \cdot \theta_{OH^*}^4 \cdot \theta_* \right) \\
r_{11}^T &= f_s \cdot \left(k_{11}^{forw,\,T} \frac{p_{C_2H_4}}{P_{ref}} \cdot \theta_* - k_{11}^{rev,\,T} \theta_{C_2H_4^*} \right) \\
r_{12}^T &= f_s \cdot \left(k_{12}^{forw,\,T} \theta_{C_2H_4/O^*} \cdot \theta_{O^*} - k_{12}^{rev,\,T} \theta_{CH_2CHOH/O^*} \cdot \theta_* \right) \\
r_{13}^T &= f_s \cdot \left(k_{13}^{forw,\,T} \theta_{CH_2CHOH/O^*} \cdot \theta_{O^*} - k_{13}^{rev,\,T} \theta_{CH_2CHO/O^*} \cdot \theta_{OH^*} \right) \\
r_{14}^T &= f_s \cdot \left(k_{14}^{forw,\,T} \theta_{CH_2CHO/O^*} \cdot \theta_{O^*}^5 - k_{14}^{rev,\,T} \theta_{CO_2^*}^2 \cdot \theta_{OH^*}^3 \cdot \theta_* \right) \\
r_{15}^T &= f_s \cdot \left(k_{15}^{forw,\,T} \theta_{OH^*}^2 - k_{15}^{rev,\,T} \theta_{H_2O^*} \cdot \theta_{O^*} \right) \\
r_{16}^T &= f_s \cdot \left(k_{16}^{forw,\,T} \theta_{CO_2^*} - k_{16}^{rev,\,T} \frac{p_{CO_2}}{P_{ref}} \cdot \theta_* \right) \\
r_{17}^T &= f_s \cdot \left(k_{17}^{forw,\,T} \theta_{H_2O^*} - k_{17}^{rev,\,T} \frac{p_{H_2O}}{P_{ref}} \cdot \theta_* \right)
\end{aligned}
$$

Where f_s is the rate factor for the step reaction, r_i^T is the overall reaction rate (s^{-1}) for step i at temperature T, $k_i^{j,\,T}$ is the rate constant (s^{-1}) in the direction j (forward, reverse), p_l is the partial pressure of component l, P_{ref} is the reference pressure and θ_k is the surface coverage of species k.

A.2 Surface coverage material balance of adsorbed species [2]

$$\frac{\partial \theta_{O_2^*}}{\partial t} = r_1 - r_2 \tag{A.1}$$

$$\frac{\partial \theta_{O^*}}{\partial t} = 2\ r_2 - 2\ r_3 - r_4 + r_5 - r_6 + r_9 - 6\ r_{10} - r_{12} - r_{13} - 5\ r_{14} + r_{15} \tag{A.2}$$

$$\frac{\partial \theta_{O/O^*}}{\partial t} = 2\ r_3 - r_5 \tag{A.3}$$

$$\frac{\partial \theta_{C_2H_4/O^*}}{\partial t} = r_4 - r_5 - r_{12} \tag{A.4}$$

$$\frac{\partial \theta_{CH_2CH_2O/O^*}}{\partial t} = r_5 - r_7 - r_8 \tag{A.5}$$

$$\frac{\partial \theta_{C_2H_4O/O^*}}{\partial t} = r_6 + r_7 \tag{A.6}$$

$$\frac{\partial \theta_{CH_3CHO/O^*}}{\partial t} = r_8 - r_9 - r_{10} \tag{A.7}$$

$$\frac{\partial \theta_{C_2H_4^*}}{\partial t} = r_{11} \tag{A.8}$$

$$\frac{\partial \theta_{CH_2CHOH/O^*}}{\partial t} = r_{12} - r_{13} \tag{A.9}$$

$$\frac{\partial \theta_{CH_2CHO/O^*}}{\partial t} = r_{13} - r_{14} \tag{A.10}$$

$$\frac{\partial \theta_{OH^*}}{\partial t} = 4\ r_{10} + r_{13} + 3\ r_{14} - 2\ r_{15} \tag{A.11}$$

$$\frac{\partial \theta_{H_2O^*}}{\partial t} = r_{15} - r_{17} \tag{A.12}$$

$$\frac{\partial \theta_{CO_2^*}}{\partial t} = 2\ r_{10} + 2\ r_{14} - r_{16} \tag{A.13}$$

A.3 Global reaction rates [2]

$$RRate_{O_2} = f_R \cdot \phi \cdot \rho_* \cdot (-r_1 - r_3) \tag{A.14}$$

$$RRate_{C_2H_4} = f_R \cdot \phi \cdot \rho_* \cdot (-r_4 - r_{11}) \tag{A.15}$$

$$RRate_{EO} = f_R \cdot \phi \cdot \rho_* \cdot (-r_6) \tag{A.16}$$

$$RRate_{ALD} = f_R \cdot \phi \cdot \rho_* \cdot (-r_9) \tag{A.17}$$

$$RRate_{CO_2} = f_R \cdot \phi \cdot \rho_* \cdot (r_{16}) \tag{A.18}$$

$$RRate_{H_2O} = f_R \cdot \phi \cdot \rho_* \cdot (r_{17}) \tag{A.19}$$

f_R represents the rate factor, ϕ represents the effectiveness factor and ρ_* represents the site density (mol kg^{-1}).

Table A.1: Stoichiometric coefficients (nu) for the global reaction rates

Components	Reactions					
	O_2	C_2H_4	EO	ALD	CO_2	H_2O
Oxygen	1	0	0	0	0	0
Ethylene	0	1	0	0	0	0
Ethylene oxide	0	0	1	0	0	0
Acetaldehyde	0	0	0	1	0	0
Carbon dioxide	0	0	0	0	1	0
Water	0	0	0	0	0	1

A.4 Literature Parameters [2]

Table A.2: Stegelmann et al. model parameters [2]

	k_0 (s^{-1})		E (kJ mol^{-1})	
	forward	reverse	forward	reverse
Step 1	2.71×10^5	1.1×10^{12}	5.7	47.3
Step 2	4.0×10^{12}	8.0×10^{14}	75.0	157.5
Step 3	2.0×10^7	1.3×10^{15}	20.0	96.9
Step 4	7.2×10^7	2.2×10^{11}	0.0	37.1
Step 5	9.0×10^{14}	5.3×10^{14}	112.0	183.3
Step 6	1.95×10^8	4.8×10^{12}	0.0	39.1
Step 7	1.13×10^{13}	2.11×10^{12}	95.0	93.5
Step 8	9.0×10^{12}	4.5×10^{10}	95.0	204.3
Step 9	2.9×10^{13}	2.6×10^9	41.9	4.4
Step 10	2.0×10^{20}	5.3×10^{13}	11.0	791.5
Step 11	7.2×10^7	2.2×10^{11}	0.0	30.1
Step 12	4.0×10^{11}	3.1×10^{14}	32.0	42.8
Step 13	2.6×10^{13}	1.3×10^9	86.0	106.1
Step 14	1.0×10^{20}	5.5×10^{13}	0.0	906.6
Step 15	1.4×10^{10}	1.0×10^{11}	65.6	50.0
Step 16	3.6×10^{14}	1.0×10^8	38.9	0.0
Step 17	5.9×10^{14}	1.4×10^9	46.6	0.0

P_{ref} is 100 kPa.

Appendix B: Sensitivity Analysis

B.1 Validity of Model Parameters

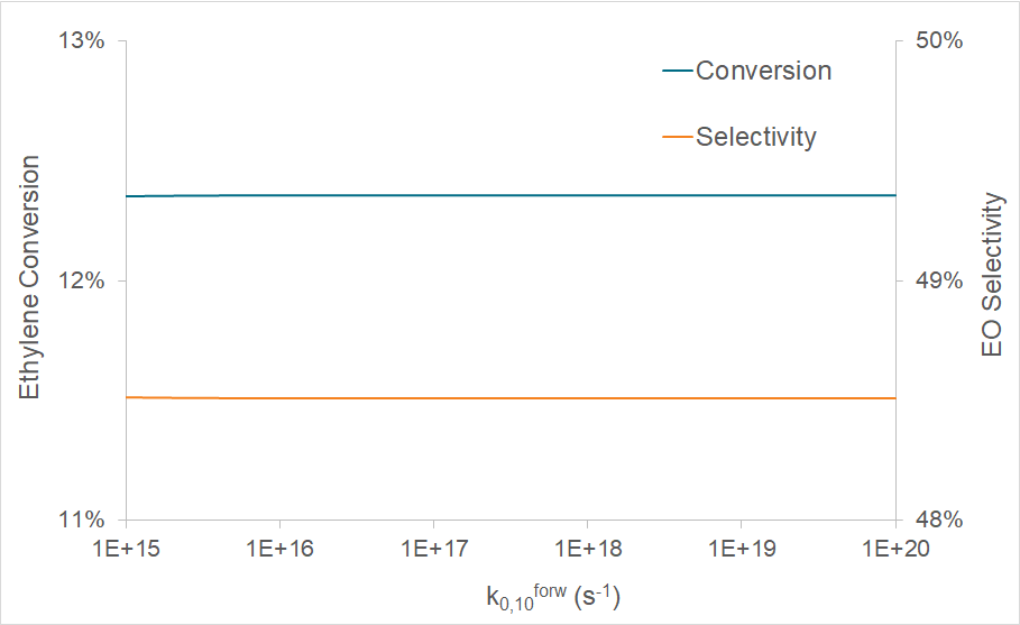

Figure B.1: Change in ethylene conversion and EO selectivity due to $k_{0,10}^{forw}$ variation

B.2 Reacting Temperature Analysis

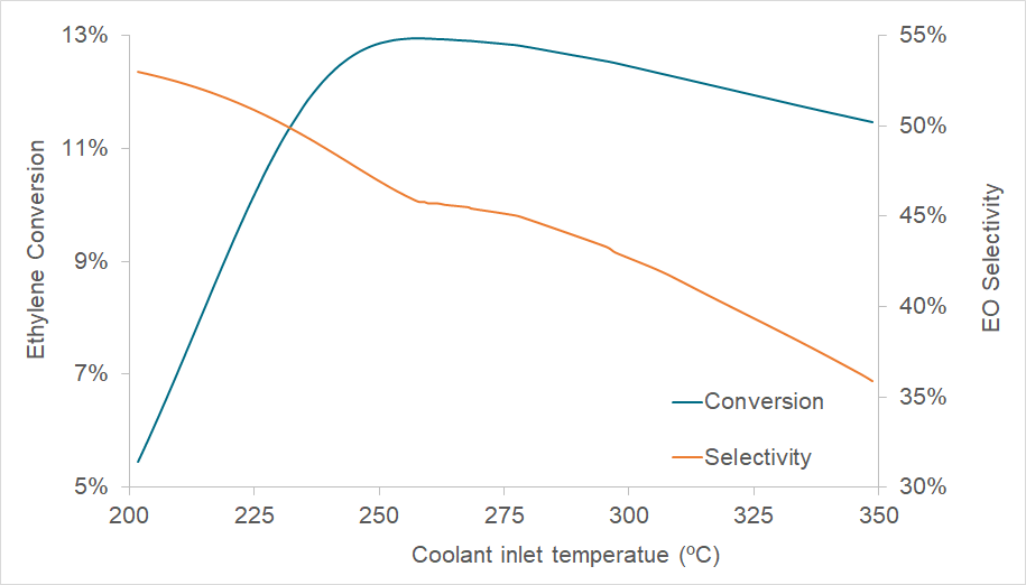

Figure B.2: Change in ethylene conversion and EO selectivity due to coolant inlet temperature variation

Appendix C: Model Extensions

C.1 Catalyst Deactivation

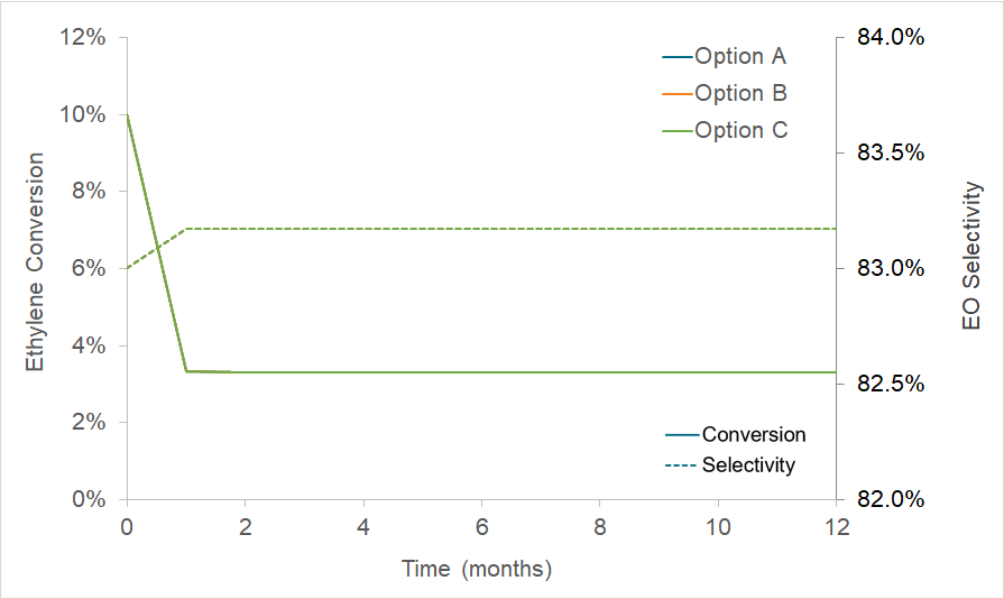

Figure C.1: Testing of the different options of deactivation kinetic parameters suggested by Zhou and Yuan [25]

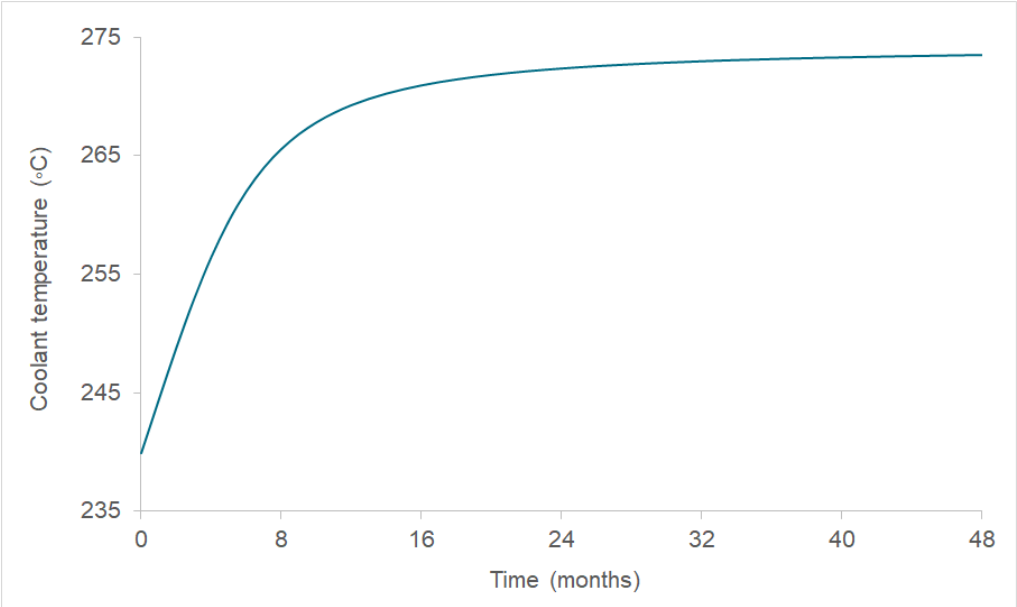

Figure C.2: Increase in coolant temperature to compensate site density deactivation using $k_{d,0}^{\rho_*}$ = 4 x 10^{11} months^{-1} and $E_d^{\rho_*}$ = 155 kJ mol^{-1}

Glossary

Foreign Object — Imported file into the gPROMS platform creating a compatible exchange of information. 16

Model Validation — gPROMS ProcessBuilder entity type in which parameter estimations and external model validations are performed. 44

Performed Experiment — gPROMS ProcessBuilder entity type required to carry out a parameter estimation. Entails data of the aimed process results. 28, 29